

Implementation of Inertia and Damping Terms into the Idealized Structural Unit Method

Dissertation

zur

Erlangung des akademischen Grades

Doktor-Ingenieur (Dr.-Ing.)

Fakultät für Maschinenbau und Schiffstechnik

Universität Rostock

vorgelegt von

M.Sc. Anna Oksina

geb. am 04.08.1991 in Leningrad

Rostock, 2017

Gutachter:

Prof. Dr.Eng/Hiroshima Univ. Patrick Kaeding

Prorektor für Studium, Lehre und Evaluation

Inhaber des Lehrstuhls Schiffstechnische Konstruktionen

Universität Rostock

Prof. Dr.-Ing. habil. Maciej Taczala

Dekan der Fakultät für Meerestechnik und Transport

Westpommersche Technische Universität Stettin

Datum der Einreichung:

01. März 2017

Datum der Verteidigung:

07. Juli 2017

ABSTRACT

Determination of the load-carrying capacity of structures is very important for the assessment of their safety. Constantly subjected to dynamic loads marine and offshore structures experience the significant rise of inertial forces in structural elements, often leading to buckling, plastic deformations or fatigue cracks. To ensure safety and reliability of structures under dynamic loading it is necessary to estimate the influence of the transient effects on the collapse behavior of plate panels.

As a possible tool for the ultimate strength analysis, the Finite Element Method (FEM) is widely spread among engineers. In spite of the great effectiveness, the transient Finite Element Analysis (FEA) remains very time consuming and sometimes difficult to accomplish well. Therefore, the Idealized Structural Unit Method (ISUM) can be applied for collapse analysis of large structures.

Within the present thesis the applicability of the ISUM is extended to dynamic collapse analyses of steel plate panels by taking the inertia and damping terms into account. Formulation of the consistent mass matrix for ISUM plate element is based on integration of the bilinear and trigonometric shape functions, which interpolate the nodal point displacements and internal deflections respectively. The latter depend on a direction of the applied load and describe buckling behaviour of plate panels. Since the investigations on a dynamic buckling behaviour of rectangular plates showed similarity with static buckling modes, shape functions for static ISUM formulation are used.

Damping effects are included to analysis by formulating the damping matrix, using Rayleigh model: damping parameters are determined for each examined plate type performing modal analysis. Based on the validation of the Rayleigh damping model on an example of the square plate panel, the damping ratio is chosen for the dynamic collapse investigations of rectangular plate panels.

The explicit central difference scheme (CDM) and the implicit Newmark's method (NMK) are introduced to perform the numerical integration of the system of nonlinear differential equations of second order. Validation is carried out on examples of simple spring-mass system (1D linear problem), 4-node membrane element (2D linear problem) and 4-node ISUM element (3D nonlinear problem). Particular attention is paid to the stability of the central difference method by adjustment an integration time step, since the prescribed scheme is only conditionally stable.

Current force control formulation does not allow to obtain the post-buckling region of the average stress - average strain curve. To provide the complete understanding of the buckling process, the enforced motion method is introduced. Corresponding numerical schemes are adjusted to the enforced motion method and validated on example of the 4-node ISUM element: new formulation provides desirable results, since the total buckling behavior of the plate structure can be obtained.

Having introduced the transient ISUM formulation, dynamic collapse analyses of different rectangular plate panes are performed. Validation of the obtained results is based on a comparison with FEA. The influence of the inertia and damping effects on the dynamic buckling behavior of rectangular plate panels is shown by the corresponding average stress - average strain curves. Factors, which effects the rise of the ultimate strength are outlined. According to the loading art, typical dynamic buckling modes are demonstrated. Newly implemented explicit central difference and implicit Newmark's time integration methods are analyzed in terms of results' reliability and computational costs. Finally, the applicability of the Idealized Structural Unit Method on dynamic collapse analyses of rectangular plates is assessed.

ACKNOWLEDGEMENTS

I would like to use the opportunity to express my sincere gratitude to people who facilitated the completion of this thesis.

First of all, I am eternally grateful to my academic supervisor *Prof. Patrick Kaeding* for making my dream come true. Without your help it would not be possible to perform an exciting doctoral research in Germany. Thanks to your support covering scientific questions as well as the administrative matters I got the DAAD scholarship and became a part of your team. You trusted me to work on the Idealized Structural Unit Method and I hope that I have met your expectations. During my research activity no questions left unanswered. Our discussions were comprehensive and informative, always carried a positive attitude and a friendly nature. Visiting your lectures was a special delight since you have an outstanding ability to explain the complicated technical things clearly and intelligibly, keep the audience's attention. I highly appreciate your assistance in preparing and submitting of papers and your approval on my participation at the conferences. I never doubted that my thesis will be successfully completed on time due to your smart guidance and efficient organization.

I very much acknowledge *Prof./Szczecin Univ. Maciej Taczala* for the review of my thesis. I highly appreciate your insightful comments, which help to improve the present work.

My special thanks go to my colleague *Dr.-Ing. Thomas Lindemann* for his comprehensive assistance and support. Also performing researches on the Idealized Structural Unit Method you gave me the valuable advises and helped to understand the specific of the Method. You have always found time to discuss the studies and answer my questions, so that it definitely accelerated my work on the project.

Furthermore, I would like to thank *Prof. Christoph Woernle* and *Prof. Robert Bronsart* for their support and discussions during my research activity. Additionally, I am deeply grateful to *Prof./St. Petersburg Univ. Vladimir Tryaskin*, *Prof./St. Petersburg Univ. Gennadiy Demeshko*, *Prof./St. Petersburg Univ. Alexander Rodionov*, *Dr.-Ing./St. Petersburg Univ. Yuri Ipatovtsev*, *Dr.-Ing./St. Petersburg Univ. Michael Mironov* for giving me the fundamental knowledges in structural mechanics and marine engineering. I express my thanks to my colleague *Dr.-Ing. Ivan Shevchuk* for his support and assistance concerning mathematics.

I would like to express my gratitude to the team of the chair for Shipbuilding Structures as well as to my fellows and all students for the comprehensive help and friendly atmosphere.

My greatest thanks I address to my mama, *Irina Oksina*, who has been always supported me and my endeavors. Your opinion and advises are the most important to me as well as mine to you. I know that you always believe in me and this feeling makes me stronger and more confident.

My stay and doctoral research in Germany have been supported by a scholarship of the German Academic Exchange Service, for which I am very grateful.

Anna Oksina

List of Figures

Figure 1: Ultimate capacity of steel plates under axial loading	1
Figure 2: Hogging (left) and Sagging (right) bending modes of the ship hull	2
Figure 3: The rectangular ISUM plate element [18].....	7
Figure 4: Buckling behavior of the square plate under uniaxial thrust	8
Figure 5: Fourier coefficients of deflected shape (left).	9
Figure 6: Buckling behavior of the rectangular plate under longitudinal thrust.....	10
Figure 7: initial deflection of rectangular plate 2400 x 835 x 15 mm in hungry-horse mode.....	10
Figure 8: Amplitudes A_l (left) and A_t (right) as additional degrees of freedom	11
Figure 9: Buckling behavior of the rectangular plate under transverse thrust.....	12
Figure 10: Plate panel under longitudinal and transverse thrust, [18]	16
Figure 11: Average stress-average strain relationship for the square	16
Figure 12: Average stress-average strain relationship for the rectangular plate	17
Figure 13: a) Force balance for a resting brick; b) Force balance acc. to d'Alembert's principle	19
Figure 14: Classification of the nonlinear analysis types.....	23
Figure 15: Spring-mass system subjected to dynamic force $F(t)$	31
Figure 16 (1)-(4): Structural response of the spring-mass system	33
Figure 17: Set-up for numerical test as a 4-Node membrane element [54]	34
Figure 18 (1)-(4): Structural response of the 4-node membrane.....	38
Figure 19: Set-up for numerical test as a 4-node ISUM element, [54]	39
Figure 20: Maximum applied force from the average stress-average strain curves.....	39
Figure 21: The applied dynamic force $F(t)$ on a 4-node ISUM element	41
Figure 22 (1),(2): Structural response of the 4-node ISUM element	43
Figure 23: Full Newton-Raphson iteration procedure	48
Figure 24 (1),(2): Displacement control vs. force control	50
Figure 25: ISUM-discretization for rectangular plate panels	53
Figure 26 (1)-(3): Dynamic collapse behavior of 15 mm square plate - different damping models	56
Figure 27 (1)-(3): Dynamic collapse behavior of the 11 mm square plate under uniaxial thrust	57
Figure 28 (1)-(3): Dynamic collapse behavior of the 15.5 mm square plate under uniaxial thrust	59
Figure 29 (1)-(3): Dynamic collapse behavior of the 19 mm square plate under uniaxial thrust	60
Figure 30 (1)-(6): Dynamic collapse behavior of longitudinally loaded plate 2400 x 835 x 15 mm.....	63
Figure 31: Influence of the reduced time step on the ISUM NMK and ISUM CDM oscillations	64
Figure 32 (1)-(6): Dynamic collapse behavior of longitudinally loaded plate 4200 x 835 x 13 mm.....	66
Figure 33 (1)-(6): Dynamic collapse behavior of longitudinally loaded plate 4200 x 835 x 22 mm.....	69
Figure 34 (1)-(6): Dynamic collapse behavior of transversely loaded plate 2400 x 835 x 15 mm	72
Figure 35 (1)-(6): Dynamic collapse behavior of transversely loaded plate 4200 x 835 x 13 mm	75
Figure 36: Collapse behavior of transversely loaded plate under velocity of 250 mm/s.....	76
Figure 37: Collapse modes of transversely loaded plate under velocity of 250 mm/s	76
Figure 38 (1)-(6): Dynamic collapse behavior of transversely loaded plate 4200 x 835 x 22 mm	79
Figure 39 (1)-(4): Dynamic collapse behavior of plate 4200 x 835 x 22 mm under biaxial thrust	82

List of Tables

Table 1: Dimensions and material properties of the square plate.....	8
Table 2: Dimensions and material properties of the rectangular plate	10
Table 3: Coefficients $A0i$ for initial deflection definition of rectangular plate 2400 x 835 x 15 mm ...	11
Table 4: Dimensions and material properties of the 4-node membrane element	34
Table 5: Source data for the problem's description.....	41
Table 6: Properties of the examined plate panels	53
Table 7: Damping parameters for the examined plate panels.....	55
Table 8: Coefficients $A0i$ for initial deflection definition of rectangular plate 4200 x 835 x 13 mm ...	64
Table 9: Coefficients $A0i$ for initial deflection definition of rectangular plate 4200 x 835 x 22 mm ...	67

List of Symbols and Abbreviations

ANSYS	ANalysis SYStem
CPU	Ratio of computing time
CSR	Common Structural Rules
ELDA	Elastic Large Deflection Analysis
FEA	Finite Element Analysis
FEM	Finite Element Method
FEM DC	Finite Element Method Displacement Control
FEM FC	Finite Element Method Force Control
FORTRAN	FORmula TRANslator
ISUM	Idealized Structural Unit Method
ISUM CDM	Idealized Structural Unit Method-Central Difference Method
ISUM NMK	Idealized Structural Unit Method- Newmark's Method
TL	Total Lagrangian formulation
UL	Updated Lagrangian formulation
$\{\Delta F\}$	Increment of the applied force vector
ΔL	Distance between the element nodes
$\{\Delta R\}$	Increment of internal force vector
$\{\Delta \varepsilon\}$	Green Strain Increment vector
$\{\Delta d\}$	Incremental displacement vector
Δt	Time step
Δt_{cr}	Critical time step value
$\Delta u_i, \Delta v_i, \Delta w_{ni}$	Increments of the local translational degrees of freedom

α, δ	Newmark's time integration parameters
α, β	Rayleigh damping parameters
$\alpha_1, \alpha_2 \dots \beta_4$	Generalized coordinates
β	Slenderness ratio
$\{\delta \varepsilon\}$	Virtual strain vector
$\{\delta d\}$	Virtual displacement vector
$\{\delta d^{S_f}\}$	Virtual displacement vector on a surface S_f
ε_Y	Yield strain
ε_x	Average compressive strain, x -component
ε_y	Average compressive strain, y -component
ξ	Damping ratio
π	Ratio of a circle's circumference to its diameter
ρ	Density
σ_{Euler}	Euler's stress
σ_Y	Yield strength
σ_x	Compressive stress, x -component
σ_y	Compressive stress, y -component
$[\tau]$	Internal stresses (Cauchy stress tensor)
ν	Poisson's ratio
ϕ_i	Eigenvectors
ω	Angular frequency
A_{ij}	Fourier coefficients of deflected shape
A_l	Longitudinal amplitude of ISUM plate element
A_t	Transverse amplitude of ISUM plate element
$[B]$	Strain-displacement matrix
$[B_L], [B_{L0}^t], [B_{Lt}^t]$	Linear strain-displacement transformation matrices
$[B_{LN0}^t], [B_{LNt}^t]$	Nonlinear strain-displacement transformation matrices
$[C]$	Damping matrix
$[C]$	Inplane stiffness
$[D]$	Material matrix
\tilde{D}	Bending stiffness
E	Young's modulus
$\{F\}$	Externally applied force vector
\tilde{F}	Airy's stress function
$[H(x, y, z)]$	Displacement interpolation matrix
H'	Hardening rate
$[K]$	Stiffness matrix
$[K^t], [K_{L0}^t], [K_{Lt}^t]$	Linear strain incremental stiffness matrices
$[K_{NL0}^t], [K_{NLt}^t]$	Nonlinear strain incremental stiffness matrices

$[M]$	Consistent mass matrix
$\{R\}$	Internal force vector
$\{R_C^i\}$	Externally applied concentrated forces
S	Body surface
$[S_0^t], [S_t^t], \{\hat{S}_t^t\}$	Matrices and vector of 2 nd Piola–Kirchhoff stresses
T	Complete time interval
$\{\hat{U}_i\}$	Nodal degree of freedom at node i of ISUM plate element
V	Body volume
$[X_0^t]$	Deformation gradient
a	Length of ISUM plate panel
a_e	Length of ISUM plate element
b	Breadth of ISUM plate panel
b_e	Breadth of ISUM plate element
$\{d\}$	Vectors of nodal point displacements
$\{d^I\}$	Total degree of freedom of ISUM plate element I
$\{\dot{d}\}$	Vectors of nodal point velocities
$\{\ddot{d}\}$	Vectors of nodal point accelerations
f	Shape function parameter
$\{f^B\}$	Externally applied force vector per unit volume
$\{f^{Sf}\}$	Externally applied force vector per unit area
$f_l(x, y)$	Longitudinal shape function of ISUM plate element
$f_t(x, y)$	Transverse shape function of ISUM plate element
i, j	Number of half-waves in x -and y -directions respectively
k	Spring stiffness
m	Special coefficient for shape function $f_l(x, y)$
m	Concentrated mass
p	Special coefficient for shape function $f_t(x, y)$
t	Thickness of ISUM plate element
t	Current time
u_i, v_i, w_{ni}	Local translational degrees of freedom at node i of ISUM plate element
v	Applied edge velocity value
$w(x, y)$	Deflection function of ISUM plate element
w_l	Longitudinal component of deflection function
w_0	Initial value of the internal deflection
w_t	Transverse component of deflection function
x, y	Global coordinates
x_e, y_e	Local element coordinates

CONTENTS

Abstract.....	ii
Acknowledgements.....	iii
List of Figures.....	iv
List of Tables.....	v
List of Symbols and Abbreviations.....	v
1 Introduction.....	1
1.1 Ultimate Strength Assessment by the Idealized Structural Unit Method	1
1.2 Subject of the Thesis	5
1.3 Composition of the Thesis	6
2 Formulation and Application of the Idealized Structural Unit Method	7
2.1 Theoretical Aspects	7
2.1.1 Square Plates under Uniaxial Thrust	8
2.1.2 Rectangular Plates under Longitudinal Thrust	10
2.1.3 Rectangular Plates under Transverse Thrust.....	12
2.2 Solution Procedure.....	13
2.3 Average Stress-Average Strain Relationships for Square and Rectangular Plates	16
2.4 Concluding Remarks.....	18
3 Fundamentals of Transient Analyses.....	19
3.1 Formulation of the Dynamic Equilibrium Equation.....	19
3.2 Direct Time Integration Methods.....	21
3.2.1 Explicit Time Integration Method.....	21
3.2.2 Implicit Time Integration Method	22
3.3 Nonlinear Structural Analyses	23
3.3.1 Incremental Step-by-Step Solution Process	24
3.3.2 Incremental Equations of Motion	25
3.3.3 Incremental Matrix Equations for Finite Element Formulations.....	27
3.4 Direct Time Integration Methods for Nonlinear Structural Analyses	28
3.4.1 Explicit Time Integration Method for Nonlinear Structural Analyses	28
3.4.2 Implicit Time Integration Method for Nonlinear Structural Analyses.....	28
3.5 Concluding Remarks.....	30

4	Application of Direct Time Integration Methods using Force Control	31
4.1	Dynamic Analysis of a Spring-Mass System.....	31
4.2	Dynamic Analysis of a 4-Node Membrane Element.....	34
4.3	Dynamic Analysis of a 4-Node ISUM Element. Formulation of consistent mass matrix.....	39
4.4	Concluding Remarks	44
5	Displacement Control Procedure for Direct Time Integration Methods.....	45
5.1	Enforced Motion Method in Structural Analysis	45
5.2	Explicit Time Integration Method with Enforced Motion Technique	46
5.3	Implicit Time Integration Method with Enforced Motion Technique	47
5.4	Displacement Control vs. Force Control.....	49
5.5	Concluding Remarks	51
6	Dynamic Collapse Analyses of ISUM Plate Panels	52
6.1	Rayleigh Damping Model	54
6.2	Dynamic Collapse Analyses of Square Panels under Uniaxial Thrust.....	57
6.3	Dynamic Collapse Analyses of Rectangular Panels under Longitudinal Thrust.....	61
6.3.1	Plate Panel 2400 x 835 x 15 mm	61
6.3.2	Plate Panel 4200 x 835 x 13 mm	64
6.3.3	Plate Panel 4200 x 835 x 22 mm	67
6.4	Dynamic Collapse Analyses of Rectangular Panels under Transverse Thrust	70
6.4.1	Plate Panel 2400 x 835 x 15 mm	70
6.4.2	Plate Panel 4200 x 835 x 13 mm	73
6.4.3	Plate Panel 4200 x 835 x 22 mm	77
6.5	Dynamic Collapse Analyses of a Rectangular Panel under Biaxial Thrust	80
6.6	Concluding Remarks	83
7	Conclusions.....	85
	References.....	86

1 Introduction

1.1 Ultimate Strength Assessment by the Idealized Structural Unit Method

Science and Technology have been developing with enormous speed in recent years. Innovations have covered all fields of knowledge, trying to make it ideal in terms of getting higher quality, increasing reliability, reducing costs and improving user friendliness.

All these benefits concerning engineering would be difficult to reach without developing of modern numerical methods and deeply studying mechanics. Taking into account nonlinearities and material behavior, initial imperfection of structures and the development of new finite element types, it has become possible to revise old regulations and to assess the load-carrying capacity from the point of the limit state. In other words, a certain structural element can operate until it reaches the ultimate strength by losing its stiffness, resulting in collapse. This means that it is necessary to analyze also the buckling behavior of structural members, since it is better when the failure takes place in the plastic range, allowing the structure to reallocate internal stresses.

The ultimate limit state design is based on the buckling analysis of steel plates, being the core element of all marine structures. There are many factors such as loading and boundary conditions, material and geometrical properties, initial imperfections, which define the buckling behavior. For example, thin plates buckle even in the elastic range, and in contrast, thick plates – at the plastic range, experiencing significant spread of yielding. Imperfect structures have a lower ultimate strength value compared with ideal ones, Figure 1:

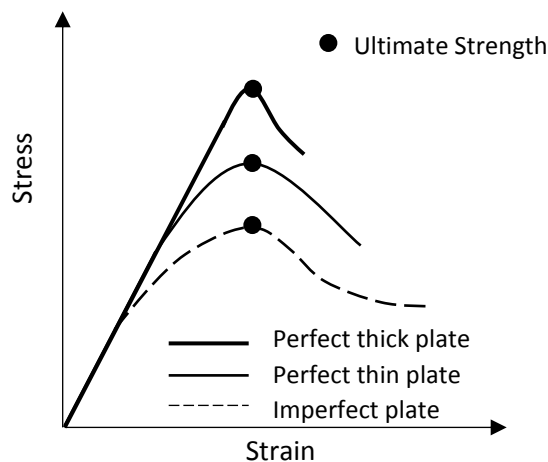


Figure 1: Ultimate capacity of steel plates under axial loading

Buckling of the ships' steel plates takes place under large in-plane compressive loads, caused by longitudinal hull bending. One can define this bending as hogging and sagging, then the middle part of the ship hull, idealized as a girder with variable characteristics of the cross-section, bends upwards and downwards respectively, Figure 2. In case of hogging, the compression of plates acts below the neutral axis. Considering sagging, plates above the neutral axis experience compression.

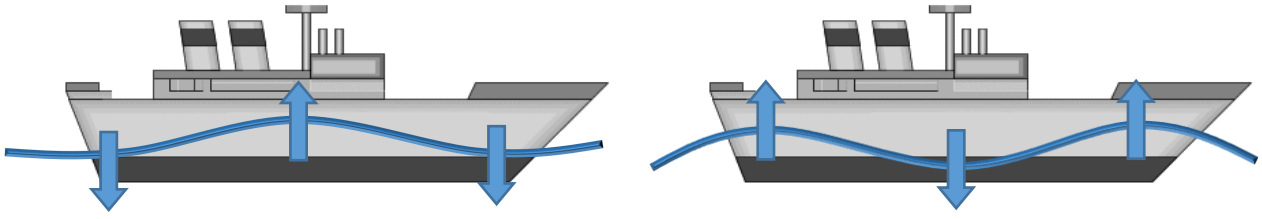


Figure 2: Hogging (left) and Sagging (right) bending modes of the ship hull











There are two principal methods to calculate the ultimate strength of steel plates [1]:

- The membrane stress method, [2]
- The rigid-plastic theory method, [3]

The first one allows getting the membrane stresses by solving the nonlinear governing differential equations of large deflection plate theory, namely the equilibrium and the compatibility equations. These will be discussed in detail in Chapter 2. As the membrane stresses reach the yield stress, collapse will occur. The spread of the yielding can be assessed by using the Mises-Hencky yield criterion, which determines the possible locations for the initial yielding as plasticity at corners and plasticity at longitudinal or transverse edges. The second approach presumes for the ultimate limit state the presence of kinematical mechanisms so that the internal strain energy is in equilibrium with the external potential energy.

According to the Common Structural Rules (CSR) safety of marine structures must be proved performing the hull girder ultimate strength check. Within the rules, collapse analysis based on the Smith's method is presented, where the ultimate hull girder capacity is defined as the maximum value of the curve, which depicts vertical bending moment versus the curvature of the ship cross section [5]. Due to this method the hull cross-section is to be divided into small elements. Vertical curvature of the hull is assumed to occur incrementally. Therefore, corresponding incremental strains can be calculated. Element stresses are derived from the incremental strains and integrated over the cross-section to obtain bending moment increments. Finally, incremental curvatures and moments are being summed to get cumulative values. Taking into account the assumption that the shear strains are neglected, the nonlinear Finite Element Method (FEM) is approved and recommended for the assessment of the ultimate strength.

The Finite Element Method (FEM) is one the most effective tools to solve such a complicated nonlinear behavior of structures. The idea of the method is to find the approximate solution of a certain problem. For this aim, the solution area is subdivided into a lot of small finite elements, representing the geometrical shape of the structure. As the approximate solution is found for each element and the equilibrium conditions are satisfied, the unknown displacements and stresses can be evaluated. The fundamental principles of the Finite Element Method were depicted in the papers of Clough [6], Argyris [7], Turner et al [8], Hrennikov [9] and many others. With the development of the computer technologies, the application of the perspective Finite Element Method grew significantly. In 1967 Zienkiewicz and Cheung [10] published the first book with the title "The Finite Element Method in structural and continuum mechanics", where they used a weighted residual Galerkin method and the least squares approach for the derivation of equations. This attracted attention of the mathematics community and gave a boost to the usage of FEM for the solution of linear and nonlinear differential equations. FEM found its application to a wide range of engineering tasks, namely for equilibrium time-independent problems, eigenvalue problems and propagation or transient problems. Some popular computer programs, which perform the Finite Element Analysis, are listed below:

- **ABAQUS** - Finite Element Analysis, 1978 
- **ANSYS** - Finite Element Analysis is, 1970 
- **COMSOL Multiphysics** - Finite Element Analysis, 1986 
- **Femap** - Finite Element Analysis, Siemens PLM Software, 1985 
- **FreeFEM++** - Finite Element Analysis, 1987 
- **LS-DYNA** - nonlinear transient dynamic Finite Element Analysis, 1987 
- **MSC.Nastran** - Finite Element Analysis, 1963 
- **SAMCEF** - Finite Element Analysis, 1965 
- **ПК Ли́ра** - Finite Element Analysis, 1963 
- **ПК СТАДИО** - Finite Element Analysis, 1991 

In spite of all the advantages of the Finite Element Method, it remains very time consuming because of the large number of unknowns involved in the solution procedure. A possible way of making analysis process faster would be the usage of special finite elements, which are larger as standard ones and therefore structures modelled with such elements would have less unknowns.

This idea of creation of the Idealized Structural Unit Method (ISUM) belongs to Ueda and Rashed [11]. The uniqueness of the method lies in the fact that unlike the traditional nonlinear FEM, one idealized structural element can model the whole structural component. Thus, the nonlinear structural analysis of square panel using ISUM takes ca. 1×10^4 less computational time than performing traditional FEA with mesh 50×50 elements.

Within the original ISUM formulation the geometrical and material nonlinearities were included in an idealized manner [12]-[16]. These idealizations are considered by special failure functions, which take the current stress-strain state of the element into account, and by the stiffness matrices defining the relationship between nodal force increments and nodal displacement increments depending on the failure functions. Material nonlinearities are included by usage of the plastic flow theory. These assumptions let a large structural unit be modeled as one element. Therefore a whole structural system can be discretized by some elements and the computational time with ISUM becomes much lower in comparison to FEM. The basic engineering concept for the plate element was defining the effective breadth of a plate after buckling.

Later, Masaoka et al. [17] have proposed to treat the amplitude of the lateral deflection of the plate panel explicitly as additional degree of freedom. This was reached by using eigenfunctions, depicting the buckling modes of the plate panels. The summation of these buckling mode shapes provided a common deflection function, where the coefficient is considered as degree of freedom. Unfortunately, this formulation was not suitable for determining the post-ultimate strength of structures accurately. The investigations of the collapse behavior of the stiffened plates did not provide accurate results as the ultimate strength was overestimated.

In the newest ISUM formulation proposed by Fujikubo and Kaeding [18] special shape functions were developed to reach highly accurate results for axially loaded plate panels with plate slenderness ratios up to 3.5. It was noticed that the deflection shape changes from the buckling mode shape to the collapse mode shape with the localization of plasticity. To simulate this complicated behavior and consider the plastic deformations, a few ISUM elements with the appropriate buckling- or collapse shape function have to be taken for modeling of one rectangular plate panel. These assumptions enabled also the combination of a beam-column element with the ISUM plate element. The applicability of the new formulation was demonstrated on examples of a double bottom structure of a bulk carrier by Fujikubo et al. [19], on a pontoon-type VLFS by Kaeding et al. [20], on different box-girder specimens in longitudinal bending by Kaeding et al. [21] and even on the 1/3 scaled welded steel frigate model by Fujikubo et al. [22].

Kaeding et al. [23] proposed further improvements of this formulation regarding the consideration of lateral pressure effects, by using the corresponding amplitude of the lateral plate panel deflection as separate degree of freedom. Ishibashi et al. [24] examined the collapse behavior of the plate panels under inplane bending and developed an approach to consider the presence of cutouts in plate panels under transverse thrust. Pei et al. [25], [26], [27] investigated the collapse behavior of the non-rectangular plates, by introducing the isoparametric ISUM element formulation. Gao et al. [28] carried out the collapse analysis of double bottom structures, taking the influence of the welding residual stresses on the ultimate strength into account.

A condensation procedure proposed by Lindemann et al. [29] was applied to the ISUM formulation and validated for plate panels and stiffened plates. This condensation allows to reduce the ISUM plate to nodal degrees of freedom so that it can be implemented in conventional FE software. Nonlinear FEA was performed to determine the collapse behavior of thin plate panels under inplane thrust and an approach to improve the shape function for such thin plates under longitudinal thrust. A new ISUM plate element formulation was developed by Lindemann [30] to perform collapse analysis of plate panels and stiffened plates under lateral pressure in geometrically nonlinear bending.

In June 2016, the world famous International Conference on Ocean, Offshore and Arctic Engineering OMAE dedicated a Special Symposium in honor of Professor Yukio Ueda, where scientific experts, industry and academic leaders, researchers and engineers discussed about modern computational methods for welding mechanics and strength of structures. Special attention was paid to the Idealized Structural Unit Method as about one third of the presentations was connected with ISUM, underlining its relevance and importance. By today, there are six available elements, ensuring the efficient analysis of the nonlinear behavior of marine structures, [31]:

- ISUM deep girder element
- ISUM plate element
- ISUM stiffened plate element
- ISUM tubular pipe element
- ISUM tubular pipe element with internal damage
- ISUM tubular joint element

Obviously the Idealized Structural Unit Method has its future and the field of application will broaden. This work is intended to enable transient analyses of shipbuilding structures within ISUM, using ISUM plate element.

1.2 *Subject of the Thesis*

Marine and offshore structures are subjected to dynamic loads during the lifetime. The values or directions of dynamic loads rapidly change in time, causing the significant rise of inertial forces in structural elements. Dynamic loads appear as result of ship's movement at sea, wind and wave acting, machinery operation, hull vibration and sometimes even as result of collision or explosion. Considering the ship's motion, three translational – surge, sway, heave – and three rotational – pitch, roll and yaw – degrees of freedom can be observed. According to these movements, the corresponding dynamic forces and moments act on the ship hull provoking the appearance of stresses, often leading to buckling, plastic deformations or fatigue cracks of the structural members.

To ensure the safety and reliability of structures under dynamic loading it is necessary to estimate the transient effects on the collapse behavior of plate panels. It was found that the strain rate, or in other words the derivative of the measured displacement with respect to time influence the mechanical properties of the steel. Lindemann et al. [32] have performed uniaxial tensile tests of mild and high tensile steel specimens to analyze this phenomenon. The experimental data showed interesting results: one could observe an increase of the yield strength. This demonstrated a good agreement with the Cooper-Symonds equation [33], which determines dynamic yield strength, using strain rate value and empirical coefficients. Due to these investigations one can presume that the load-carrying capacity of the steel marine structures under dynamic loading can be higher compared with the static loading.

To simulate dynamic collapse behavior of ship hull girder in waves, Pei et al. [34] developed a simulation system combining load/motion analysis of a ship's hull and progressive collapse analysis on a full ship model. The time domain load/motion calculation was performed to obtain time history of pressure distribution and acceleration of the ship. Then, the obtained pressure distribution and corresponding inertia force are applied to the full ship model, and the progressive collapse analysis is performed with combined ISUM/FEM analysis. Within the present thesis the applicability of the Idealized Structural Unit Method is extended to dynamic collapse analyses of steel plate panels. Since the transient analysis can be considered as set of equilibrium states at particular time points, the following additions were implemented to the static ISUM FORTRAN code:

- Inertia effects, by formulating the consistent mass matrix for ISUM plate element. In contrast to the previous investigations mass matrix construction method is based on a variational formulation, according to the FEM philosophy.
- Damping effects, by formulating the damping matrix, using the Rayleigh damping model;
- New solution procedures, which enable to find the unknown displacements and internal forces. The explicit central difference scheme and the implicit Newmark's method are implemented to perform the numerical integration of the system of nonlinear differential equations of second order.

This thesis covers a thorough study of the Idealized Structural Element Method, Finite Element Method and the numerical integration schemes. The following chapters give the detailed description of the mentioned theoretical aspects and include the practical implementation mechanisms and the results, presented by stress-strain relationships.

1.3 Composition of the Thesis

The present thesis consists of seven Chapters, which reflect the essence of the performed research and give the gradual presentation of information.

The *Introduction* in Chapter 1 provides a general information about the Idealized Structural Unit Method, gives an overview of the method's evolution, making a bridge to the objective and scope of the present study.

In Chapter 2 *Formulation and Application of the Idealized Structural Unit Method* the idea and the main theoretical aspects of ISUM are expounded. On an example of the rectangular plate panel under static longitudinal and transverse thrust the description of the new shape functions developed by Fujikubo and Kaeding [18] is presented. A brief introduction of the principle of virtual work and its application to the finite element formulation of ISUM is outlined. The assessment of the load-carrying capacity is successfully performed using the average stress-average strength curves.

In Chapter 3 *Fundamentals of the Transient Analysis* the derivation of the linear and nonlinear dynamic equilibrium equations is introduced. The direct explicit central difference scheme and the implicit Newmark's method are presented as suitable numerical solution procedures. Both schemes are analyzed in terms of stability, possible advantages and disadvantages are discussed. The comprehensive procedure description enables the direct implementation of these methods in ISUM program code.

In Chapter 4 *Application of the Direct Time Integration Methods using Force Control* the validation of the explicit central difference and the implicit Newmark's time integration methods is outlined on an example of the simple spring-mass system (1D linear problem), of the 4-node membrane element (2D linear problem) and of the 4-node ISUM element (3D nonlinear problem). The consistent mass matrix for ISUM plate element subjected to the uniaxial and biaxial loading is presented using the bilinear and trigonometric shape functions of the static formulation in [18].

In Chapter 5 *Application of the Displacement Control Procedure to the Direct Time Integration Methods* the formulation of the enforced motion method is introduced. This technique is applied to the explicit and implicit time integration schemes; results of the dynamic collapse analysis of the 4-node ISUM element performing displacement control (enforced motion) and force control are compared to each other.

In Chapter 6 *Dynamic Collapse Analysis of ISUM Plate Panels* the dynamic buckling behavior of different square and rectangular plate panels under longitudinal, transverse and biaxial thrust is investigated. The Rayleigh damping model is introduced. The influence of the damping forces is considered. The explicit central difference and the implicit Newmark's time integration methods are analyzed in terms of reliability of the obtained results and reducing the computational costs.

The last Chapter 7 *Conclusions* introduces the summary of the main features of the present study, denotes the possible improvements and future tasks.

2 Formulation and Application of the Idealized Structural Unit Method

2.1 Theoretical Aspects

The basic idea of the Idealized Structural Unit Method is to perform nonlinear analyses of marine structures faster than with using of the standard Finite Element Method. Since the number of equilibrium equations is equal to the degree of freedom number, the possible way of producing results effective in terms of time is to reduce the number of elements. With smart idealizations, it has become possible to model the standard shipbuilding steel plate even with very few elements.

Rectangular ISUM plate element developed by Fujikubo and Kaeding [18] with four corner nodes is taken as basis in this thesis. In Figure 3, a simply supported plate is subdivided by three ISUM plate elements indicated by Roman numerals. Three translational degrees of freedom u , v and w_n are defined at each node and interpolated bilinear within ISUM plate element. Overall bending deflection w_n is used in analyses of stiffened plates so that the plate panels “follow” the deflections of stiffeners modelled by beam elements, as described in [35]. In analysis of plate panels, w_n is equal to zero.

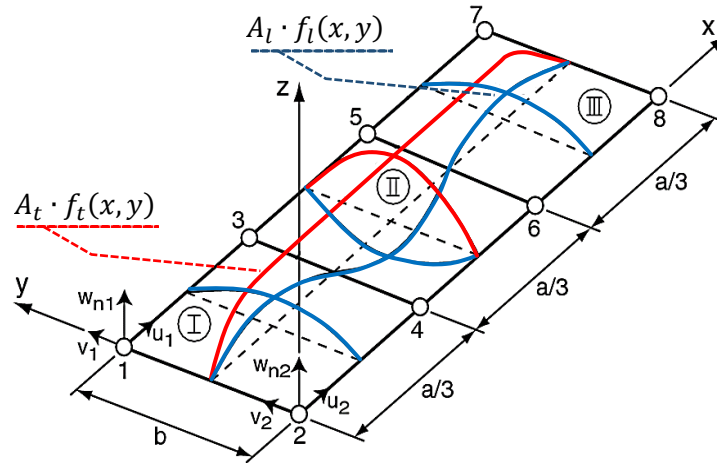


Figure 3: The rectangular ISUM plate element [18]

The deflection of the plate panel can be represented by the sum of two functions w_l and w_t , each describing according to the subscripts the buckling modes of the plate under longitudinal and transverse loading, Eq. 1:

$$w(x, y) = w_l + w_t = A_l \cdot f_l(x, y) + A_t \cdot f_t(x, y) \quad (1)$$

The shape functions $f_l(x, y)$ and $f_t(x, y)$ are multiplied with the amplitudes A_l and A_t , which are used within ISUM formulation as the additional degrees of freedom. In case of the biaxial thrust, the both amplitudes A_l and A_t are nonzero. Under longitudinal thrust the transverse amplitude A_t becomes zero and vice versa. Thereby one can describe the nodal degrees of freedom \hat{U}_i at node i with Eq. 2 and the total degrees of freedom d^I of element \textcircled{I} with Eq. 3:

$$\hat{U}_i = \{u_i, v_i, w_{ni}\} \quad (2)$$

$$d^I = \{\hat{U}_i, \hat{U}_i, \hat{U}_i, \hat{U}_i, A_l^I, A_t^I\}^T \quad (3)$$

2.1.1 Square Plates under Uniaxial Thrust

To understand the collapse behavior of the plate panels the FEA was performed. As the first case, the simple supported square plate with the following dimensions and material properties was considered:

Table 1: Dimensions and material properties of the square plate

Length, breadth	a, b	1000	mm
Thickness	t	15.5	mm
Yield strength	σ_Y	313.6	MPa
Young's modulus	E	205.8	MPa
Poisson's ratio	ν	0.3	-
Hardening rate	H'	0	-

The FE-model simulates the shipbuilding plating between longitudinal and transverse stiffeners. All edges of the plate are kept straight within the coupling conditions to satisfy the condition of continuity of plate edges. A discretization scheme of 50×50 shell elements is used. Initial lateral deflection with a magnitude of 10% of the thickness value is applied to simulate the buckling state. Uniaxial thrust is applied by inplane edge displacements. The buckling behavior and spread of yielding on the middle layer is shown in Figure 4:

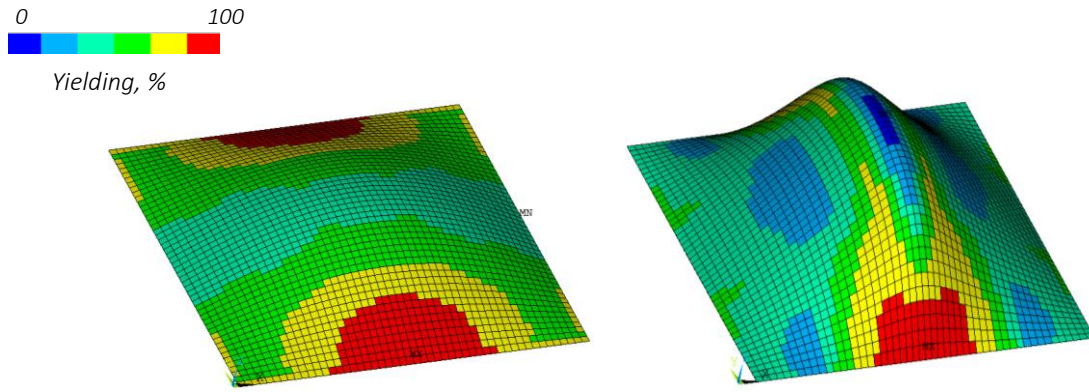


Figure 4: Buckling behavior of the square plate under uniaxial thrust at the ultimate strength $\varepsilon_x/\varepsilon_Y^* = 1$ (left) and at the post-ultimate strength $\varepsilon_x/\varepsilon_Y = 3$ (right). Deflection scale: 6

Due to the analysis the sinusoidal buckling shape can be observed at the ultimate strength but at the post-buckling region it changes to the roof mode. Fujikubo and Kaeding [18] expressed this change of the shape by the coefficients of the Fourier series, Eq. 4. Numbers of half-waves in x - and y - directions are represented by indices i and j respectively.

$$w = \sum_i \sum_j A_{ij} \sin \frac{i\pi x}{a} \sin \frac{j\pi y}{b} \quad (4)$$

* ε_x - Average compressive strain

ε_Y - Yield strain

The coefficients A_{11} and A_{31} are playing the main role by describing of the buckling behavior of the square plates, since the building of the roof mode can be explained by the great influence of the coefficients A_{31} beyond the ultimate strength. The relative values of the coefficients are presented in Figure 5 (left). As A_{31} becomes negative, the overlapping of the both shapes with one and three half-waves leads to the straightening in x - direction and as result to the formation of the roof mode.

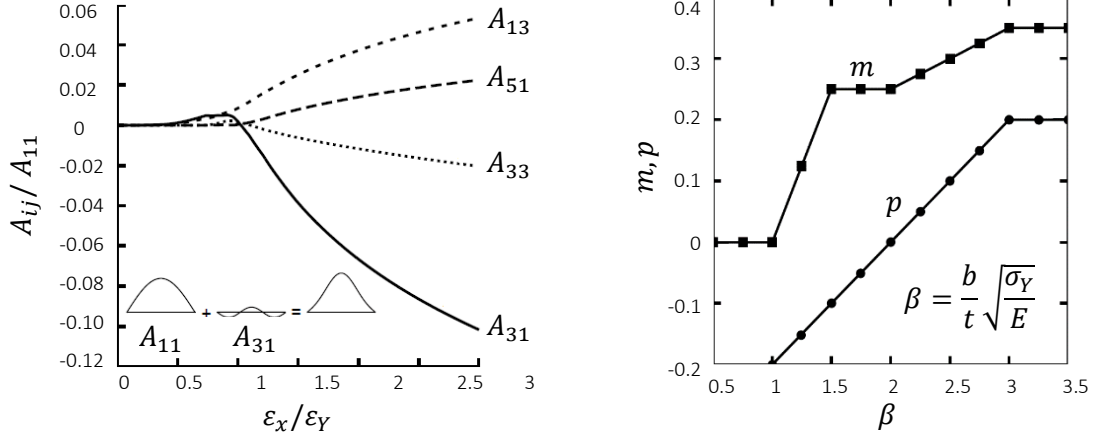


Figure 5: Fourier coefficients of deflected shape (left).
Definition of the coefficients m and p (right), [18]

To model the same behavior using the Idealized Structural Unit Method, Fujikubo et al. [36] created the shape function, which accounts the above considered transformation of the buckling mode in the post-ultimate range, Eq. 5:

$$w = A_l \sin \frac{n\pi x}{a} \sin \frac{\pi y}{b} + f A_l \sin \frac{3n\pi x}{a} \sin \frac{\pi y}{b} \quad (5)$$

The parameter f , Eq. 6, reproduces the relationship A_{31}/A_{11} and becomes the nonzero value, as the buckling mode must change to the roof mode. Itself it is a function of the dimensionless relation $\varepsilon_x/\varepsilon_Y$ and special coefficients m and p , obtained by the FEA of the buckling behaviour of square plates [36], Figure 5 (right). One can see that the increasing of the slenderness ratio β (for e.g. by reducing of the plate thickness) speeds up the changing from the sinusoidal to the roof mode. The numbers of half-waves n for the square plate is equal to one and therefore, such a plate panels can be modelled using only one ISUM plate element.

$$f = \begin{cases} 0, & \frac{\varepsilon_x}{\varepsilon_Y} < 1 - p \\ -m \ln \left(\frac{\varepsilon_x}{\varepsilon_Y} + p \right), & \frac{\varepsilon_x}{\varepsilon_Y} \geq 1 - p \end{cases} \quad (6)$$

2.1.2 Rectangular Plates under Longitudinal Thrust

Considering the collapse behavior of the rectangular plates under longitudinal thrust the FEA showed that they buckle unlike the square plates into several number of half-waves. Exemplary, the rectangular plate panel, which buckles into three half-waves, is represented on Figure 6. The principal dimensions and material properties of the FE-model of the rectangular plate are given in Table 2. Discretization scheme of 10×30 shell elements is used.

Table 2: Dimensions and material properties of the rectangular plate

Length	a	2400	mm
Breadth	b	835	mm
Thickness	t	15.5	mm
Yield strength	σ_Y	313.6	MPa
Young's modulus	E	205.8	MPa
Poisson's ratio	ν	0.3	-
Hardening rate	H'	0	-

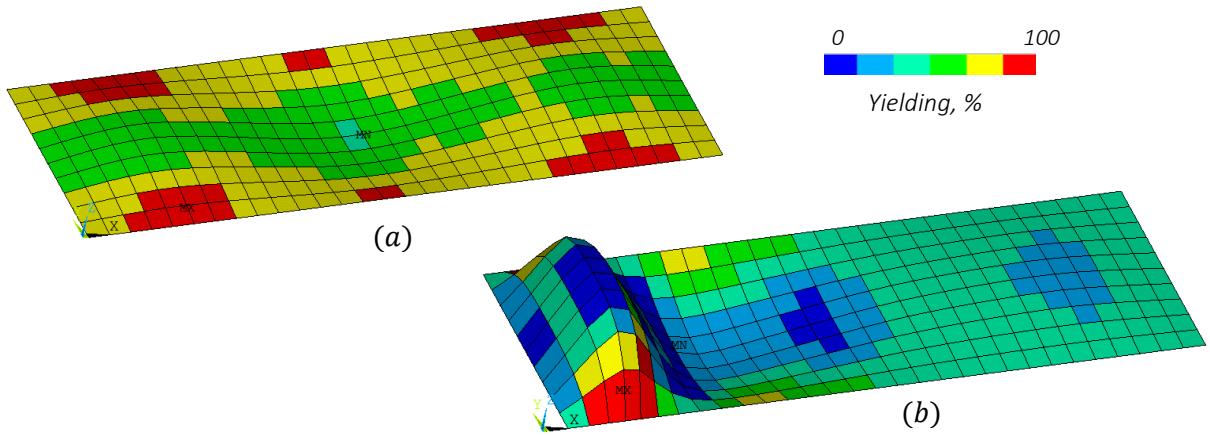


Figure 6: Buckling behavior of the rectangular plate under longitudinal thrust at the ultimate strength $\varepsilon_x/\varepsilon_Y = 1$ (a) and at the post-ultimate strength $\varepsilon_x/\varepsilon_Y = 4$ (b). Deflection scale: 6

One can see that the deflections are not the same in different half waves. This is the result of the non-symmetrical initial deflection, taking place in real structures. Like the square plate, one half-wave changes its shape from the sinusoidal to the roof mode beyond the ultimate strength. This half-wave collapses and the rest of the plate unloads. The initial deflection of the rectangular plate panels being a part of marine structures has a complicated non-uniform shape. It represents the so-called hungry-horse mode, Figure 7, and can be described by Eq. 7.

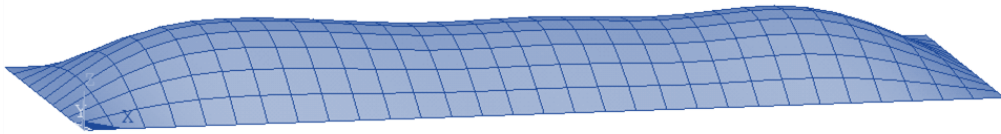


Figure 7: initial deflection of rectangular plate 2400 x 835 x 15 mm in hungry-horse mode. Deflection scale: 6

$$w = \sum_i A_{0i} \sin \frac{i\pi x}{a} \sin \frac{\pi y}{b} \quad (7)$$

The coefficients A_{0i} were defined experimentally by Ueda and Yao [37] for different rectangular plates according to the number of half-waves. For the considered rectangular plate with three half waves the coefficients A_{0i} are presented in Table 3:

Table 3: Coefficients A_{0i} , [mm] for initial deflection definition of rectangular plate 2400 x 835 x 15 mm

A_{01}	A_{02}	A_{03}	A_{04}	A_{05}	A_{06}	A_{07}	A_{08}	A_{09}	A_{010}	A_{011}
3.96	0.22	1.20	0.09	0.36	0.02	-0.02	0.08	-0.14	-0.02	-0.02

To model the same buckling behavior using the Idealized Structural Unit Method the shape function given by Eq. 5 is used, which enables describing the change from the sinusoidal to the roof mode within one half-wave. For this purpose, the number of elements of ISUM model has to be equal to the number of the buckling half-waves. The prescribed half-wave, which is going to reach the roof mode, gets the non-zero coefficients m and p , Figure 5, and therefore parameter f can be evaluated, Eq. 6. Only one component of the initial deflection is used for the ISUM model. The full value A_{0n} is assigned to the one ISUM element, and half of this value to the others. Exemplary the above-examined plate with three buckling half-waves gets for the first element the initial deflection A_{03} equal to the 1.20 mm, and the two rest elements the value of 0.6 mm. Keeping equal degrees of freedom A_l for the second and third element, but different from the degree of freedom A_l of the first element enables the modelling of localization of the plastic deformation, Figure 8 (left).

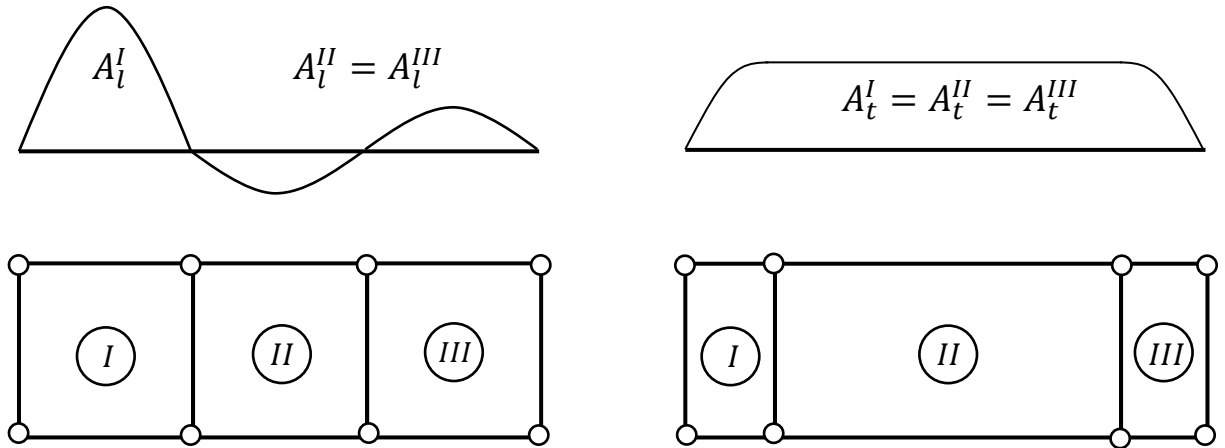


Figure 8: Amplitudes A_l (left) and A_t (right) as additional degrees of freedom for simulation of plastic deformation localization, [18]

2.1.3 Rectangular Plates under Transverse Thrust

To analyze the collapse behavior of the rectangular panel under transverse thrust, the FEA of the plate with dimensions and material properties given in Table 2 was performed. The FE-model with discretization scheme of 10×30 shell elements is used and the initial deflection in a hungry-horse mode according to the Eq. 7 was applied. The rectangular plate under transverse thrust buckles into one half wave, Figure 9. At the ultimate strength the cylindrical middle part is already formed. It remains longitudinally constant but in transverse direction represents the sinusoidal shape. The end parts behave as half of a square plate. Beyond the ultimate strength, the roof mode seems to be formed as the shape becomes more and more straightened in loading direction.

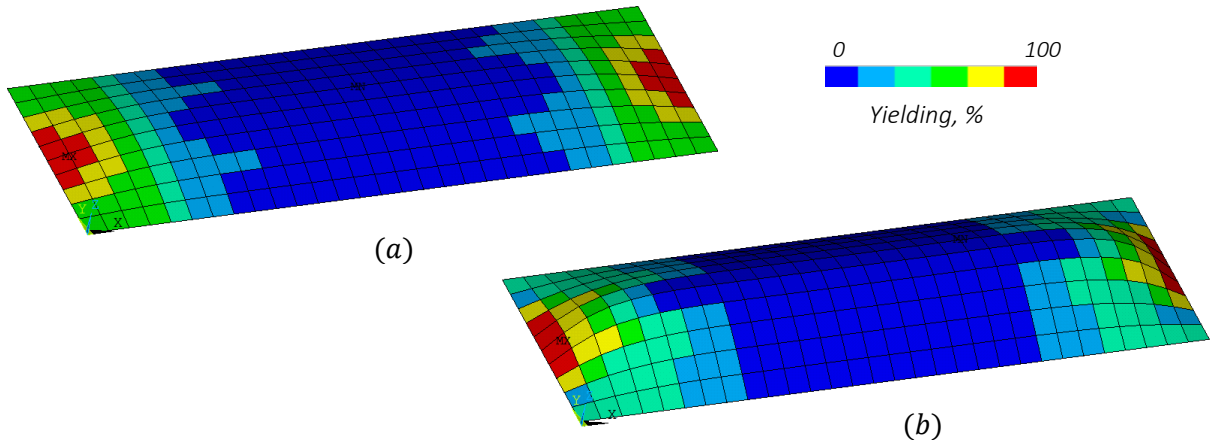


Figure 9: Buckling behavior of the rectangular plate under transverse thrust at the ultimate strength $\epsilon_x/\epsilon_Y = 1$ (a) and at the post-ultimate strength $\epsilon_x/\epsilon_Y = 4$ (b). Deflection scale: 6

To repeat the same buckling behavior using the Idealized Structural Unit Method at least three ISUM plate elements must be used, Figure 8 (right). The first and the third elements simulate the collapse of the end parts, which behave like the half of the square plate. That is why the length of these elements should be equal to the half of the plate breadth so that bringing them together would build the square plate. The second element is the biggest one and it simulates the cylindrical buckling behavior of the middle part of the rectangular plate. Keeping for each element the same degree of freedom, represented by the amplitude A_t , guarantees the continuous deflection all over the plate panel.

The shape function, Eq. 8 proposed by Fujikubo et al. [36] describes the buckling behavior of the rectangular plates under transverse thrust. Divided on three intervals according to the current x -coordinate it shows the good agreement with FEA.

$$w = A_t \begin{cases} \sin \frac{\pi x}{a} \sin \frac{\pi y}{b}, & 0 \leq x \leq \frac{b}{2} \\ \sin \frac{\pi y}{b}, & \frac{b}{2} \leq x \leq a - \frac{b}{2} \\ \sin \frac{\pi(x - (a - b))}{a} \sin \frac{\pi y}{b}, & a - \frac{b}{2} \leq x \leq a \end{cases} \quad (8)$$

2.2 Solution Procedure

The principle of virtual work is the basis of FE-solution process. According to this principle, the deformable body is in equilibrium if for any small virtual displacement, applied on the body, which was in equilibrium state, the total internal virtual work is equal to the total external virtual work, Eq. 9. The term “virtual” in this context means that the virtual displacements are not the real ones, which appear during the loading. It is just used to derive the governing differential equations of motion, integrating the principle of virtual work by parts.

$$\int \{\delta \varepsilon\}^T \{\tau\} dV = \int \{\delta d\}^T \{f^B\} dV + \int \{\delta d^{S_f}\}^T \{f^{S_f}\} dS + \sum_i \{\delta d^i\}^T \{R_C^i\} \quad (9)$$

In the above given equation one can see:

- $\{\delta d\}, \{\delta \varepsilon\}$ - virtual displacement vector and corresponding virtual strain vector;
- $\{\delta d^{S_f}\}$ - virtual displacement vector on surface area S_f , on which known tractions are applied;
- $\{\tau\}$ - stress vector, which balance the externally applied forces;
- $\{f^B\}, \{f^{S_f}\}$ - externally applied force vector per unit current volume and area;
- $\{R_C^i\}$ - externally applied concentrated force vector;
- S, V - body surface and volume.

For ISUM plate element the stress-state is defined by stress resultants per unit width:

$$\{\tau\} = \{N\} = \{N_x, N_{xy}, N_{xy}, M_x, M_y, M_{xy}\}^T \quad (10)$$

N_x, N_{xy}, N_{xy} – membrane force components per unit width;

M_x, M_y, M_{xy} – bending moment components per unit width.

Analogously to the stresses, the vector of the applied nodal forces can be expressed as:

$$\int f^B dV = \{F\} = \{F_{u_1} \ F_{u_2} \ F_{u_3} \ F_{u_4} \ F_{v_1} \ F_{v_2} \ F_{v_3} \ F_{v_4} \ F_{w_{n1}} \ F_{w_{n2}} \ F_{w_{n3}} \ F_{w_{n4}} \ F_{A_l} \ F_{A_t}\}^T \quad (11)$$

Components of vector $\{F\}$ are defined according to the degrees of freedom of ISUM plate element.

A distinctive feature of the nonlinear analysis is that the obtained displacements d are no more the linear function of the applied load F . Within the geometrical and material nonlinearities, the current body configuration can significantly change during the loading history. Therefore, the main difficulty of the nonlinear analysis is that the equilibrium equation must be satisfied at any possible configurations, whether the large displacements or large rotations appear. The incremental approach is successfully applied to cope with this problem. To build such a scheme one can presume that for the certain moment the solution is known and to get the solution in the next step the incremental values must be found.

Thus, performing two-dimensional analysis without consideration of surface and concentrated forces ($f^S = R_C^i = 0$) the principle of virtual work in an incremental form can be written as:

$$\int \{\delta \Delta \varepsilon\}^T (\{N\} + \{\Delta N\}) dA = \{\delta \Delta d\}^T (\{F\} + \{\Delta F\}) \quad (12)$$

In the following paragraphs a brief summary of the solution procedure is given based on [38]. The total strain increment $\Delta \varepsilon$ represents the updated Green Strain Increment [39], which introduces the difference between the two adjacent configurations. It consist of the linear part (the first term on the right-hand side), obtained from the nodal inplane displacements and of the nonlinear part (the second term on the right-hand side), calculated using the Elastic Large Deflection Analysis (ELDA):

$$\begin{Bmatrix} \Delta \varepsilon_x \\ \Delta \varepsilon_y \\ \Delta \gamma_{xy} \end{Bmatrix} = \begin{Bmatrix} \Delta \varepsilon_x^{linear} \\ \Delta \varepsilon_y^{linear} \\ \Delta \gamma_{xy}^{linear} \end{Bmatrix} + \begin{Bmatrix} \Delta \varepsilon_x^{ELDA} \\ \Delta \varepsilon_y^{ELDA} \\ \Delta \gamma_{xy}^{ELDA} \end{Bmatrix} \quad (13)$$

The linear inplane strains can be obtained calculating the partial derivatives of the bilinear shape functions, which represent the interpolation of the nodal inplane displacements u and v . The subscripts by the displacements u and v mean the node number according to the Figure 3, a_e and b_e represent the length and breadth of the element respectively:

$$\begin{aligned} \Delta \varepsilon_x^{linear} &= \frac{\partial \Delta u}{\partial x} = \frac{\partial}{\partial x} \left[\left(1 - \frac{x_e}{a_e}\right) \frac{y_e}{b_e} \Delta u_1 + \left(1 - \frac{x_e}{a_e}\right) \left(1 - \frac{y_e}{b_e}\right) \Delta u_2 + \frac{x_e}{a_e} \frac{y_e}{b_e} \Delta u_3 + \frac{x_e}{a_e} \left(1 - \frac{y_e}{b_e}\right) \Delta u_4 \right] \\ \Delta \varepsilon_y^{linear} &= \frac{\partial \Delta v}{\partial y} = \frac{\partial}{\partial y} \left[\left(1 - \frac{x_e}{a_e}\right) \frac{y_e}{b_e} \Delta v_1 + \left(1 - \frac{x_e}{a_e}\right) \left(1 - \frac{y_e}{b_e}\right) \Delta v_2 + \frac{x_e}{a_e} \frac{y_e}{b_e} \Delta v_3 + \frac{x_e}{a_e} \left(1 - \frac{y_e}{b_e}\right) \Delta v_4 \right] \\ \Delta \gamma_{xy}^{linear} &= \frac{\partial \Delta u}{\partial y} + \frac{\partial \Delta v}{\partial x} \end{aligned} \quad (14)$$

The derivation of the nonlinear strain can be performed by the Elastic Large Deflection Analysis (ELDA) for the certain shape function w , which depends on the loading direction. For longitudinal thrust application Eq. (5 is taken as shape function, for transverse – Eq. (8 and for biaxial – Eq. (1. The chosen shape function w can be substituted into the compatibility condition for large deflections, [40], [41], where w_0 represents the initial value of the internal deflection described by the same shape function w :

$$\frac{\partial^4 \tilde{F}}{\partial x^4} + 2 \frac{\partial^4 \tilde{F}}{\partial x^2 \partial y^2} + \frac{\partial^4 \tilde{F}}{\partial y^4} = E \left[\left(\frac{\partial^2 w}{\partial x \partial y} \right)^2 - \frac{\partial^2 w}{\partial x^2} \frac{\partial^2 w}{\partial y^2} - \left(\frac{\partial^2 w_0}{\partial x \partial y} \right)^2 + \frac{\partial^2 w_0}{\partial x^2} \frac{\partial^2 w_0}{\partial y^2} \right] \quad (15)$$

Having solved the Airy's stress function \tilde{F} , the nonlinear strain components can be found using the following equation, where E is the Young's modulus and ν is the Poisson's ratio:

$$\begin{aligned} \Delta \varepsilon_x^{ELDA} &= \frac{1}{E} \left(\frac{\partial^2 \tilde{F}}{\partial y^2} - \nu \frac{\partial^2 \tilde{F}}{\partial x^2} \right) \\ \Delta \varepsilon_y^{ELDA} &= \frac{1}{E} \left(\frac{\partial^2 \tilde{F}}{\partial x^2} - \nu \frac{\partial^2 \tilde{F}}{\partial y^2} \right) \\ \Delta \gamma_{xy}^{ELDA} &= - \frac{\partial^2 \tilde{F}}{\partial x \partial y} \frac{2(1 + \nu)}{E} \end{aligned} \quad (16)$$

Having found the total strain increment, Eq. 13, the increment of the stress resultants ΔN can be calculated by:

$$\{\Delta N\} = [D]\{\Delta \varepsilon\} \quad (17)$$

Vector $\{\Delta \varepsilon\}$ composes the inplane strain increments of Eq. 13 and the classical three curvature terms of Kirchhoff plates, which are evaluated linearly, as given in detail by [38].

The material matrix $[D]$ depends on the stress state. In the elastic range, taking into account the inplane stiffness $C = Et/(1 - \nu^2)$ and the bending stiffness $\tilde{D} = \frac{Et^3}{12}/(1 - \nu^2)$ of the plate element with a certain thickness t , matrix $[D]$ can be obtained as:

$$[D] = \begin{bmatrix} C & C\nu & 0 & 0 & 0 & 0 \\ C\nu & C & 0 & 0 & 0 & 0 \\ 0 & 0 & C(1-\nu)/2 & 0 & 0 & 0 \\ 0 & 0 & 0 & \tilde{D} & \tilde{D}\nu & 0 \\ 0 & 0 & 0 & \tilde{D}\nu & \tilde{D} & 0 \\ 0 & 0 & 0 & 0 & 0 & \tilde{D}(1-\nu)/2 \end{bmatrix} \quad (18)$$

In the plastic range, the material matrix $[D]$ can be evaluated using the plastic flow law, yield functions and the yield criteria, based on the von Mises hypothesis and giving the estimation, whether the initial, intermediate or fully plastic state takes place, Eggers and Kröplin, [42]. A complete description of the evaluating of the material matrix is given by [30].

Finally, the principle of virtual work in an incremental form yields:

$$[K]\{\Delta d\} = \{\Delta F\} + (\{F\} - \{R\}), \quad (19)$$

with tangential stiffness matrix $[K]$, incremental displacement vector $\{\Delta d\}$, applied force vector $\{F\}$ and its increment $\{\Delta F\}$ and internal force vector $\{R\}$. Element stiffness matrices and internal force vectors are assembled over the whole structure as in conventional FEA. Taking into account the material nonlinearities, the order of integration plays an important role for a large ISUM element, as the check of yielding is performed at the integration points.

This means that usage of the low integration order would not give an accurate picture of material nonlinearities distribution. Therefore, within the Idealized Structural Unit Method (ISUM) 7×7 integration points placed equidistant over the element area are used for each plate element. Integration of stiffness matrix and internal force vector is carried out numerically, by the trapezoidal rule. Solution of the above-obtained incremental Eq. 19 is performed numerically by the widely used Newton-Raphson Method. It is an effective scheme, which allows reaching an equilibrium state within a certain tolerance for each new body configuration, performing an iterative procedure for determination of the approximate displacement values. Formulation of the Newton-Raphson Method will be discussed in Chapter 3.3.1.

2.3 Average Stress-Average Strain Relationships for Square and Rectangular Plates

One of the main purposes of engineering analysis is to predict how material will respond to the loading, acting on the structures. This analysis can be performed experimentally by applying forces to a specimen and then determining the resulting stress using sensors. Using the obtained results one can derive the stress–strain curve, which enables determination of the material properties such as yield strength, ultimate strength, Young’s modulus, Poisson’s ratio and others. Performing the FEA of the structures the stress–strain curve gives analogously the comprehensive information on the collapse behavior, giving the opportunity to analyze the whole loading process.

The dimensionless average stress-average strain curves will be presented within this work for both FEA and ISUM to make the data handling more convenient. Assuming the applied by displacements longitudinal or transverse thrust, according to the current deformation the resulting internal forces are summed up on a subjected by the loading element face and divided by area of this face, Figure 10.

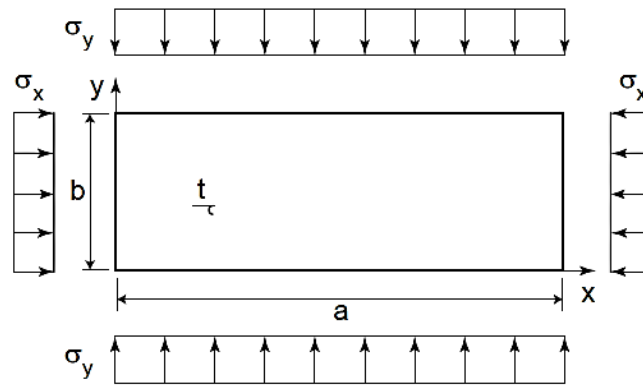


Figure 10: Plate panel under longitudinal and transverse thrust, [18]

Exemplary, the average stress-average strain relationships for square and rectangular plates are presented in Figure 11 and Figure 12 respectively. The obtained stresses σ_x and σ_y are divided by the yield strength value σ_Y , and the obtained strains ε_x and ε_y are divided by the yield strain $\varepsilon_Y = \frac{\sigma_Y}{E}$.

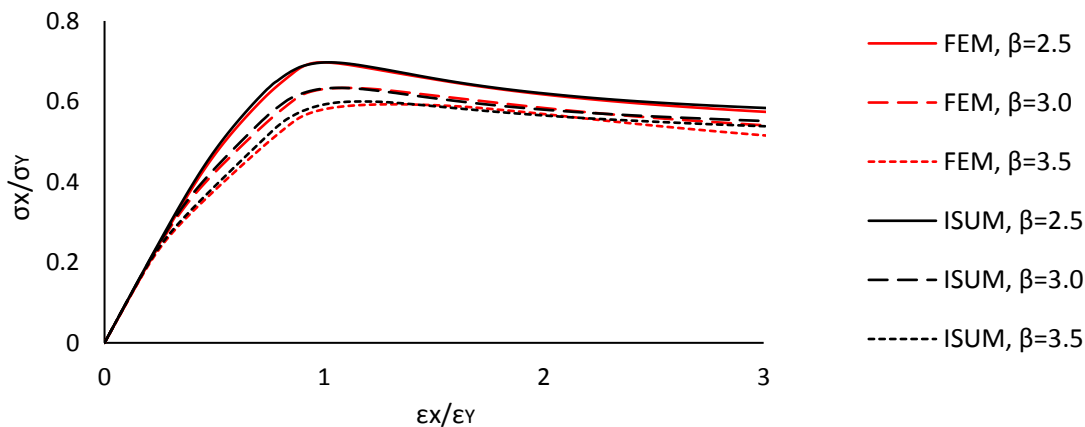


Figure 11: Average stress-average strain relationship for the square plate with different slenderness ratio

Three square plates with slenderness ratios β equal to 2.5, 3.0 and 3.5 with dimensions and material properties given in Table 1 have the similar collapse behavior under uniaxial loading. Buckling is observed by the change of the slope of the corresponding average stress-average strain curve. After buckling, the initial yielding is reached. This means that the material extension takes place more quickly with little increase in load. The peak points on the diagram correspond to the ultimate strength, which is the maximum strength that material is able to withstand before breaking.

One can see that the ultimate strength values increase with increasing slenderness ratio. In other words, the logical assumption that the load-carrying capacity of the thicker plates are higher is proved by the obtained average stress-average strain curves. In the post-ultimate strength range the load-carrying capacity decreases. The results of FEA (by "ANSYS 15.0") and ISUM analysis have very good agreement.

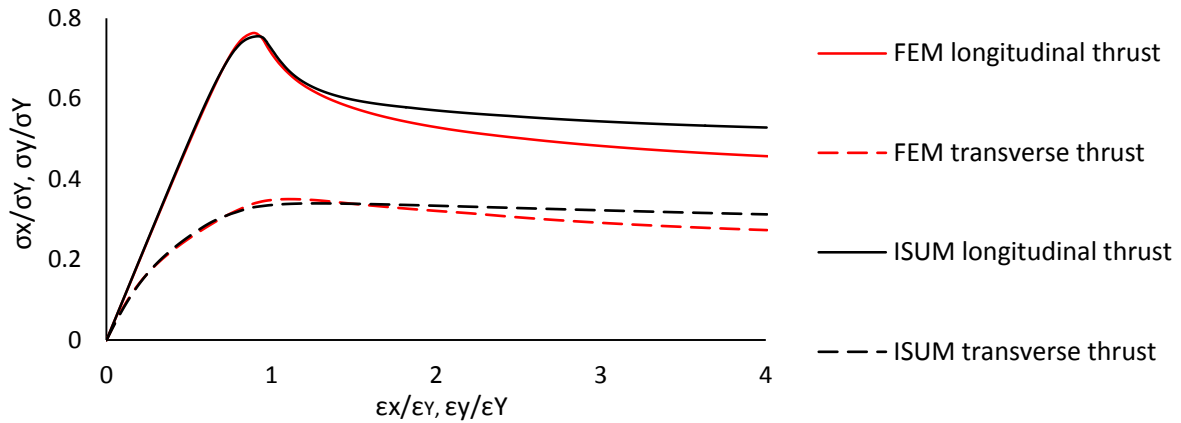


Figure 12: Average stress-average strain relationship for the rectangular plate under longitudinal and transverse thrust

The collapse behavior of the rectangular plate with dimensions and material properties, given in Table 2 under longitudinal and transverse thrust is no more the same, Figure 12. The first thing that catches the eye is that the ultimate strength value of the longitudinally loaded plate is two times higher as of the transversely loaded plate. This can be explained theoretically by the comparison of the Euler's stresses [43]: under the uniaxial compression along the long side of the plate the Euler's stress is $\sigma_{Euler} = 4\pi^2 \tilde{D}/b^2 t$, and $\sigma_{Euler} = \left(1 + \left(\frac{b}{a}\right)^2\right)^2 \pi^2 \tilde{D}/b^2 t$ under the uniaxial compression along the short side of the plate, with bending stiffness \tilde{D} and plate geometrical characteristics a , b and t . Assuming that the value $\left(\frac{b}{a}\right)^2$ is small compared to 1, the Euler's stress for the plate under longitudinal loading is approximately four times higher as under transverse loading. That is why the longitudinal framing is more preferable for maritime structures from the point of considering the hull's bending.

As one can see, ISUM solution exactly follows the FE-curve for both longitudinal and transverse thrust cases, and only in the post-buckling range they slightly depart from the FEA results.

2.4 Concluding Remarks

In Chapter *Formulation and Application of the Idealized Structural Unit Method* the following subjects were highlighted and discussed as basis for the developments in the following Chapters:

- Formulation of the rectangular ISUM plate element developed by Fujikubo and Kaeding [18]: within the new ISUM formulation the amplitudes of the shape functions are treated as additional degrees of freedom.
- Main features of the buckling behavior of rectangular plates under longitudinal and transverse thrust: for rectangular plates under longitudinal thrust, the sinusoidal buckling shape is typical. However, the presence of the initial deflection causes the non-symmetrical yielding distribution that leads to the formation of the roof mode beyond the ultimate strength for one half-wave. The same happens to the square plate, which collapses in the only half-wave. For rectangular plates under transverse thrust, the cylindrical middle part forms at the ultimate strength. It remains longitudinally constant during the buckling process and in transverse direction it represents the sinusoidal shape, becoming more and more straightened as the deformations increase.
- New shape function, presented by Fujikubo and Kaeding [18] for rectangular plates under longitudinal and transverse thrust: in case of the longitudinal loading, the special parameter is introduced within the new formulation, which multiplied with the trigonometric function models the change from the sinusoidal to the roof mode. In case of the transverse thrust, the shape function is defined on the intervals, limited by the length of the elements. According to the buckling behavior the amplitudes of the shape functions are whether the same for each element (by transverse thrust) or not (by longitudinal thrust). The number of ISUM plate elements must be equal to the number of half-waves.
- The principle of virtual work in application to the static ISUM formulation: the incremental approach for derivation and solution of the equation of motion is introduced together with the technique of the Green Strain Increment definition [39]. Importance of an integration order for establishment of the stiffness matrix and internal force vector is highlighted.
- Average stress-average strain relationship as a suitable tool for the buckling behavior analysis: the assessment of the load-carrying capacity is presented on examples of the uniaxial loaded square plate with different slenderness ratios and on examples of the longitudinally and transversely loaded rectangular plate. The results obtained by the static ISUM analysis show very good agreement with the static FEA results. The visible advantage of the Idealized Structural Unit Method is that the calculation time with ISUM is much shorter than with FEA.

3 Fundamentals of Transient Analyses

3.1 Formulation of the Dynamic Equilibrium Equation

The main difference between static and transient analysis is that the dynamic loads are time-dependent. They are applied as a function of time and therefore, time represents the additional parameter in transient analysis. Moreover, the dynamic loads induce the time-varying response of internal forces and stresses, displacements, velocities, and accelerations. These time-dependent parameters make dynamic analysis more difficult to perform, but one should not forget that considering the real physical processes as well as the operation conditions of machineries and structures the influence of the dynamic effects can play the significant role in the total force-balance.

Let us consider the interpretation of forces on an example of the brick, lying on a horizontal surface:

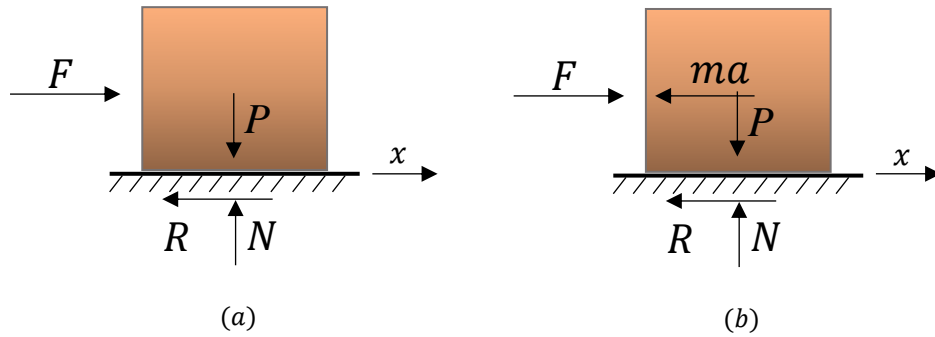


Figure 13: a) Force balance for a resting brick; b) Force balance according to d'Alembert's principle

The ground reactions can be simply evaluated from the static equilibrium equations, Figure 13 a). But as soon as the brick starts to move with acceleration a , the Newton's second law yields $F - R = ma$, where the inertia force ma turns the task to the transient one. This dynamic problem can be brought to the equilibrium rewriting $F - R - ma = 0$. This technique is known as d'Alembert's principle, [44], which means that for the dynamic equilibrium the inertia force $-ma$, acting opposite the motion's direction must be considered in addition to the real forces, acting on a structure, Figure 13 b). For solution of the dynamic problems the d'Alembert's principle is widely used and its' application will be shown below.

There are some important assumptions and hypotheses, which must be clarified to derive the dynamic equilibrium equation for the finite element application. Performing the FEA a real structure is treated as an assemblage of the finite elements, connected at the nodal points. Apart from a global coordinate system u, v, w each element has its' own local coordinate system x, y, z and the displacements inside each element $\{d(x, y, z)\}$ are represented as a function of the nodal displacements $\{\hat{d}(u, v, w)\}$, where $[H(x, y, z)]$ is the displacement interpolation matrix (shape function):

$$\{d\} = [H]\{\hat{d}\} \quad (20)$$

Analog to displacements, the components of strain $\{\varepsilon(x, y, z)\}$ can be described as a function of the nodal displacements $\{\hat{d}(u, v, w)\}$, where $[B(x, y, z)]$ is the strain-displacement matrix, based on the shape function:

$$\{\varepsilon\} = [B]\{\hat{d}\} \quad (21)$$

The stresses in the finite elements $\{\tau(x, y, z)\}$ can be calculated using the material matrix $[D]$ and strains $\{\varepsilon(x, y, z)\}$:

$$\{\tau\} = [D]\{\varepsilon\} \quad (22)$$

Substitution of the above given equations 20-22 into the principle of virtual work, Eq. 9, without consideration of surface and concentrated forces ($f^{Sf}=R_C^i=0$) yields the static finite element equilibrium equation, [45]:

$$\left[\int [B^T][D][B]dV \right] \{\hat{d}\} = \left[\int [H^T]\{f^B\}dV \right] \quad (23)$$

Stiffness matrix $[K]$ Force vector $\{F\}$

Finally, according to the d'Alembert's principle it remains to include the inertia forces to the acting body forces. Apart from it, due to the energy dissipation, which takes place during vibration of real structures, the damping forces depending on velocities should be also added to the body forces. Assuming that velocities and accelerations can be approximated by derivatives of displacements in Eq. 20 the body force vector yields:

$$\{F\} = \int [H^T](\{f^B\} - \rho[H]\{\ddot{d}\} - k[H]\{\dot{d}\})dV \quad (24)$$

In Eq. 24 the parameters ρ and k denote density and damping properties of the elements, $\{\dot{d}\}$ and $\{\ddot{d}\}$ represent the vectors of the nodal point velocities and accelerations respectively. For further convenience it is considered that $\{d\} \equiv \{\hat{d}\}$. Thereby, the dynamic equilibrium equation in finite element formulation can be written as:

$$\left[\int \rho[H^T][H]dV \right] \{\ddot{d}\} + \left[\int k[H^T][H]dV \right] \{\dot{d}\} + \left[\int [B^T][D][B]dV \right] \{d\} = \left[\int [H^T]\{f^B\}dV \right] \quad (25)$$

Mass matrix $[M]$ Damping matrix $[C]$ Stiffness matrix $[K]$ Force vector $\{F\}$

Practically, it is quite difficult to get the damping properties of the elements as they depend on the frequencies. Nevertheless, damping matrix $[C]$ can be obtained using the mass and stiffness properties of the whole finite element model together with the experimental data on the damping characteristics. Damping will be considered later by the Rayleigh damping model.

3.2 Direct Time Integration Methods

The dynamic equilibrium equation represents the linear differential equation of second order whose solution can be successfully obtained performing the direct time integration. The term “direct” means that there is no need to transform the primary differential equation into another form. The solution is searched on the discrete time intervals Δt where the displacements, velocities and accelerations are supposed to vary.

Building the solution scheme it is assumed that at time $t = 0$ the displacements $\{d\}^0$, velocities $\{\dot{d}\}^0$ and accelerations $\{\ddot{d}\}^0$ are known. The complete time range T is divided into n equal time intervals Δt , therefore, the approximate solution is determined on time intervals $0, \Delta t, 2\Delta t, 3\Delta t \dots T - \Delta t, T$.

3.2.1 Explicit Time Integration Method

A grate number of finite difference expressions can be employed for approximation of the velocities and accelerations in terms of displacements within the time interval Δt . One of the most effective schemes is the central difference method, which represents the direct explicit time integration procedure. The term “explicit” means that utilization of the equilibrium conditions at time t yields the required solution at time $t + \Delta t$. Let us consider the basic approximation relationships for the explicit time integration method [46]:

$$\begin{aligned}\{\dot{d}\}^t &= \frac{1}{2\Delta t} (\{d\}^{t+\Delta t} - \{d\}^{t-\Delta t}) \\ \{\ddot{d}\}^t &= \frac{1}{(\Delta t)^2} (\{d\}^{t+\Delta t} - 2\{d\}^t + \{d\}^{t-\Delta t})\end{aligned}\tag{26}$$

Considering the dynamic equilibrium equation at time t , the Eq. 25 can be introduced in the way:

$$[M]\{\ddot{d}\}^t + [C]\{\dot{d}\}^t + [K]\{d\}^t = \{F\}^t\tag{27}$$

Substituting Eq. 26 into Eq. 27 the governing central difference equation can be solved relative to $\{d\}^{t+\Delta t}$:

$$\left(\frac{1}{(\Delta t)^2}[M] + \frac{1}{2\Delta t}[C]\right)\{d\}^{t+\Delta t} = \{F\}^t - \left([K] - \frac{2}{(\Delta t)^2}[M]\right)\{d\}^t - \left(\frac{1}{(\Delta t)^2}[M] - \frac{1}{2\Delta t}[C]\right)\{d\}^{t-\Delta t}\tag{28}$$

On the first time step a starting procedure must be used to get $\{d\}^{-\Delta t}$. Assuming that $t = t_0 = 0$ and $\{d\}^0$ with $\{\dot{d}\}^t$ are known, accelerations $\{\ddot{d}\}^0$ can be obtained by Eq. 27. Then, the required vector $\{d\}^{-\Delta t}$ is evaluated from Eq. 26:

$$\{d\}^{-\Delta t} = \{d\}^0 - \Delta t\{\dot{d}\}^0 + \frac{(\Delta t)^2}{2}\{\ddot{d}\}^0\tag{29}$$

The important role for the accuracy and stability of the central difference method plays the choice of the time step value Δt , which must not exceed a special critical value: $\Delta t \leq \Delta t_{cr}$. This critical value can be assessed by $\Delta t_{cr} = \Delta L \sqrt{\frac{\rho}{E}}$, where ΔL is the lowest distance between the element nodes [45]. Such a requirement makes the central difference integration scheme only conditionally stable. In other words, the time step Δt must be very small, to get adequate results.

For example, assuming the lowest distance between nodes $\Delta L = 0.1$ m and material properties for steel with $\rho = 7850$ kg/m³ and $E = 2.058 \cdot 10^{11}$ MPa, the critical time step is $\Delta t_{cr} \approx 2 \cdot 10^{-5}$. This means that performing the transient FEA of a structure, subjected to the dynamic loading during two seconds, 10^5 steps have to be reviewed. That is why the central difference method is worth doing, when the governing Eq. 28 can be simplified – by neglecting of the matrix $[C]$ in case of no damping influence or by consideration of the diagonal mass matrix $[M]$ since the solution can be easily obtained without matrix factorization.

3.2.2 Implicit Time Integration Method

The Newmark's implicit time integration method is implemented and primary used in most FEM programs, as in contrast to the central difference scheme it is an unconditionally stable tool with the certain parameters. Term "implicit" means that the equation of motion is considered at time $t + \Delta t$:

$$[M]\{\ddot{d}\}^{t+\Delta t} + [C]\{\dot{d}\}^{t+\Delta t} + [K]\{d\}^{t+\Delta t} = \{F\}^{t+\Delta t} \quad (30)$$

Approximation relations for the Newmark's implicit time integration method are presented by [46]:

$$\{d\}^{t+\Delta t} = \{d\}^t + \{\dot{d}\}^t \Delta t + \left[\left(\frac{1}{2} - \alpha \right) \{\ddot{d}\}^t + \alpha \{\ddot{d}\}^{t+\Delta t} \right] (\Delta t)^2 \quad (31)$$

$$\{\dot{d}\}^{t+\Delta t} = \{\dot{d}\}^t + \left[(1 - \delta) \{\ddot{d}\}^t + \delta \{\ddot{d}\}^{t+\Delta t} \right] \Delta t \quad (32)$$

Parameters $\alpha = 1/4$ and $\delta = 1/2$ ensure an unconditional stability of the Newmark's time integration method, which represents in this case the constant-average-acceleration approximation scheme. Solving Eq. 31 with respect to $\{\ddot{d}\}^{t+\Delta t}$ and then substituting the obtained expression into the Eq. 32, the unknown velocities $\{\dot{d}\}^{t+\Delta t}$ and accelerations $\{\ddot{d}\}^{t+\Delta t}$ can be inserted to the equation of motion, Eq. 30 that yields:

$$\begin{aligned} \left(\frac{1}{\alpha(\Delta t)^2} [M] + \frac{\delta}{\alpha \Delta t} [C] + [K] \right) \{d\}^{t+\Delta t} = \{F\}^{t+\Delta t} + [M] \left[\frac{1}{\alpha(\Delta t)^2} \{d\}^t + \frac{1}{\alpha \Delta t} \{\dot{d}\}^t + \left(\frac{1}{2\alpha} - 1 \right) \{\ddot{d}\}^t \right] \\ + [C] \left[\frac{\delta}{\alpha \Delta t} \{d\}^t + \left(\frac{\delta}{\alpha} - 1 \right) \{\dot{d}\}^t + \frac{\Delta t}{2} \left(\frac{\delta}{\alpha} - 2 \right) \{\ddot{d}\}^t \right] \end{aligned} \quad (33)$$

As it was already mentioned, the Newmark's implicit time integration method is an unconditionally stable scheme with the parameters taken as $\alpha = 1/4$ and $\delta = 1/2$. This means that there is no restrictions in choosing the time step Δt . That would be an advantage in case of the dynamic loading, acting on the structure during a relative long period. Exemplary, let us consider such a period equal to 20 seconds: due to the explicit scheme with a required time step Δt not less then $2 \cdot 10^{-5}$ s one need to perform 10^6 calculation steps. Using the Newmark's implicit method one could accept the time step $\Delta t = 2 \cdot 10^{-2}$ s and calculate the same problem performing only 10^3 integration steps. Nevertheless, in case of the impact loads, acting in a short period of time, $2 \cdot 10^{-1}$ seconds exemplary, the Newmark's implicit method with time step $\Delta t = 2 \cdot 10^{-2}$ s would not be able to supply an accurate structural response within 10 steps. Considering a new time step $\Delta t = 2 \cdot 10^{-4}$ s for an implicit Newmark's scheme versus time step $\Delta t = 2 \cdot 10^{-5}$ s for an explicit central difference scheme one can benefit no more so much in computational time as in the case of long-lasting dynamic loading. Thereby the choice of one or another method depends on the problem formulation, but the Newmark's implicit time integration scheme seems to be more versatile.

3.3 Nonlinear Structural Analyses

As it was already mentioned in Chapter 2, due to the geometrical and/or material nonlinearities, the obtained deformations are no more a linear function of the applied loads, and therefore, the nonlinear structural analysis has to be performed.

Considering the operation conditions of the shipbuilding structures the presence of the tensile stresses, which would exceed the yield strength, often lead to the formation of the plastic zones. In this case, the deformations can be small but the danger of possible cracks generation appears. Analysing such a process the material nonlinearities must be taken into account. Studying the collapse behaviour or assessing the load-carrying capacity, we consider the structure in its critical state, just before it collapses, and in this case not only material nonlinearities are to be considered, but also the geometrical nonlinearities, as large deformation appears.

Performing the nonlinear structural analysis it is important to categorize the real physical problem since the different formulations are used for each analysis type. In Figure 14 the classification of the nonlinear analysis types is presented [48]:

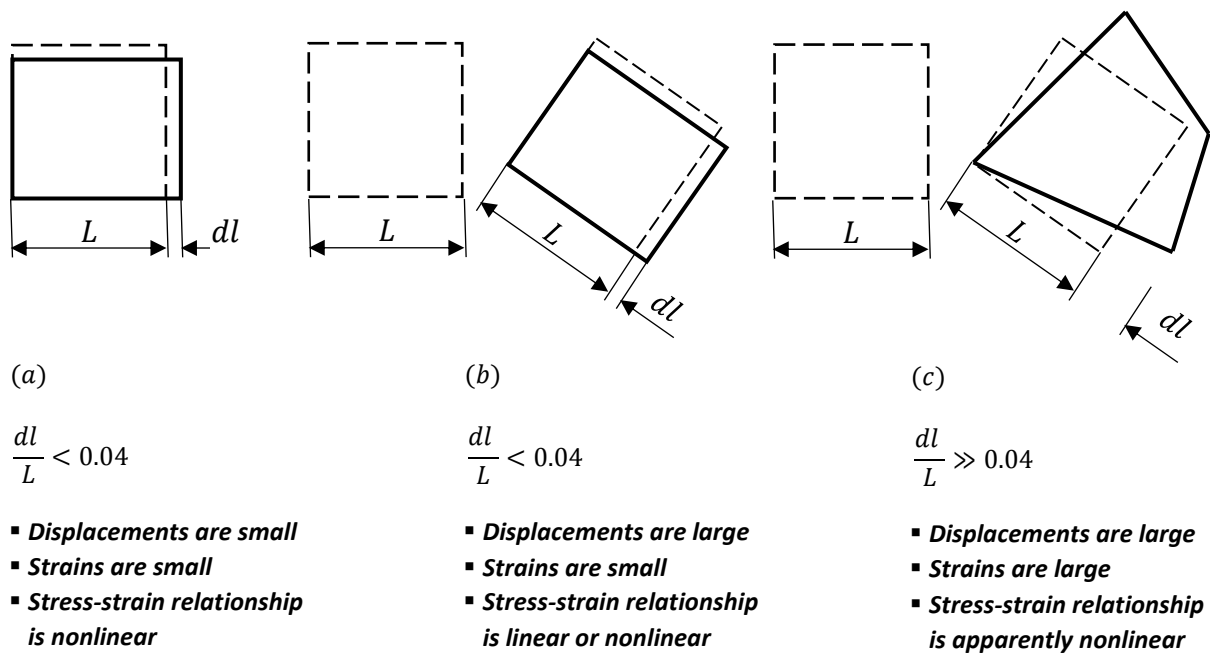


Figure 14: Classification of the nonlinear analysis types. a) Materially-nonlinear-only analysis; b), c) Geometrically-nonlinear analysis

Considering the materially-nonlinear-only analysis, the presence of the nonlinear effect can be described by the nonlinear stress-strain relation. The displacements and strains are infinitesimally small and therefore the usual engineering stress and strain measures can be employed in the equation of motion. The geometrically-nonlinear analysis is the most common case since the large displacement and the nonlinear stress-strain relationship most likely cause the appearance of the large strains.

3.3.1 Incremental Step-by-Step Solution Process

Within an incremental nonlinear analysis it is presumed that the externally applied forces or displacements represent the function of time and that the body configuration, subjected to the loading is changing. Simultaneously, the initial configuration at time t is known and one searches for a solution for the next configuration at time $t + \Delta t$, where Δt represents the chosen time increment. Thus, applying the principle of virtual work for the unknown state at time $t + \Delta t$ one can write an equilibrium equation for the vector of externally applied nodal point forces $\{F\}^{t+\Delta t}$ and for the vector of nodal point forces $\{R\}^{t+\Delta t}$, equivalent to the internal element stresses, [48]:

$$\{F\}^{t+\Delta t} - \{R\}^{t+\Delta t} = 0 \quad (34)$$

It is important to point out that in case of the static analysis, when the frequencies of applied forces are much smaller than the natural frequencies of the structure, time variable t only denotes the different state configurations due to the different load intensities. For the transient analysis with the frequencies of loads, lying in the range of the natural frequencies of the structure, time t is an actual physical variable and the force vector $\{F\}^{t+\Delta t}$ must include the inertia forces. Considering that the internal reactions $\{R\}^t$ at time t are known, the required reactions $\{R\}^{t+\Delta t}$ at time $t + \Delta t$ can be expressed by adding of the increment value of $\{\Delta R\}$ to the $\{R\}^t$:

$$\{R\}^{t+\Delta t} = \{R\}^t + \{\Delta R\} \quad (35)$$

Approximately, the incremental vector $\{\Delta R\}$ can be calculated multiplying the tangential stiffness matrix $[K]^t$, corresponding to the geometrical and material nonlinearities, with the increment of the nodal point displacements $\{\Delta d\}$:

$$\{\Delta R\} \cong [K]^t \{\Delta d\} \quad (36)$$

Substitution Eq. 35 into the Eq. 34 gives:

$$[K]^t \{\Delta d\} = \{F\}^{t+\Delta t} - \{R\}^t \quad (37)$$

Solving the above equation with respect to $\{\Delta d\}$ one can approximate the required displacements at time $t + \Delta t$:

$$\{d\}^{t+\Delta t} \cong \{d\}^t + \{\Delta d\} \quad (38)$$

Further, one can repeat the incremental procedure to get the exact displacements by using the Newton-Raphson approach [49] within corresponding iterations $i = 1, 2, 3 \dots n_{iter}$, assuming for the first iteration that $\{d\}^{t+\Delta t(0)} = \{d\}^t$ and $\{R\}^{t+\Delta t(0)} = \{R\}^t$:

$$\begin{aligned} [K]^t \{\Delta d\}^{(i)} &= \{F\}^{t+\Delta t} - \{R\}^{t+\Delta t(i-1)} \\ \{d\}^{t+\Delta t(i)} &= \{d\}^{t+\Delta t(i-1)} + \{\Delta d\}^{(i)} \end{aligned} \quad (39)$$

The updating of the nodal point displacements continues until the out-of-balance force vector $\{F\}^{t+\Delta t} - \{R\}^{t+\Delta t(i-1)}$ is small enough.

3.3.2 Incremental Equations of Motion

In nonlinear structural mechanics an effective analysis can be performed considering the Lagrangian formulation of the problem meaning that from the original to the final configuration of the body we follow all the particles and “record” the trajectory of motion. Using this formulation the equilibrium of the body in an incremental Lagrangian analysis at time $t + \Delta t$ can be expressed introducing the principle of virtual work in this way [50]:

$$\int [\tau]^{t+\Delta t} \{\delta \varepsilon\}^{t+\Delta t} dV^{t+\Delta t} = \int \{\delta d\}^T \{f^B\}^{t+\Delta t} dV^{t+\Delta t} \quad (40)$$

In the above given equation one can see:

- $[\tau]^{t+\Delta t}$ - Cauchy stress tensor* at time $t + \Delta t$;
- $\{\delta \varepsilon\}^{t+\Delta t}$ - Virtual strain vector at time $t + \Delta t$;
- $V^{t+\Delta t}$ - Volume at time $t + \Delta t$;
- $\{\delta d\}$ - Virtual displacement vector;
- $\{f^B\}^{t+\Delta t}$ - Externally applied force vector per unit volume at time $t + \Delta t$.

The main problem in the formulation of Eq. 40 is that the configuration of the body at time $t + \Delta t$ is unknown and therefore, one cannot integrate over the unknown volume. Apart from it, the Cauchy stresses at time $t + \Delta t$ cannot be calculated by adding to the Cauchy stresses at time t the stress increment, since the rigid body rotation of material influence on the stress-state.

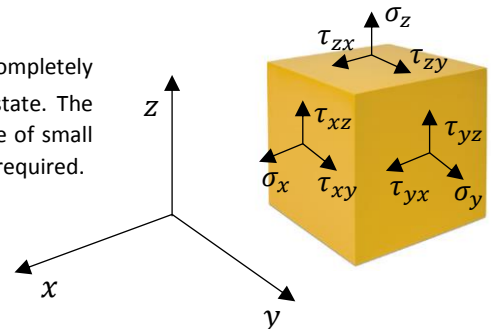
To deal with this problem special stress and strain measures have to be introduced. Such a principal measure of the deformation of the body can be given by the deformation gradient $[X]_0^t$, [51]:

$$[X]_0^t = \begin{bmatrix} \frac{\partial x_1^t}{\partial x_1^0} & \frac{\partial x_1^t}{\partial x_2^0} & \frac{\partial x_1^t}{\partial x_3^0} \\ \frac{\partial x_2^t}{\partial x_1^0} & \frac{\partial x_2^t}{\partial x_2^0} & \frac{\partial x_2^t}{\partial x_3^0} \\ \frac{\partial x_3^t}{\partial x_1^0} & \frac{\partial x_3^t}{\partial x_2^0} & \frac{\partial x_3^t}{\partial x_3^0} \end{bmatrix} \quad (41)$$

The deformation gradient $[X]_0^t$ describes the deformations and rotations that material have experienced from time 0 (coordinates x_1^0, x_2^0, x_3^0) to time t (coordinates x_1^t, x_2^t, x_3^t).

* Cauchy stress tensor $[\tau]$, [52], consist of the nine components τ_{ij} that completely define the stress-state at a point inside a material in the deformed state. The Cauchy stress tensor is used for linear analysis, presuming the presence of small deformations. For nonlinear analysis the Piola–Kirchhoff stress tensor is required.

$$[\tau] = \begin{bmatrix} \sigma_x & \tau_{xy} & \tau_{xz} \\ \tau_{yx} & \sigma_y & \tau_{yz} \\ \tau_{zx} & \tau_{zy} & \sigma_z \end{bmatrix}$$



Using the deformation gradient $[X]_0^t$ one can describe the Green-Lagrange strain tensor $[\varepsilon]_0^t$, which measures the stretching deformations, and the 2nd Piola–Kirchhoff stress tensor $[S]_0^t$, [48]:

$$\begin{aligned} [\varepsilon]_0^t &= \frac{1}{2} \left([X]_0^t{}^T [X]_0^t - [I] \right) \\ [S]_0^t &= \frac{\rho^0}{\rho^t} [X]_t^0 [\tau]^t [X]_t^0{}^T \end{aligned} \quad (42)$$

To obtain the incremental equation of motion one can now implement the Green-Lagrange strain tensor $[\varepsilon]_0^t$ and the 2nd Piola–Kirchhoff stress tensor $[S]_0^t$ to the Eq. 40 and refer them to the known equilibrium configuration. Here, one can choose between two common configurations, namely the initial configuration at time 0 (Total Lagrangian TL formulation) or the last calculated configuration at time t (Updated Lagrangian UL formulation), [48]:

$$\begin{aligned} \int [S]_0^{t+\Delta t} \{\delta \varepsilon\}_0^{t+\Delta t} dV^0 &= \int \{\delta d\}^T \{f^B\}_0^{t+\Delta t} dV^0 \quad (TL) \\ \int [S]_t^{t+\Delta t} \{\delta \varepsilon\}_t^{t+\Delta t} dV^t &= \int \{\delta d\}^T \{f^B\}_0^{t+\Delta t} dV^0 \quad (UL) \end{aligned} \quad (43)$$

The both TL and UL formulations for the equation of motion can be linearized by performing the incremental decompositions of stresses and strains*. Detailed description of the linearization procedure is given in [48]. These two formulations are almost similar and they supply the identical results with the only difference that the incremental linear strains in the TL formulation contain the initial displacement effect that makes the strain-displacement matrix more complicated compared with the UL formulation.

* Within the TL and UL formulation the Green-Lagrange strain tensor and the 2nd Piola–Kirchhoff stress tensor can be decomposed into the linear and nonlinear parts [48]:

<p>TL formulation:</p> $\begin{aligned} \varepsilon_{ij_0}^{t+\Delta t} &= \varepsilon_{ij_0}^t + \varepsilon_{ij_0} \\ S_{ij_0}^{t+\Delta t} &= S_{ij_0}^t + S_{ij_0} \end{aligned}$	<p>with:</p>	$\begin{aligned} \varepsilon_{ij_0} &= e_{ij_0} + \eta_{ij_0} \\ S_{ij_0} &= D_{ijrs_0} e_{rs_0} \end{aligned}$
<p>UL formulation:</p> $\begin{aligned} \varepsilon_{ij_t}^{t+\Delta t} &= \varepsilon_{ij_t} \\ S_{ij_t}^{t+\Delta t} &= S_{ij_t}^t + S_{ij_t} \end{aligned}$	<p>with:</p>	$\begin{aligned} \varepsilon_{ij_t} &= e_{ij_t} + \eta_{ij_t} \\ S_{ij_t} &= D_{ijrs_t} e_{rs_t} \end{aligned}$

Where D_{ijrs_0} and D_{ijrs_t} represent the incremental stress-strain tensors at time t referred to the configurations at times 0 and t respectively.

3.3.3 Incremental Matrix Equations for Finite Element Formulations

The approach for the formulation of the nonlinear matrix equations for the FEA is the same as for the linear analysis – the chosen displacement interpolations can be substituted directly to the governing equation of motion. Let us review the linearized equations of motion for different types of nonlinear analysis without surface and concentrated forces ($f^S = R_C^i = 0$) and rewrite them into a matrix form [48]:

Materially-nonlinear-only analysis

$$\begin{aligned} \int D_{ijrs} e_{rs} \delta e_{ij} dV &= \int \{\delta d\}^T \{f^B\}_0^{t+\Delta t} dV^0 - \int \sigma_{ij} \delta e_{ij} dV \\ \left(\int [B_L]^T [D] [B_L] dV \right) \{\Delta d\} &= \int [H]^T \{f^B\}_0^{t+\Delta t} dV^0 - \int [B_L]^T \{\Sigma\}^t dV \\ [K]^t \{\Delta d\} &= \{F\}^{t+\Delta t} - \{R\}^t \end{aligned} \quad (44)$$

Geometrically-nonlinear analysis. TL formulation

$$\begin{aligned} \int D_{ijrs_0} e_{rs_0} \delta e_{ij_0} dV^0 + \int S_{ij_0}^t \delta \eta_{ij_0} dV^0 &= \int \{\delta d\}^T \{f^B\}_0^{t+\Delta t} dV^0 - \int S_{ij_0}^t \delta e_{ij_0} dV^0 \\ \left(\int [B_L]_0^t [D]_0 [B_L]_0^t dV^0 \right) \{\Delta d\} + \left(\int [B_{LN}]_0^t [S]_0^t [B_{LN}]_0^t dV^0 \right) \{\Delta d\} &= \int [H]^T \{f^B\}_0^{t+\Delta t} dV^0 - \int [B_L]_0^t \{S\}_0^t dV^0 \\ \underbrace{\int [B_L]_0^t [D]_0 [B_L]_0^t dV^0}_{\text{Tangential stiffness matrix}} + \underbrace{\int [B_{LN}]_0^t [S]_0^t [B_{LN}]_0^t dV^0}_{[K_{NL}]_0^t} \{\Delta d\} &= \{F\}^{t+\Delta t} - \{R\}_0^t \end{aligned} \quad (45)$$

Geometrically-nonlinear analysis. UL formulation

$$\begin{aligned} \int D_{ijrs_t} e_{rs_t} \delta e_{ij_t} dV^t + \int S_{ij_t}^t \delta \eta_{ij_t} dV^t &= \int \{\delta d\}^T \{f^B\}_0^{t+\Delta t} dV^0 - \int S_{ij_t}^t \delta e_{ij_t} dV^t \\ \left(\int [B_L]_t^t [D]_t [B_L]_t^t dV^t \right) \{\Delta d\} + \left(\int [B_{LN}]_t^t [S]_t^t [B_{LN}]_t^t dV^t \right) \{\Delta d\} &= \int [H]^T \{f^B\}_0^{t+\Delta t} dV^0 - \int [B_L]_t^t \{S\}_t^t dV^t \\ \underbrace{\int [B_L]_t^t [D]_t [B_L]_t^t dV^t}_{\text{Tangential stiffness matrix}} + \underbrace{\int [B_{LN}]_t^t [S]_t^t [B_{LN}]_t^t dV^t}_{[K_{NL}]_0^t} \{\Delta d\} &= \{F\}^{t+\Delta t} - \{R\}_0^t \end{aligned} \quad (46)$$

- $[K]^t, [K_L]_0^t, [K_L]_t^t$ - Linear strain incremental stiffness matrices;
- $[K_{NL}]_0^t, [K_{NL}]_t^t$ - Nonlinear strain incremental stiffness matrices;
- $\{\Delta d\}$ - Unknown displacement vector;
- $\{F\}^{t+\Delta t}$ - Vector of externally applied forces at time $t + \Delta t$;
- $\{R\}^t, \{R\}_0^t, \{R\}_t^t$ - Vectors of nodal point forces equivalent to the element stresses at time t ;
- $[B_L], [B_L]_0^t, [B_L]_t^t$ - Linear strain-displacement transformation matrices;
- $[B_{LN}]_0^t, [B_{LN}]_t^t$ - Nonlinear strain-displacement transformation matrices;
- $[D], [D]_0, [D]_t$ - Stress-strain material matrices;
- $[H]$ - Displacement interpolation matrix;
- $\{\Sigma\}$ - Stress vector, containing components of σ_{ij}^t ;
- $[S]_0^t, [S]_t^t, \{S\}_0^t, \{S\}_t^t$ - Matrices and vectors of second Piola-Kirchhoff stresses.

3.4 Direct Time Integration Methods for Nonlinear Structural Analyses

To perform the transient nonlinear structural analysis the direct explicit and implicit time integration schemes are used. These procedures can be realized in the same way, as it was discussed for the transient linear analysis application, but using as a basis nonlinear incremental equation of motion obtained in the previous subchapter. Although the required equation was derived for the static analysis, one can just add the inertia (and damping) forces to the acting body forces according to d'Alembert's principle, see Eq.24.

3.4.1 Explicit Time Integration Method for Nonlinear Structural Analyses

The explicit central difference scheme is successfully used for the transient nonlinear structural analysis. Analogously to the linear analysis we consider the equilibrium equation at time t to get the structural response at time $t + \Delta t$, [48]:

$$[M]\{\ddot{d}\}^t + [C]\{\dot{d}\}^t = \{F\}^t - \{R\}^t \quad (47)$$

Substitution of the approximations for velocities $\{\dot{d}\}^t$ and accelerations $\{\ddot{d}\}^t$ (see Eq. 26) to the above given equation yields:

$$\left(\frac{1}{(\Delta t)^2}[M] + \frac{1}{2\Delta t}[C]\right)\{d\}^{t+\Delta t} = \{F\}^t - \{R\}^t + \frac{2}{(\Delta t)^2}[M]\{d\}^t - \left(\frac{1}{(\Delta t)^2}[M] - \frac{1}{2\Delta t}[C]\right)\{d\}^{t-\Delta t} \quad (48)$$

As one can see, the obtained formula is very similar to the one, derived for the linear analysis. Nevertheless, the nodal point force vector $\{R\}^t$ includes the nonlinear effects due to the second Piola-Kirchhoff stresses and must be evaluated using the Eqns. 44 -46. The advantages and disadvantages of the central difference scheme discussed within the linear analysis also remain valid for the nonlinear analysis.

3.4.2 Implicit Time Integration Method for Nonlinear Structural Analyses

The Newmark's method with integration parameters $\alpha = 1/4$ and $\delta = 1/2$ represents a very effective tool for the performance of the nonlinear dynamic analysis, [48]. Being an implicit scheme, the equilibrium is considered at time $t + \Delta t$. Therefore, dealing with the nonlinear analysis it is necessary to fulfill the iteration procedure, exemplary Newton-Raphson method, see Eq. 39, to reach the equilibrium state minimizing the out-of-balance vector:

$$\begin{aligned} [M]\{\ddot{d}\}^{t+\Delta t(i)} + [C]\{\dot{d}\}^{t+\Delta t(i)} + [K]^{t+\Delta t(i-1)}\{\Delta d\}^{t(i)} &= \{F\}^{t+\Delta t} - \{R\}^{t+\Delta t(i-1)} \\ \{d\}^{t+\Delta t(i)} &= \{d\}^{t+\Delta t(i-1)} + \{\Delta d\}^{t(i)} \end{aligned} \quad (49)$$

Approximations for the displacements and velocities can be obtained using the trapezoidal rule:

$$\{d\}^{t+\Delta t} = \{d\}^t + \frac{\Delta t}{2}(\{\dot{d}\}^t + \{\dot{d}\}^{t+\Delta t}) \quad (50)$$

$$\{\dot{d}\}^{t+\Delta t} = \{\dot{d}\}^t + \frac{\Delta t}{2}(\{\ddot{d}\}^t + \{\ddot{d}\}^{t+\Delta t}) \quad (51)$$

Solving Eq. 50 with respect to $\{\dot{d}\}^{t+\Delta t}$ and then substituting the obtained expression into Eq. 51, the unknown velocities $\{\dot{d}\}^{t+\Delta t}$ and accelerations $\{\ddot{d}\}^{t+\Delta t}$ can be expressed by:

$$\begin{aligned}\{\dot{d}\}^{t+\Delta t} &= \frac{2}{\Delta t}(\{d\}^{t+\Delta t} - \{d\}^t) - \{\dot{d}\}^t \\ \{\ddot{d}\}^{t+\Delta t} &= \frac{4}{(\Delta t)^2}(\{d\}^{t+\Delta t} - \{d\}^t) - \frac{4}{\Delta t}\{\dot{d}\}^t - \{\ddot{d}\}^t\end{aligned}\quad (52)$$

In the incremental form, Eq. 52 can be written as:

$$\begin{aligned}\{\dot{d}\}^{t+\Delta t(i)} &= \frac{2}{\Delta t}(\{d\}^{t+\Delta t(i-1)} + \{\Delta d\}^{(i)} - \{d\}^t) - \{\dot{d}\}^t \\ \{\ddot{d}\}^{t+\Delta t(i)} &= \frac{4}{(\Delta t)^2}(\{d\}^{t+\Delta t(i-1)} + \{\Delta d\}^{(i)} - \{d\}^t) - \frac{4}{\Delta t}\{\dot{d}\}^t - \{\ddot{d}\}^t\end{aligned}\quad (53)$$

Using the obtained incremental approximations, the nonlinear equilibrium equation yields, [48]:

$$\begin{aligned}\left(\frac{4}{(\Delta t)^2}[M] + \frac{2}{\Delta t}[C] + [K]^{t+\Delta t(i-1)}\right)\{\Delta d\}^{(i)} &= \{F\}^{t+\Delta t} - \{R\}^{t+\Delta t(i-1)} \\ &\quad - [M]\left(\frac{4}{(\Delta t)^2}(\{d\}^{t+\Delta t(i-1)} - \{d\}^t) - \frac{4}{\Delta t}\{\dot{d}\}^t - \{\ddot{d}\}^t\right) \\ &\quad - [C]\left(\frac{2}{\Delta t}(\{d\}^{t+\Delta t(i-1)} - \{d\}^t) - \{\dot{d}\}^t\right)\end{aligned}\quad (54)$$

The tangential stiffness matrix $[K]^t$ and the nodal point force vector $\{R\}^{t+\Delta t}$ contain the nonlinear effects and can be obtained using Eqns. 44 - 46.

As it was already mentioned, the iteration procedure with $i = 1, 2, 3 \dots n_{iter}$ repeats until the out-of-balance vector becomes small enough. For this aim, the convergence check should be performed after each iteration, and if the chosen convergence criterion is satisfied, one can proceed to the next step. As a possible convergence criterion, the out-of-balance convergence [53] can be introduced:

$$\left\| \{F\}^{t+\Delta t} - \{R\}^{t+\Delta t(i-1)} - [M]\{\ddot{d}\}^{t+\Delta t(i-1)} - [C]\{\dot{d}\}^{t+\Delta t(i-1)} \right\|_2 \leq \gamma \|\{F\}^{t+\Delta t}\| \quad (55)$$

In the above given equation $\{F\}^{t+\Delta t} - \{R\}^{t+\Delta t(i-1)} - [M]\{\ddot{d}\}^{t+\Delta t(i-1)} - [C]\{\dot{d}\}^{t+\Delta t(i-1)}$ represents the out-of-balance (residual) vector.

The tolerance is represented by γ and $\|\{F\}^{t+\Delta t}\|$ is the reference force value.

3.5 Concluding Remarks

In Chapter *Fundamentals of the Transient Analysis* the following subjects were highlighted and discussed:

- Derivation of the linear dynamic equilibrium equation: using the principle of virtual work the static equilibrium state is described in matrix form for the finite element application, [45]. The required kinematic parameters such as displacements and strains are presented in dependence on the nodal displacement values, using special shape functions. The extension on the dynamic analysis is introduced by application of d'Alembert's principle, [44].
- Numerical integration methods for the solution of the linear dynamic differential equation of 2nd order: the direct explicit central difference method and direct implicit Newmark's method are presented as the most common techniques, [46]. Approximation relationships and a comprehensive description are given that enable the direct implementation of these methods into ISUM program code. The discussed advantages and disadvantages of both schemes, connected with important characteristics such as stability of the method or time step definition, give a helpful starting point performing dynamic structural analyses.
- Special features of nonlinear structural analysis: the classification of nonlinearities is performed taking into account varying body configurations with corresponding nonlinear stress-strain relationships, large displacement and large strain values, [47]. Derivation of the nonlinear dynamic equilibrium equation is presented by use of the principle of virtual work, which is related to the body configuration varying in time, [50]. This assumption does not allow Cauchy stresses and variations in small strains to be used as it was done within the linear analysis, since these quantities now refer to the unknown configurations. The deformation gradient is introduced to solve this problem and to move from the linear parameters to the 2nd Piola-Kirchhoff stress tensor and Green-Lagrange strain tensor, [48]. The corresponding nonlinear dynamic incremental equilibrium equations are presented according to the type of nonlinear analysis and the body configuration – initial configuration (total Lagrangian formulation) or previously calculated configuration (updated Lagrangian formulation), [48].
- Numerical integration methods for the solution of the nonlinear dynamic differential equation of 2nd order, [48]: the direct explicit central difference method and direct implicit Newmark's method can be successfully extended on the nonlinear analysis with some considerations. Using the central difference method an incremental solution procedure is not required. This means that it totally repeats the corresponding integration scheme used for the linear analysis, taking into account the nonlinear effects that appear in the formulation of the finite element matrices. The implicit Newmark's integration method additionally requires for the nonlinear analysis an iterative approach to fulfill the equilibrium state within each time step. Newton-Raphson technique with the out-of-balance convergence check enables minimization of the residual force vector with prescribed tolerance, [49], [53].

4 Application of Direct Time Integration Methods using Force Control

Having defined in the previous chapter the basic principles of the transient Finite Element Analysis, we get closer to the subject of the present thesis and shall focus on the implementation of the inertia and damping effects to the Idealized Structural Unit Method. But as one could see in Chapter 2, being a kind of Finite Element Method, the Idealized Structural Unit Method has its' specific features concerning the element sizing: treatment of the internal deflection [18]. That is why one should start from simple examples first performing the transient analysis of systems without considering the nonlinearities and damping effects. The present chapter is devoted to verify the direct explicit and implicit time integration methods on a couple of simple examples.

4.1 Dynamic Analysis of a Spring-Mass System

Let us consider the simple spring-mass system with a mass $m = 1$ kg, spring stiffness $k = 1000$ N/m, Figure 15. The applied dynamic force $F(t)$ increases linearly in time interval $0 \leq t \leq t_1$ from zero value to $F_{max} = 10$ N and then stays constant. The purpose of the analysis is to get the structural dynamic response in terms of displacements using the explicit and implicit time integration schemes.

For the both schemes the initial conditions are set to: $d^0 = \dot{d}^0 = \ddot{d}^0 = 0$. The time step is considered to be $\Delta t = 1 \cdot 10^{-2}$ s. The Newmark's integration parameters are $\alpha = 1/4$ and $\delta = 1/2$. The loading is provided by force control – the dynamic force $F(t)$ is substituted into Eqns. 28 and 33 directly, according to the prescribed loading path and varying within time. In the present analysis, four test cases describe different loading paths:

Test 1: $t_1 = 0.01$ s; Test 2: $t_1 = 0.25$ s;

Test 3: $t_1 = 1.00$ s; Test 4: $t_1 = 10.00$ s;

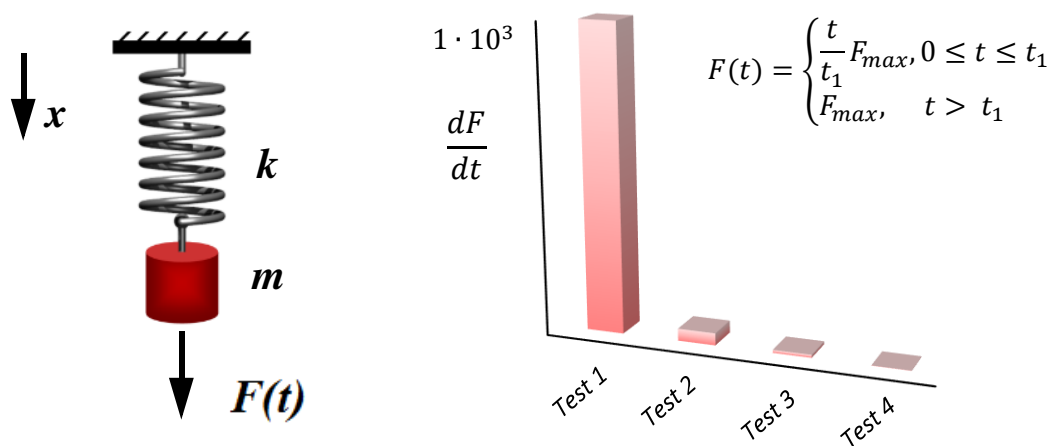


Figure 15: Spring-mass system subjected to dynamic force $F(t)$

For the given system with one degree of freedom, the dynamic equilibrium equation in explicit form, Eq. 28, reduces to:

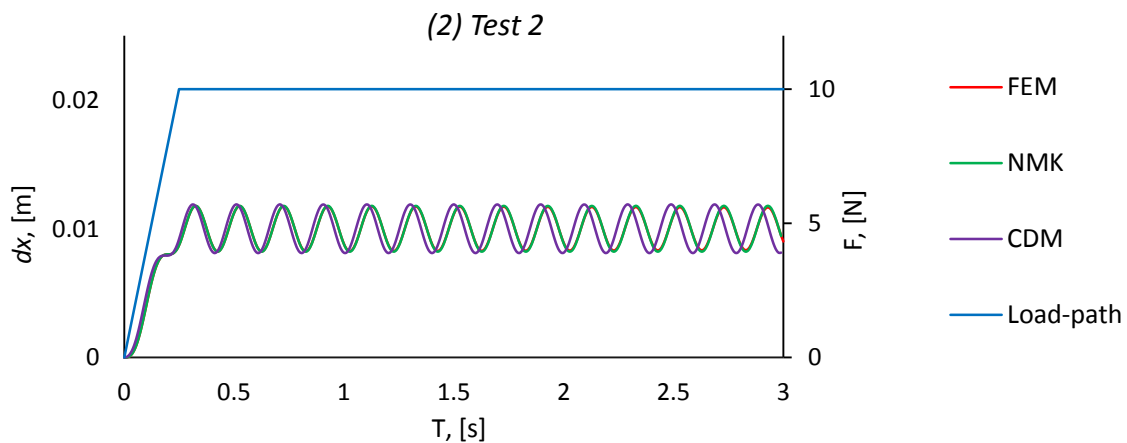
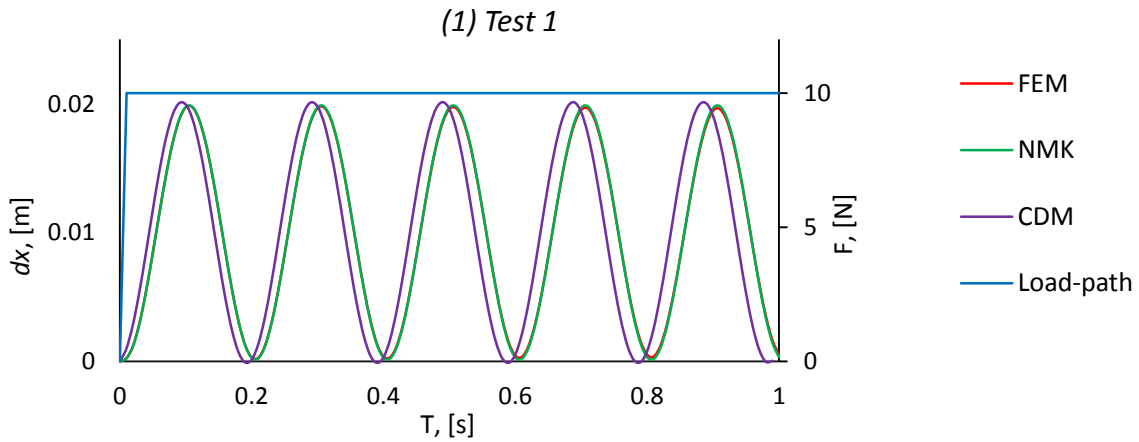
$$\frac{1}{(\Delta t)^2} m d^{t+\Delta t} = F^t - \left(k - \frac{2}{(\Delta t)^2} m \right) d^t - \left(\frac{1}{(\Delta t)^2} m \right) d^{t-\Delta t} \quad (56)$$

The dynamic equilibrium equation in implicit form, Eq. 33, yields:

$$\left(\frac{1}{\alpha(\Delta t)^2} m + k \right) d^{t+\Delta t} = F^{t+\Delta t} + m \left(\frac{1}{\alpha(\Delta t)^2} d^t + \frac{1}{\alpha \Delta t} \dot{d}^t + \left(\frac{1}{2\alpha} - 1 \right) \ddot{d}^t \right) \quad (57)$$

To assess the structural response of the system, here, and on the following examples presented in this thesis, the results obtained with the Newmark's (NMK) and central difference (CDM) methods are compared with the results from the Finite Element Analysis (FEM), performed using the program complex "ANSYS 15.0". The following element types are used within the "ANSYS analysis" for the prescribed task:

- 2-D longitudinal spring-damper of unit length COMBIN14;
- 2-D structural mass without rotary inertia MASS21.



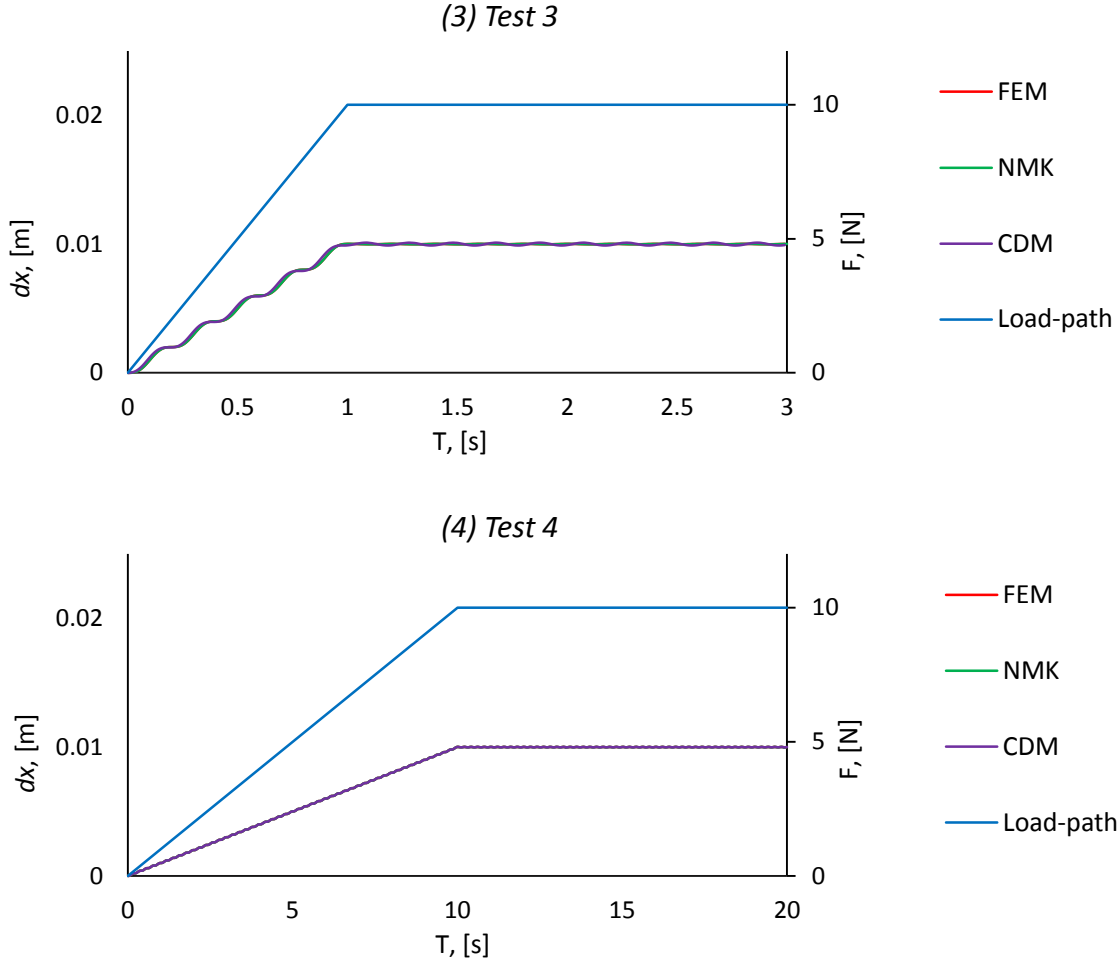


Figure 16 (1)-(4): Structural response of the spring-mass system

The first conclusion which can be made analyzing the presented results, Figure 16 (1)-(4), is that the considered numerical integration schemes supply reliable results: the curve obtained with the Newmark's (NMK) method completely coincides with the curve depicting the results of the Finite Element Analysis (FEM). The curve, which corresponds to the central difference method (CDM), slightly delays the (NMK) and (FEM) solutions, within the first and second test cases. This can be explained by the fact that exactly the Newmark's scheme is used as a time integration tool within the program complex "ANSYS 15.0". On the other hand, analyzing the test cases three and four one can note that the (CDM) solution coincides with the two other curves. This happens since the inertia effects decrease and therefore, the problem turns from the dynamic formulation to the quasi-static one. Indeed, on this simple example one can clearly observe the influence of the inertia: the same system with the same properties, subjected to the dynamic force with the same maximum value shows completely different behavior, according to the way how the load was applied. In the first test case the load reaches its' maximum value very rapidly, within only one time step. This causes the significant undamped oscillations. In the second test case, the amplitude of the oscillations becomes smaller, since the dynamic load grows up within twenty-five time steps. In the third test case we can distinguish just small oscillations, which disappear in the fourth test case completely. Here the frequency of the applied load is much smaller than the natural frequency of the system: $1/t_1 \ll 2\pi\sqrt{k/m}$ that enables considering the static formulation of the problem and the displacements are linearly proportional to the applied load: $kd = F$.

4.2 Dynamic Analysis of a 4-Node Membrane Element

As a second example let us examine the dynamic structural response of a 4-Node membrane, which can be considered as a prototype of ISUM element without internal deflection, Figure 17. Constraints are applied where the edges between nodes 1-2 and 1-3 can move in x and y direction and the other two edges are fixed. Dimensions and material properties are given in Table 4.

Analogously to the previous example the dynamic force $F(t)$, applied on the nodes 1 and 2, increases linearly in time interval $0 \leq t \leq t_1$ from zero value to $F_{max} = 1 \cdot 10^5$ N and then stays constant. Four different test cases are presumed for this analysis:

Test 1: $t_1 = 0.0001$ s; Test 2: $t_1 = 0.0025$ s;

Test 3: $t_1 = 0.0075$ s; Test 4: $t_1 = 0.03$ s;

Table 4: Dimensions and material properties of the 4-node membrane element

Length, breadth	a, b	1000	mm
Thickness	t	15.5	mm
Yield strength	σ_Y	313.6	MPa
Young's modulus	E	205.8	MPa
Density	ρ	7850	kg/m ³
Poisson's ratio	ν	0.3	-

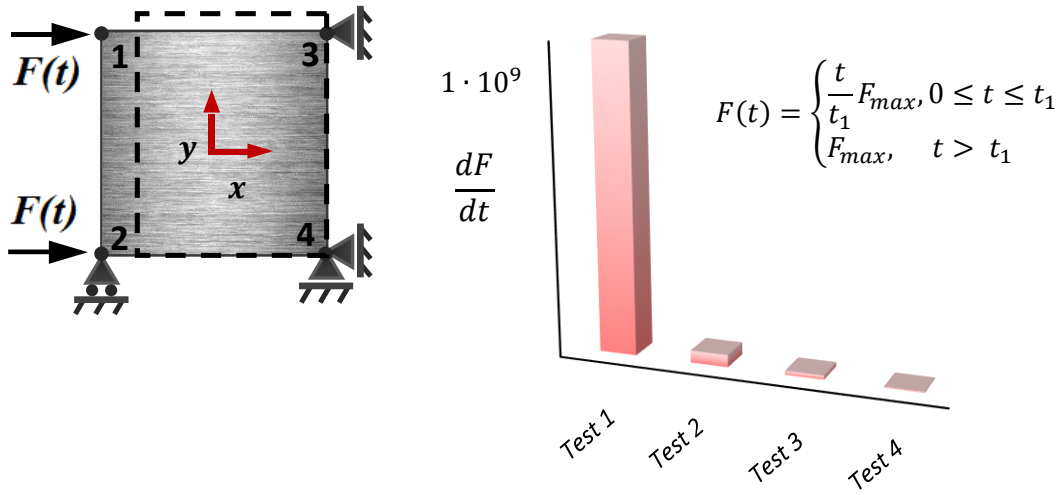


Figure 17: Set-up for numerical test as a 4-Node membrane element [54]

Within the FEA performed with the program complex “ANSYS 15.0” one 4-node structural shell element SHELL181 is used to model the membrane. Material and geometrical properties of the element are specified according to the Table 4. Bending stiffness of the shell element is not considered by activating the option KEYOPT (1) = 1, [55]

To define the stiffness $[K]$ and mass $[M]$ matrices for the 2-dimensional structural analysis of the 4-node membrane element, one should determine the integrands $[H]$, $[B]$ and $[D]$ and perform the integration over the element's area A :

$$\begin{aligned} [K] &= \int [B^T][D][B]dA \\ [M] &= \int \rho[H^T][H]dA \end{aligned} \quad (58)$$

For two-dimensional elements, we can assume that the local element displacements u and v are represented by polynomials in the local coordinate variables x and y with the unknown coefficients $\alpha_1, \alpha_2 \dots \beta_4$, which are called the generalized coordinates [48]:

$$\begin{aligned} u(x, y) &= \alpha_1 + \alpha_2 x + \alpha_3 y + \alpha_4 xy \\ v(x, y) &= \beta_1 + \beta_2 x + \beta_3 y + \beta_4 xy \end{aligned} \quad (59)$$

In matrix form one can rewrite Eq. 59 as:

$$\begin{Bmatrix} u(x, y) \\ v(x, y) \end{Bmatrix} = [\Phi]\{a\}$$

where

$$[\Phi] = \begin{bmatrix} 1 & x & y & xy & 0 & 0 & 0 & 0 \\ 0 & 0 & 0 & 0 & 1 & x & y & xy \end{bmatrix} \quad (60)$$

$$\{a\}^T = \{\alpha_1 \quad \alpha_2 \quad \alpha_3 \quad \alpha_4 \quad \beta_1 \quad \beta_2 \quad \beta_3 \quad \beta_4\}$$

Therefore, the nodal point displacements can be described as:

$$\{\hat{d}\} = [A]\{a\} \quad (61)$$

where the matrix $[A]$ contains the local coordinates x_i and y_i of the point i . Thus, for the examined membrane with the local coordinate system, placed in the area center of gravity, matrix $[A]$ looks like:

$$[A] = \begin{bmatrix} [\hat{A}] & [0] \\ [0] & [\hat{A}] \end{bmatrix} \quad [\hat{A}] = \begin{bmatrix} 1 & x_1 & y_1 & x_1 y_1 \\ 1 & x_2 & y_2 & x_2 y_2 \\ 1 & x_3 & y_3 & x_3 y_3 \\ 1 & x_4 & y_4 & x_4 y_4 \end{bmatrix} \quad [\hat{A}] = \begin{bmatrix} 1 & -\frac{a}{2} & \frac{b}{2} & -\frac{ab}{4} \\ 1 & -\frac{a}{2} & -\frac{b}{2} & \frac{ab}{4} \\ \frac{a}{2} & \frac{b}{2} & \frac{ab}{4} & 1 \\ 1 & \frac{a}{2} & -\frac{b}{2} & -\frac{ab}{4} \end{bmatrix} \quad (62)$$

Solving from Eq. 61 for $\{a\}$ and substituting into Eq. 60, one obtains the interpolation matrix $[H]$:

$$\begin{Bmatrix} u(x,y) \\ v(x,y) \end{Bmatrix} = \underbrace{[\Phi][A]^{-1}}_{\substack{\text{Displacement} \\ \text{interpolation matrix } [H]}} \{\hat{d}\} \quad (63)$$

For plane stress conditions the strains can be calculated as $\{\varepsilon\}^T = \left\{ \frac{\partial u(x,y)}{\partial x} \quad \frac{\partial v(x,y)}{\partial y} \quad \frac{\partial u(x,y)}{\partial y} + \frac{\partial v(x,y)}{\partial x} \right\}$, therefore, the strain-displacement matrix $[B]$ is to be obtained by taking the partial derivatives of the displacement interpolation matrix $[H]$.

According to the isotropic linear elastic material behavior, the material matrix $[D]$ can be defined as:

$$[D] = \frac{E}{1-\nu^2} \begin{bmatrix} 1 & \nu & 0 \\ \nu & 1 & 0 \\ 0 & 0 & \frac{1-\nu}{2} \end{bmatrix} \quad (64)$$

Having established the integrands $[H]$, $[B]$ and $[D]$, the stiffness $[K]$ and mass $[M]$ matrices are to be defined as:

$$[K] = \int_{-\frac{b}{2}}^{\frac{b}{2}} \int_{-\frac{a}{2}}^{\frac{a}{2}} t[B]^T [D] [B] \, dx dy; \quad [M] = \int_{-\frac{b}{2}}^{\frac{b}{2}} \int_{-\frac{a}{2}}^{\frac{a}{2}} \rho t [H]^T [H] \, dx dy \quad (65)$$

The integration was performed using the program complex "Mathcad 14". The obtained matrices $[K]$ and $[M]$ have dimension 8×8 . Reducing the matrices to the nodal degrees of freedom, we obtain:

$$[K] = \begin{bmatrix} 1.527 \cdot 10^9 & -5.512 \cdot 10^8 & 1.696 \cdot 10^8 & 4.24 \cdot 10^7 \\ -5.512 \cdot 10^8 & 1.527 \cdot 10^9 & 4.24 \cdot 10^7 & 1.696 \cdot 10^8 \\ 1.696 \cdot 10^8 & 4.24 \cdot 10^7 & 1.527 \cdot 10^9 & -5.512 \cdot 10^8 \\ 4.24 \cdot 10^7 & 1.696 \cdot 10^8 & -5.512 \cdot 10^8 & 1.527 \cdot 10^9 \end{bmatrix} \quad [M] = \begin{bmatrix} 13.083 & 0 & 6.542 & 0 \\ 0 & 13.083 & 0 & 6.542 \\ 6.542 & 0 & 13.083 & 0 \\ 0 & 6.542 & 0 & 13.083 \end{bmatrix}$$

Proceeding to the implicit and explicit integration procedures, we set for both methods the zero initial conditions: $d^0 = \dot{d}^0 = \ddot{d}^0 = 0$ and assume the time step $\Delta t = 1 \cdot 10^{-5} s$ according to the recommendation given in [45]: $\Delta t \leq \Delta L \sqrt{\frac{\rho}{E}}$. For the implicit integration scheme Newmark's integration parameters are $\alpha = 1/4$ and $\delta = 1/2$. The influence of damping is not considered.

For the examined membrane with four degrees of freedom, the dynamic equilibrium equation in explicit form, Eq. 28, yields:

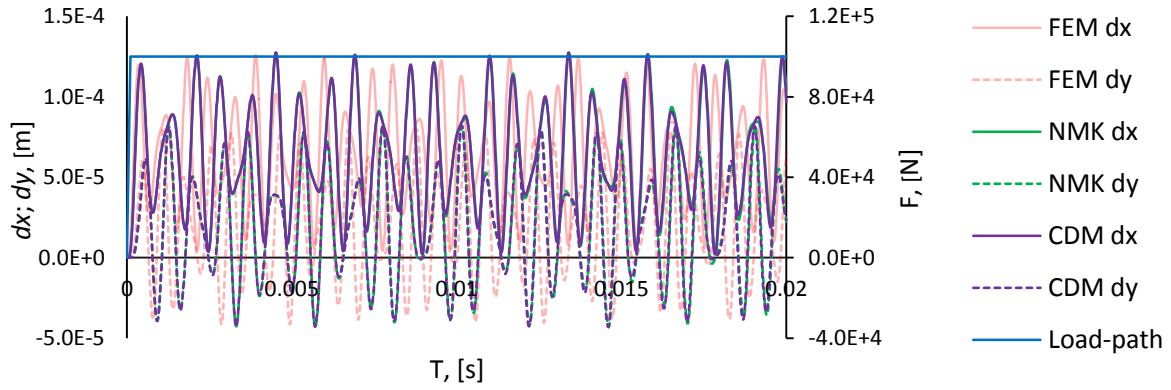
$$\frac{1}{(\Delta t)^2} [M] \{d\}^{t+\Delta t} = \{F\}^t - \left([K] - \frac{2}{(\Delta t)^2} [M] \right) \{d\}^t - \frac{1}{(\Delta t)^2} [M] \{d\}^{t-\Delta t} \quad (66)$$

The dynamic equilibrium equation in implicit form, Eq. 33, yields:

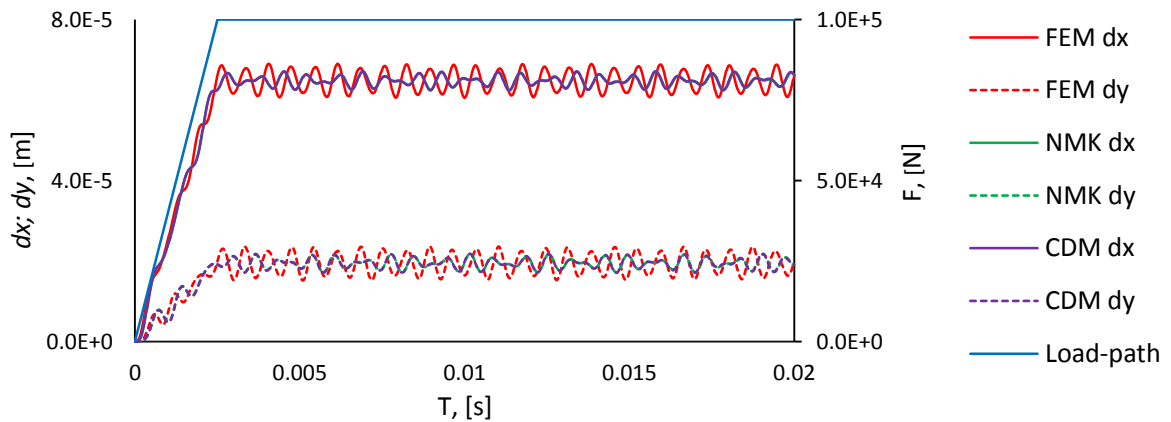
$$\left(\frac{1}{\alpha(\Delta t)^2} [M] + [K]\right) \{d\}^{t+\Delta t} = \{F\}^{t+\Delta t} + [M] \left[\frac{1}{\alpha(\Delta t)^2} \{d\}^t + \frac{1}{\alpha \Delta t} \{\dot{d}\}^t + \left(\frac{1}{2\alpha} - 1\right) \{\ddot{d}\}^t \right] \quad (67)$$

Note that the searched vector $\{d\}$ contains four displacements: two displacements in x -direction for nodes 1 and 2 and two displacements in y -direction for nodes 1 and 3. Taking into account that the external dynamical loading applied on node 1 is equal to the external dynamical loading applied on node 2, the displacements of these nodes are the same in x -direction. Analogously, the displacements of nodes 1 and 3 are the same in y -direction. Therefore, on the diagrams below the displacements in x -direction (dx) and the displacements in y -direction (dy) are displayed only for node 1.

(1) Test 1



(2) Test 2



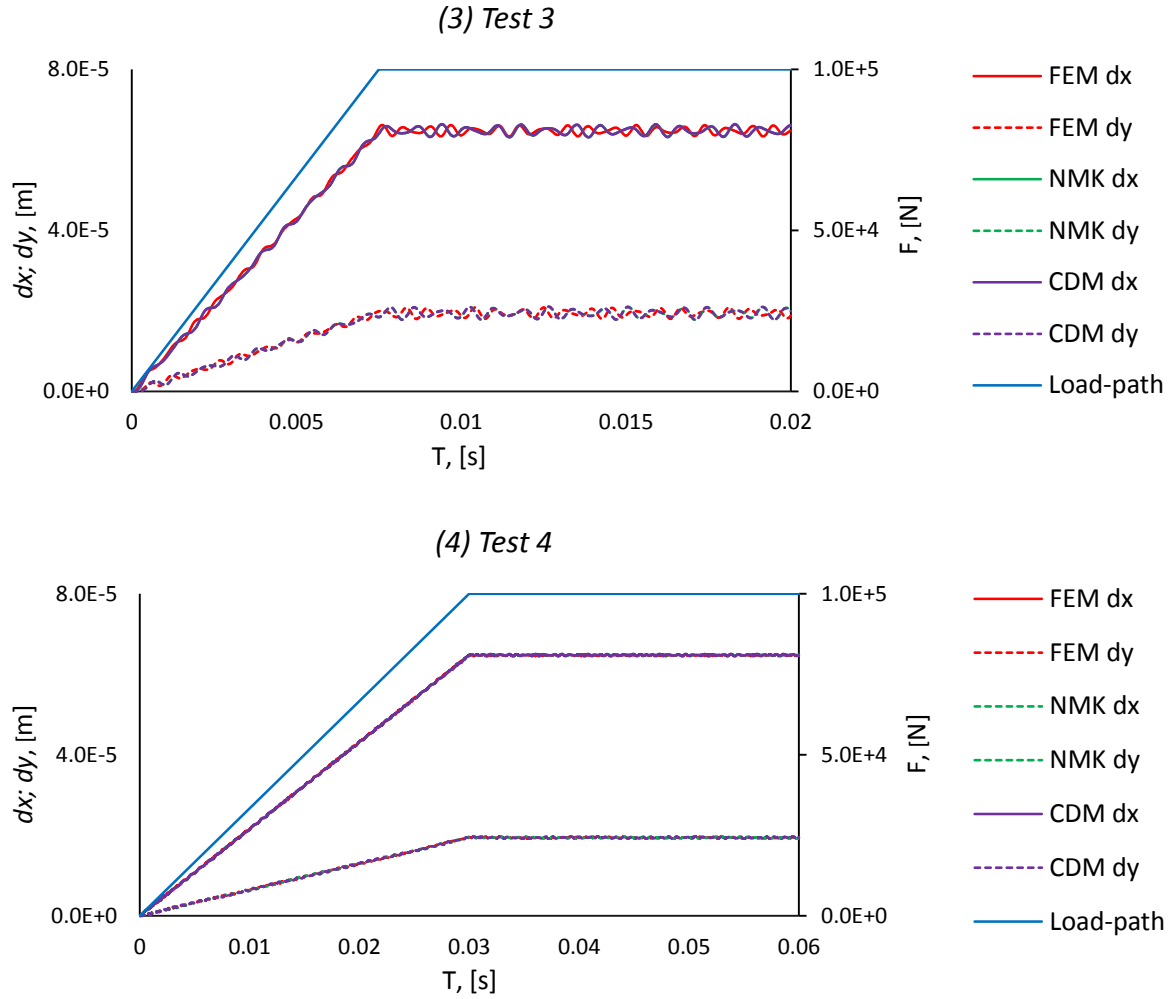


Figure 18 (1)-(4): Structural response of the 4-node membrane

Analogously to the spring-mass system, one can observe large oscillations of the solution for the first test case. The displacements in x -direction (dx) and the displacements in y -direction (dy) take also negative values and the amplitudes of the oscillations are high. This happens due to the significant influence of the inertia effects, since the frequency of the externally applied dynamic force is much bigger than the natural frequencies of the structure. Indeed, the externally applied force reaches its' maximum value within a very short period of time (10 time steps).

Examining the other test cases one can notice that the inertia effects decrease and the corresponding curves tend to oscillate closer and closer to the static solution. In the fourth test case, we cannot observe any swaying of the curves that means that the inertia forces can be neglected and the task can be considered as the static problem. As for the reliability of the explicit and implicit time integration schemes, one can see that they supply adequate results.

The curves obtained with the central difference (CDM) and Newmark's (NMK) methods coincide with each other and show good agreement with the FEM solutions. In the first two test cases, demonstrating especially strong inertia effects, one can notice the similar characteristics but also a difference in results, provided by the central difference (CDM) or Newmark's (NMK) method and the FEM. A reason is that within the "ANSYS 15.0" there is an isoparametric finite element formulation, [55], which is different to the one used for CDM and NMK.

4.3 Dynamic Analysis of a 4-Node ISUM Element. Formulation of consistent mass matrix

Having obtained the reliable results of the linear dynamical structural analysis of the spring-mass system and four-node membrane using the explicit and implicit integration methods, one can proceed to the nonlinear structural analysis of ISUM plate element and introduce the mass matrix formulation.

Within ISUM element formulation, the internal deflection is considered for a one ISUM element set-up, as shown in Figure 19. Again, constraints are given in such a way that the edges between the nodes 1-2 and 1-3 can move as straight lines in x and y direction and the other two edges are fixed. The difference compared to the previous membrane test is that ISUM element possesses the additional degree of freedom A_l , which multiplied with the shape function $f_l(x, y)$, Eq. 5, gives the distribution of the lateral deflection w_l within the element [18]:

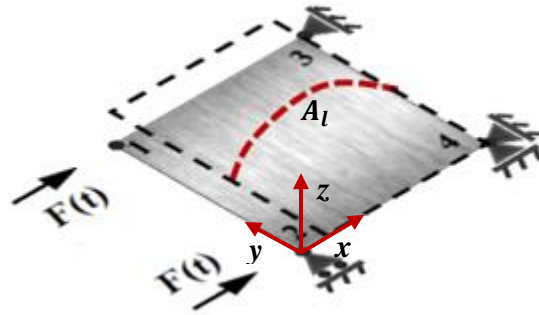


Figure 19: Set-up for numerical test as a 4-node ISUM element, [54]

The dynamic force $F(t)$ is applied on the nodes 1 and 2 within one time interval $0 \leq t \leq t_1$, linearly increasing from the zero value to the maximum value F_{max} . This maximum value F_{max} is defined according to the dynamic collapse analysis of the square plate, performed with “ANSYS 15.0” and corresponds to the ultimate force, Figure 20. Thus, one obtains for four test cases with different edge velocities V the maximum values of externally applied load F_{max} .

For the nonlinear FEA a discretization scheme of 50×50 shell elements SHELL181 is used. Geometrical and material properties of the finite element model are given in Table 1. Initial lateral deflection with a magnitude of 10% of the thickness value is applied to simulate the buckling state. Influence of damping is not considered.

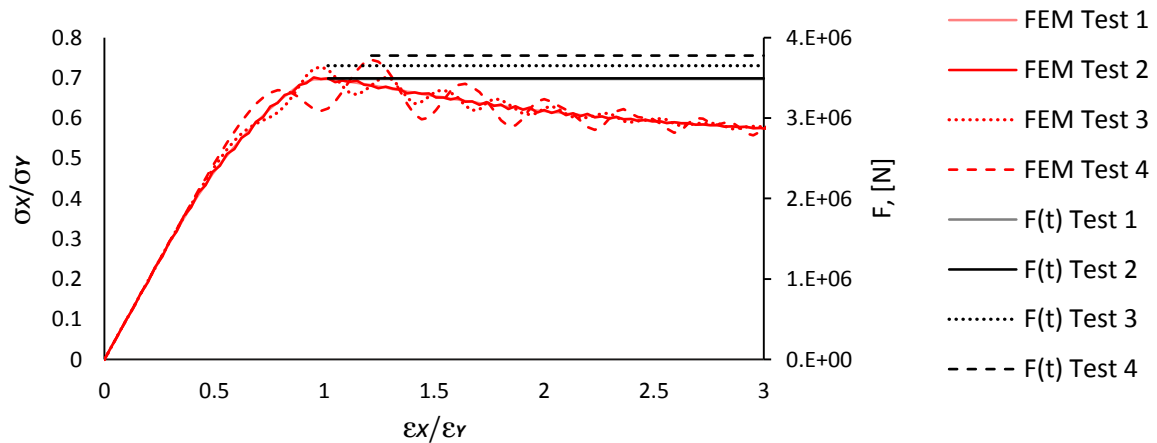


Figure 20: Definition of the maximum applied force from the average stress-average strain curves

Before implementing the implicit and explicit time integration methods into ISUM program code, one needs to formulate the finite element matrices. The tangential stiffness matrix $[K]$ is already presented within ISUM program code for the static analysis [38]. To enable the dynamic analysis, the consistent mass matrix $[M]$ must be added to the program, Eq. 65. For ISUM plate element without nodal lateral deflection the displacements $d(x, y, z)$ can be interpolated as:

$$\{d\} = [H]\{\hat{d}\}, \text{ or} \quad (68)$$

$$\begin{Bmatrix} u(x, y) \\ v(x, y) \\ w(x, y) \end{Bmatrix} = \begin{bmatrix} f_1 & f_2 & f_3 & f_4 & 0 & 0 & 0 & 0 & 0 & 0 \\ 0 & 0 & 0 & 0 & f_1 & f_2 & f_3 & f_4 & 0 & 0 \\ 0 & 0 & 0 & 0 & 0 & 0 & 0 & 0 & f_5 & f_6 \end{bmatrix} \{u_1 \ u_2 \ u_3 \ u_4 \ v_1 \ v_2 \ v_3 \ v_4 \ A_l \ A_t\}^T$$

Integrands $f_1 \dots f_4$ are the bilinear shape functions, which describe the nodal point displacements:

$$f_1 = \left(1 - \frac{x_e}{a_e}\right) \frac{y_e}{b_e}; \quad f_2 = \left(1 - \frac{x_e}{a_e}\right) \left(1 - \frac{y_e}{b_e}\right); \quad f_3 = \frac{x_e}{a_e} \frac{y_e}{b_e}; \quad f_4 = \frac{x_e}{a_e} \left(1 - \frac{y_e}{b_e}\right) \quad (69)$$

Integrands f_5 and f_6 are represented by trigonometric shape functions, which interpolate internal deflection of ISUM plate element according to the loading case, [18]:

longitudinal thrust application, $A_l \neq 0, A_t = 0$, see Eq. 5:

$$f_5 = \sin \frac{n\pi x_e}{a_e} \sin \frac{\pi y_e}{b_e} + f \sin \frac{3n\pi x_e}{a_e} \sin \frac{\pi y_e}{b_e} \quad (70)$$

transverse thrust application, $A_l = 0, A_t \neq 0$, see Eq. 8:

$$f_6 = \begin{cases} \sin \frac{\pi x_e}{a_e} \sin \frac{\pi y_e}{b_e}, & 0 \leq x \leq \frac{b}{2} \\ \sin \frac{\pi y_e}{b_e}, & \frac{b}{2} \leq x \leq a - \frac{b}{2} \\ \sin \frac{\pi(x_e - (a_e - b_e))}{a_e} \sin \frac{\pi y_e}{b_e}, & a - \frac{b}{2} \leq x \leq a \end{cases} \quad (71)$$

biaxial thrust application, $A_l \neq 0, A_t \neq 0$, see Eq. 1:

The integrands f_5 and f_6 can be obtained using Eqns. 70 and 71.

In the above given expressions parameters a_e and b_e represent the length and breadth of the element respectively. For any rectangular plate panel subjected to the axial loading, the obtained shape functions $[H]$ allow to perform a numerical integration of mass matrix $[M]$ by the trapezoidal rule with 7×7 equidistant integration points over element area, Eq. 65.

Coming back to the collapse analysis of 4-node square ISUM element, Figure 19, the degree of freedom A_t is equal to zero. Stiffness and mass matrices are reduced to the nodal degrees of freedom – two translations in x - and y - directions (displacements dx and dy for the first node) and lateral deflection A_l , according to the set-up for numerical test. The integrand f_5 of the shape function $[H]$ correspond to Eq. 70, since the sinusoidal buckling shape of square plate changes into the roof mode at the post-buckling region, Figure 4.

To start the calculations one need to know the time t_1 during that the externally applied dynamic force reaches its' maximum value. Within the FEA, the maximal applied edge displacement and the prescribed edge velocity define the total time of the thrust's application T . Further, using the average stress-average strain relationship and determining the strain (displacement), corresponding to the ultimate strength (force F_{max}) the required time t_1 can be found. Bringing together all discussed above, one can formulate the conditions for four test cases:

Table 5: Source data for the problem's description

	$V, \text{mm/s}$	F_{max}, N	T, s	t_1, s
Test 1	5	$3.39 \cdot 10^6$	1	0.3
Test 2	25	$3.40 \cdot 10^6$	0.2	0.06
Test 3	50	$3.55 \cdot 10^6$	0.1	0.03
Test 4	83	$3.67 \cdot 10^6$	0.06	0.02

Visually the applied dynamic force $F(t)$ can be presented for four test cases as:

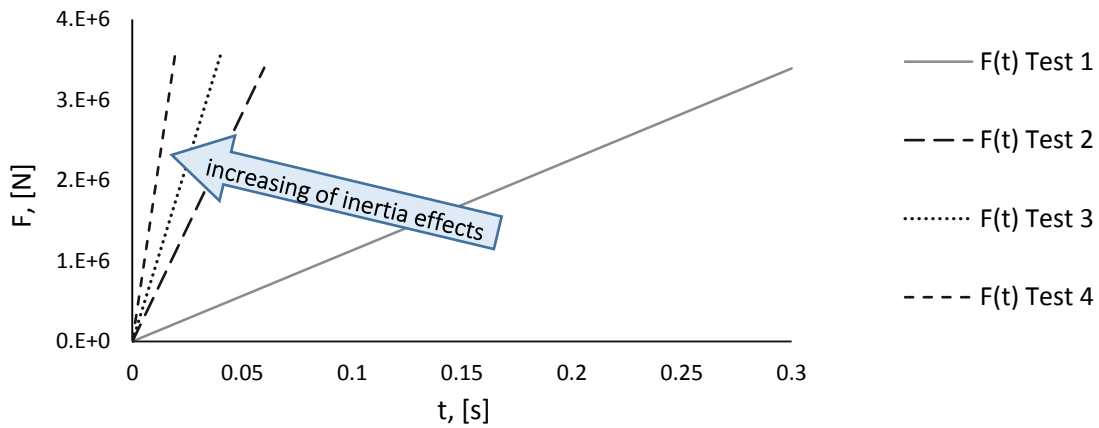


Figure 21: The applied dynamic force $F(t)$ on a 4-node ISUM element

The dynamic equilibrium equations in explicit and implicit forms without consideration of damping are presented by Eqns. 72 and 73 respectively:

$$\frac{1}{(\Delta t)^2} [M]\{d\}^{t+\Delta t} = \{F\}^t - \{R\}^t + \frac{2}{(\Delta t)^2} [M]\{d\}^t - \frac{1}{(\Delta t)^2} [M]\{d\}^{t-\Delta t} \quad (72)$$

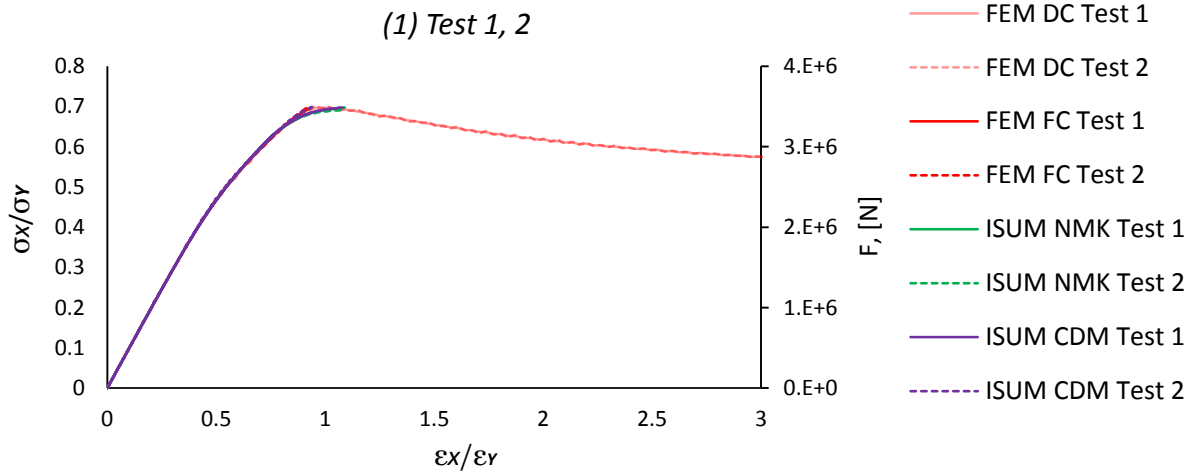
$$\left([K]^t + \frac{4}{(\Delta t)^2} [M]\right) \{\Delta d\}^{(i)} = \{F\}^{t+\Delta t} - \{R\}^{t+\Delta t(i-1)} - [M] \left(\frac{4}{(\Delta t)^2} (\{d\}^{t+\Delta t(i-1)} - \{d\}^t) - \frac{4}{\Delta t} \{\dot{d}\}^t - \{\ddot{d}\}^t \right) \quad (73)$$

For both schemes the zero initial conditions $d^0 = \dot{d}^0 = \ddot{d}^0 = 0$ are presumed. For the implicit integration scheme Newmark's integration parameters are $\alpha = 1/4$ and $\delta = 1/2$.

Here and further the time step Δt is calculated using the formula: $\Delta t = T/n$, where for the current task the total time of the thrust's application $T = t_1$. The number of calculation steps n should be a multiple of 100. Being only a conditionally stable scheme, the time step for the explicit time integration method must not exceed the value $\Delta t = 1 \cdot 10^{-5} s$ according to the recommendation given in [45]. Thus, the obtained time step values for the explicit (CDM) and implicit (NMK) integration methods are presented by:

	CDM	NMK
Test 1	$3 \cdot 10^{-6}$	$3 \cdot 10^{-4}$
Test 2	$6 \cdot 10^{-6}$	$6 \cdot 10^{-4}$
Test 3	$3 \cdot 10^{-6}$	$3 \cdot 10^{-4}$
Test 4	$2 \cdot 10^{-6}$	$2 \cdot 10^{-4}$

In Figure 22 (1), (2) the structural response of the 4-node ISUM element is presented. The FEA results are presented by two curves for each test: one obtained with displacement control – external dynamical thrust is applied by displacements FEM DC – and one obtained with force control – external dynamical thrust is applied by force.



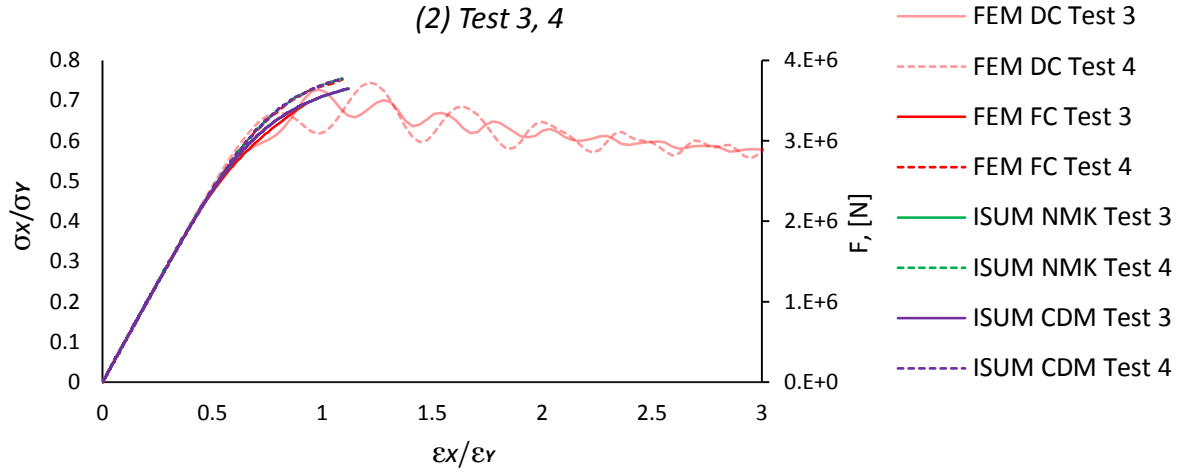


Figure 22 (1),(2): Structural response of the 4-node ISUM element

The results obtained using the implicit (NMK) and explicit (CDM) integration schemes, successfully implemented in the Idealized Structural Unit Method, completely coincide with the results provided with the commercial finite element program FEM FC. This proves the correctness of the consistent mass matrix formulation and implementation in the program code.

For the first and second test cases, the results obtained using the force control thrust application ISUM NMK, ISUM CDM and FEM FC exactly follow the solution performed with the displacement control thrust application FEM DC from the beginning until reaching the ultimate strength. For the third and fourth test cases, the differences in results provided with force and displacement control thrust application can be seen in the early plastic range. The ISUM NMK, ISUM CDM and FEM FC curves bend around the FEM DC solution and the ultimate strength is reached slightly beyond the yield strain ($\epsilon_x/\epsilon_y \approx 1.12$)

As one can see the direct application of the dynamic external load in the numerical implicit and explicit schemes – force control realization – does not lead to the full picture of the buckling behavior, since the increasing deformations in the post-buckling range do not imply a further increase in externally applied loads. In contrast, the loads tend to decrease in an oscillating manner (FEM DC), and the amplitudes of these oscillations are the most significant in the fourth test case. Small oscillations are already visible in the elastic region and they develop into large ones in the plastic region. With the growth of average strains ($\epsilon_x/\epsilon_y > 1$), the oscillation amplitudes of the applied loads gradually decrease in spite of the absence of damping.

Since the presented algorithms provide incomplete information about the buckling behavior of ISUM element, which is based on the average stress-average strain diagram, it is necessary to adjust the above considered implicit and explicit numerical schemes so that the external thrust can be applied by displacements (displacement control realization).

4.4 Concluding Remarks

In Chapter *Application of the Direct Time Integration Methods using Force Control* the following subjects were highlighted and discussed:

- Validation of the explicit central difference time integration method (CDM) and the implicit Newmark's time integration method (NMK) on an example of a simple spring-mass system, assuming the one-dimensional problem formulation: for four test cases with different frequencies of the applied load, the displacements obtained with the (CDM) and (NMK) integration schemes show good agreement with the results provided by the commercial program complex "ANSYS 15.0". The corresponding diagrams depict the influence of the inertia effects on the system's response, which is expressed in increasing oscillations of displacements at high frequencies of applied load.
- Validation of the explicit central difference time integration method (CDM) and the implicit Newmark's time integration method (NMK) on an example of a 4-node membrane element, assuming the two-dimensional problem formulation, [54]: the integration of the stiffness and mass matrices for the 4-node membrane element is performed using the program complex "Mathcad 14". Again, four test cases with different frequencies of applied load are considered and the corresponding displacements in x - and y -directions are presented as a result of the dynamic analysis. The curves obtained with the central difference (CDM) and Newmark's (NMK) methods coincide with each other and follow the FEM solutions quite well.
- Formulation of the consistent mass matrix for ISUM plate element: based on the bilinear and trigonometric shape functions, [38], described for longitudinal, transverse and biaxial thrust applications, the integration of mass matrix for the 4-node ISUM element is performed numerically by trapezoidal rule with 7×7 equidistant integration points.
- Validation of the explicit central difference time integration method (CDM) and the implicit Newmark's time integration method (NMK) on an example of the 4-node ISUM element, assuming the three-dimensional problem formulation, [54]: the maximum values of the applied dynamic load for each of four test cases correspond to the ultimate strength values, provided with the FEA of the square plate.
- The central difference time integration method (CDM) and the Newmark's time integration method (NMK) are directly implemented into the ISUM FORTRAN program code so that the externally applied dynamic thrust is applied by forces (force control). The results of the dynamic collapse analysis are presented by the average stress-average strain curves. The ISUM CDM and ISUM NMK solutions completely coincide with the FE-solutions FEM FC, obtained for the square plate with a 50×50 elements discretization that proves correct implementation of the consistent mass matrix and the integration procedures in the ISUM program code. The dynamic collapse analysis of the same structure performed with ISUM takes much less computational time than with the standard FEA. Comparing the implicit and explicit time integration schemes, the implicit one seems to be less time consuming, since the time step values can be much larger than for the explicit scheme.
- To provide the full picture of dynamic collapse behavior, including the post-buckling region, the formulation of the central difference and Newmark's time integration methods must be redefined so that the externally applied dynamic thrust can be applied by displacements (displacement control).

5 Displacement Control Procedure for Direct Time Integration Methods

Within the fourth chapter the important milestone was reached: consistent mass matrix of ISUM plate element was formulated and the explicit central difference time integration method (CDM) together with the implicit Newmark's time integration method (NMK) were successfully implemented in the Idealized Structural Unit Method. At the same time the current formulation of the numerical dynamic equation, assuming that the external thrust is applied by forces, does not provide the complete understanding of the buckling process. That is why the present chapter is dedicated to the new formulation of motion equation considering application of external dynamic thrust by displacements.

5.1 Enforced Motion Method in Structural Analysis

The enforced motion method is widely used to find the structural response of buildings, fundaments, bridges, etc., subjected to vibrations, earthquakes, and other loads, which can be described rather by displacements than by forces, [55]. Thus, the enforced motion method can be explained on an example of the linear dynamic equation of motion:

$$\begin{bmatrix} [M_{11}] & [M_{12}] \\ [M_{21}] & [M_{22}] \end{bmatrix} \begin{Bmatrix} \{\ddot{d}_1\} \\ \{\ddot{d}_2\} \end{Bmatrix} + \begin{bmatrix} [C_{11}] & [C_{12}] \\ [C_{21}] & [C_{22}] \end{bmatrix} \begin{Bmatrix} \{\dot{d}_1\} \\ \{\dot{d}_2\} \end{Bmatrix} + \begin{bmatrix} [K_{11}] & [K_{12}] \\ [K_{21}] & [K_{22}] \end{bmatrix} \begin{Bmatrix} \{d_1\} \\ \{d_2\} \end{Bmatrix} = \begin{Bmatrix} \{0\} \\ \{F\} \end{Bmatrix} \quad (74)$$

Here, the displacements (also velocities and accelerations) are subdivided into two parts, where $\{d_1\}$ are the "free" degrees of freedom and $\{d_2\}$ are the "enforced" degrees of freedom. According to this, the components of the load vector applied on the "free" degrees of freedom $\{d_1\}$ contains zeroes and the components of the load vector applied on the "enforced" degrees of freedom $\{d_2\}$ contains the unknown forces. The upper part of the Eq. 74 can be rearranged as:

$$[M_{11}]\{\ddot{d}_1\} + [C_{11}]\{\dot{d}_1\} + [K_{11}]\{d_1\} = -[M_{12}]\{\ddot{d}_2\} - [C_{12}]\{\dot{d}_2\} - [K_{12}]\{d_2\} \quad (75)$$

The above given equation can be solved for the displacements $\{d_1\}$ since the accelerations $\{\ddot{d}_1\}$ and velocities $\{\dot{d}_1\}$ can be approximated by displacements $\{d_1\}$ and the "enforced" displacements $\{d_2\}$, velocities $\{\dot{d}_2\}$ and accelerations $\{\ddot{d}_2\}$ are known. Having obtained all the kinematic parameters the unknown applied forces $\{F\}$ are to be evaluated from the lower part of the Eq. 75.

The same tactic of the external loads treatment can be used dealing with the nonlinear dynamic equation of motion performing the explicit and implicit time integration procedures. The detailed derivation of the numerical nonlinear dynamic equations assuming the enforced motion technique is introduced in the following subchapters.

5.2 Explicit Time Integration Method with Enforced Motion Technique

To enable the formulation of the explicit central difference time integration scheme with respect to the enforced motion technique, the nonlinear Eq. 48 should be rewritten according to the concept, considered in the previous subchapter, Eq. 74:

$$\begin{aligned} & \left(\frac{1}{(\Delta t)^2} [M_{11}] [M_{12}] + \frac{1}{2\Delta t} [C_{11}] [C_{12}] \right) \begin{Bmatrix} d_1 \\ d_2 \end{Bmatrix}^{t+\Delta t} + \begin{Bmatrix} R_1 \\ R_2 \end{Bmatrix}^t - \frac{2}{(\Delta t)^2} [M_{11}] [M_{12}] \begin{Bmatrix} d_1 \\ d_2 \end{Bmatrix}^t \\ & + \left(\frac{1}{(\Delta t)^2} [M_{21}] [M_{22}] - \frac{1}{2\Delta t} [C_{21}] [C_{22}] \right) \begin{Bmatrix} d_1 \\ d_2 \end{Bmatrix}^{t-\Delta t} = \begin{Bmatrix} 0 \\ F \end{Bmatrix}^t \end{aligned} \quad (76)$$

Having established the initial conditions for displacements at time t and $t - \Delta t$, the unknown displacements $\{d_1\}^{t+\Delta t}$ can be obtained from the upper part of Eq. 76:

$$\begin{aligned} & \left(\frac{1}{(\Delta t)^2} [M_{11}] + \frac{1}{2\Delta t} [C_{11}] \right) \{d_1\}^{t+\Delta t} = - \left(\frac{1}{(\Delta t)^2} [M_{12}] + \frac{1}{2\Delta t} [C_{12}] \right) \{d_2\}^{t+\Delta t} - \{R_1\}^t \\ & + \frac{2}{(\Delta t)^2} [M_{11}] [M_{12}] \begin{Bmatrix} d_1 \\ d_2 \end{Bmatrix}^t - \left(\frac{1}{(\Delta t)^2} [M_{11}] [M_{12}] - \frac{1}{2\Delta t} [C_{11}] [C_{12}] \right) \begin{Bmatrix} d_1 \\ d_2 \end{Bmatrix}^{t-\Delta t} \end{aligned} \quad (77)$$

To solve the above given system of equations the Gaussian elimination algorithm is implemented to the Idealized Structural Unit Method. It is necessary to note that the correct arrangement of the degrees of freedom and the corresponding components of the mass and damping matrices is very important performing such an analysis. Thus, within the Idealized Structural Unit Method the “enforced” degrees of freedom get the last (highest) sequence number to be placed in the lower line in the displacement vector. The lower part of the Eq. 76 yields the solution for the applied load $\{F\}^t$:

$$\begin{aligned} & \left(\frac{1}{(\Delta t)^2} [M_{21}] [M_{22}] + \frac{1}{2\Delta t} [C_{21}] [C_{22}] \right) \begin{Bmatrix} d_1 \\ d_2 \end{Bmatrix}^{t+\Delta t} + \{R_2\}^t - \frac{2}{(\Delta t)^2} [M_{21}] [M_{22}] \begin{Bmatrix} d_1 \\ d_2 \end{Bmatrix}^t \\ & + \left(\frac{1}{(\Delta t)^2} [M_{21}] [M_{22}] - \frac{1}{2\Delta t} [C_{21}] [C_{22}] \right) \begin{Bmatrix} d_1 \\ d_2 \end{Bmatrix}^{t-\Delta t} = \{F\}^t \end{aligned} \quad (78)$$

The obtained results can be concluded as correct if the equilibrium state of the system is satisfied on each time step:

$$[M]\{\ddot{d}\}^t + [C]\{\dot{d}\}^t = \{F\}^t - \{R\}^t$$

5.3 Implicit Time Integration Method with Enforced Motion Technique

The same procedure of matrix subdivision with respect to the “enforced” and “free” degrees of freedom should be realized to enable the formulation of the implicit Newmark’s time integration scheme within the enforced motion technique. In contrast to the explicit time integration scheme, the implicit numerical formulation requires the performance of the iteration procedure for the nonlinear analysis, and the Eq. 54 yields:

$$\begin{aligned} & \left(\frac{4}{(\Delta t)^2} [M_{11}] [M_{12}] + \frac{2}{\Delta t} [C_{11}] [C_{12}] + [K_{11}] [K_{12}] \right)^{t+\Delta t(i-1)} \left\{ \begin{matrix} \Delta d_1 \\ \Delta d_2 \end{matrix} \right\}^{(i)} + \left\{ \begin{matrix} R_1 \\ R_2 \end{matrix} \right\}^{t+\Delta t(i-1)} \\ & + [M_{11}] [M_{12}] \left(\frac{4}{(\Delta t)^2} \left(\left\{ \begin{matrix} d_1 \\ d_2 \end{matrix} \right\}^{t+\Delta t(i-1)} - \left\{ \begin{matrix} d_1 \\ d_2 \end{matrix} \right\}^t \right) - \frac{4}{\Delta t} \left\{ \begin{matrix} \dot{d}_1 \\ \dot{d}_2 \end{matrix} \right\}^t - \left\{ \begin{matrix} \ddot{d}_1 \\ \ddot{d}_2 \end{matrix} \right\}^t \right) \\ & + [C_{11}] [C_{12}] \left(\frac{2}{\Delta t} \left(\left\{ \begin{matrix} d_1 \\ d_2 \end{matrix} \right\}^{t+\Delta t(i-1)} - \left\{ \begin{matrix} d_1 \\ d_2 \end{matrix} \right\}^t \right) - \left\{ \begin{matrix} \dot{d}_1 \\ \dot{d}_2 \end{matrix} \right\}^t \right) = \left\{ \begin{matrix} 0 \\ F \end{matrix} \right\}^{t+\Delta t} \end{aligned} \quad (79)$$

Having established the initial conditions for displacements, velocities and accelerations at time t , and assuming that for $i = 1$ $\{R\}^{t+\Delta t(i-1)} = \{R\}^t$ and $\{d\}^{t+\Delta t(i-1)} = \{d\}^t$, the unknown incremental displacements $\{\Delta d_1\}^{(i)}$ can be obtained from the upper part of Eq. 79:

$$\begin{aligned} & \left(\frac{4}{(\Delta t)^2} [M_{11}] + \frac{2}{\Delta t} [C_{11}] + [K_{11}] \right)^{t+\Delta t(i-1)} \{\Delta d_1\}^{(i)} = - \left(\frac{4}{(\Delta t)^2} [M_{12}] + \frac{2}{\Delta t} [C_{12}] + [K_{12}] \right)^t \{\Delta d_2\}^{(i)} \\ & - \{R_1\}^{t+\Delta t(i-1)} - [M_{11}] [M_{12}] \left(\frac{4}{(\Delta t)^2} \left(\left\{ \begin{matrix} d_1 \\ d_2 \end{matrix} \right\}^{t+\Delta t(i-1)} - \left\{ \begin{matrix} d_1 \\ d_2 \end{matrix} \right\}^t \right) - \frac{4}{\Delta t} \left\{ \begin{matrix} \dot{d}_1 \\ \dot{d}_2 \end{matrix} \right\}^t - \left\{ \begin{matrix} \ddot{d}_1 \\ \ddot{d}_2 \end{matrix} \right\}^t \right) \\ & - [C_{11}] [C_{12}] \left(\frac{2}{\Delta t} \left(\left\{ \begin{matrix} d_1 \\ d_2 \end{matrix} \right\}^{t+\Delta t(i-1)} - \left\{ \begin{matrix} d_1 \\ d_2 \end{matrix} \right\}^t \right) - \left\{ \begin{matrix} \dot{d}_1 \\ \dot{d}_2 \end{matrix} \right\}^t \right) \end{aligned} \quad (80)$$

The unknown kinematic parameters can be obtained using the defined incremental displacements:

$$\begin{aligned} & \{d_1\}^{t+\Delta t(i)} = \{d_1\}^{t+\Delta t(i-1)} + \{\Delta d_1\}^{(i)} \\ & \{\dot{d}_1\}^{t+\Delta t(i)} = \frac{2}{\Delta t} \left(\{d_1\}^{t+\Delta t(i-1)} + \{\Delta d_1\}^{(i)} - \{d_1\}^t \right) - \{\dot{d}_1\}^t \\ & \{\ddot{d}_1\}^{t+\Delta t(i)} = \frac{4}{(\Delta t)^2} \left(\{d_1\}^{t+\Delta t(i-1)} + \{\Delta d_1\}^{(i)} - \{d_1\}^t \right) - \frac{4}{\Delta t} \{\dot{d}_1\}^t - \{\ddot{d}_1\}^t \end{aligned} \quad (81)$$

The externally applied forces $\{F\}$ are to be updated within the Newton-Raphson iterations using the obtained displacements:

$$\begin{aligned}\{F\}^{t+\Delta t(i)} &= \{F\}^{t+\Delta t(i-1)} + \{\Delta F\}^{(i)} \\ \{\Delta F\}^{(i)} &= [\hat{K}_{21}][\hat{K}_{22}] \begin{Bmatrix} \{\Delta d_1\} \\ \{\Delta d_2\} \end{Bmatrix}^{(i)} - (\{F\}^{t+\Delta t(i-1)} - \{\hat{R}\}),\end{aligned}\tag{82}$$

where

$$\begin{aligned}\hat{K} &= \left(\frac{4}{(\Delta t)^2} [M_{11}][M_{12}] + \frac{2}{\Delta t} [C_{11}][C_{12}] + [K_{11}][K_{12}] \right)^{t+\Delta t(i-1)} \\ \{\hat{R}\} &= \{R_2\}^{t+\Delta t(i-1)} + [M_{21}][M_{22}] \left(\frac{4}{(\Delta t)^2} \begin{Bmatrix} \{d_1\} \\ \{d_2\} \end{Bmatrix}^{t+\Delta t(i-1)} - \begin{Bmatrix} \{d_1\} \\ \{d_2\} \end{Bmatrix}^t \right) - \frac{4}{\Delta t} \begin{Bmatrix} \{\dot{d}_1\} \\ \{\dot{d}_2\} \end{Bmatrix}^t - \begin{Bmatrix} \{\ddot{d}_1\} \\ \{\ddot{d}_2\} \end{Bmatrix}^t \\ &\quad + [C_{21}][C_{22}] \left(\frac{2}{\Delta t} \begin{Bmatrix} \{d_1\} \\ \{d_2\} \end{Bmatrix}^{t+\Delta t(i-1)} - \begin{Bmatrix} \{d_1\} \\ \{d_2\} \end{Bmatrix}^t \right) - \begin{Bmatrix} \{\dot{d}_1\} \\ \{\dot{d}_2\} \end{Bmatrix}^t\end{aligned}$$

The illustration of the first step of the Newton-Raphson iteration procedure is presented in Figure 23. A characteristic of this iteration is that a new tangent stiffness matrix is calculated in each iteration, which is why this method is called the full Newton-Raphson method, [48]. The iterations continues until the out-of-balance force vector $\{F\}^{t+\Delta t(i-1)} - \{\hat{R}\}$ (vertical dashed lines) is small enough, Eq. 55.

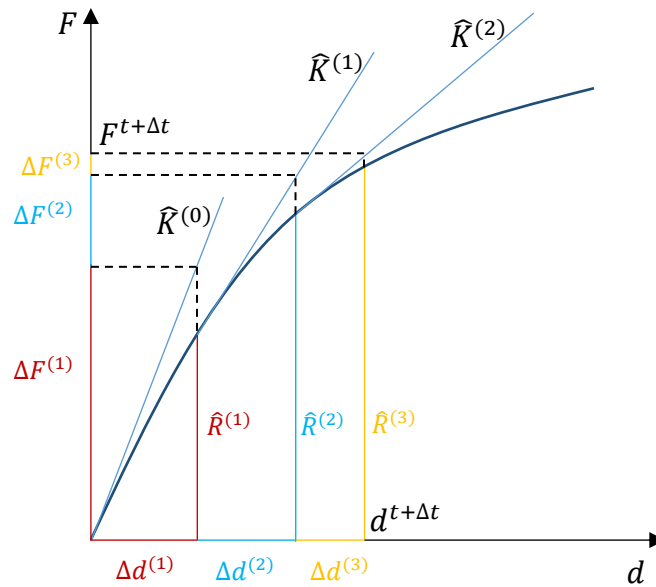


Figure 23: Full Newton-Raphson iteration procedure

5.4 Displacement Control vs. Force Control

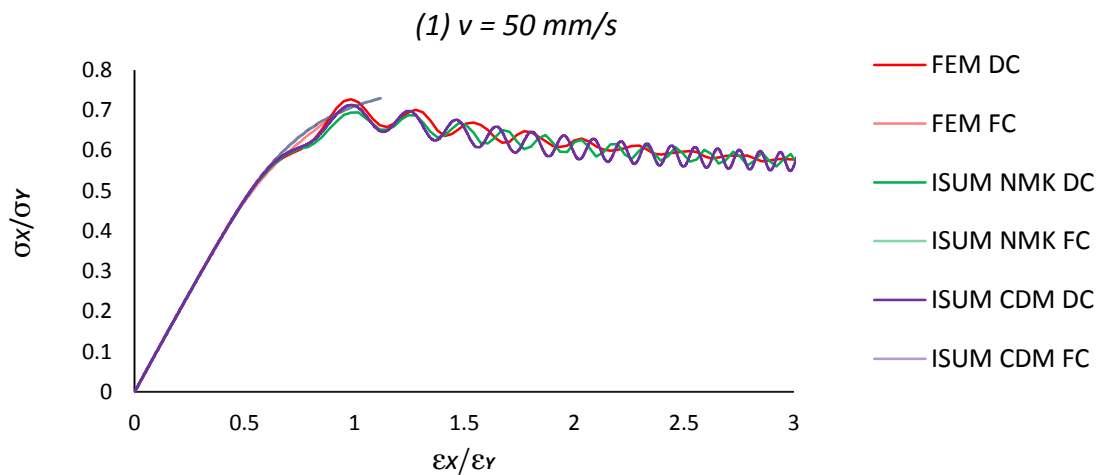
Algorithms of the enforced motion technique described in the previous subsections application to the implicit and explicit time integration procedures were implemented into the Idealized Structural Unit Method. On an example of the dynamically loaded 4-node ISUM element the two considered approaches of the load application – force control and displacement control (enforced motion) will be shown and compared with the results of the Finite Element Analysis. Geometrical and material properties of ISUM element are given in Table 1.

The task formulation for the force control load application remains the same, see subchapter 4.3. Exemplary, the cases Test 3 and Test 4 are considered. To perform the dynamic analysis of the 4-node ISUM element using the enforced motion method (displacement control), the external dynamic load is applied by displacements, with the edge velocity of 50 mm/s (Test 3) and 83 mm/s (Test 4). Within the FEA the external loads are applied in the same way (displacement control).

Here and further, the following interpretation of the edge velocity will be used: $V = d_{max}/T$, where d_{max} is the maximum applied edge displacement and T is the total time of the thrust's application. In case of the longitudinal thrust action, the d_{max} can be obtained from: $\frac{d_{max}}{a} / \frac{\sigma_Y}{E} = \frac{\varepsilon_x}{\varepsilon_Y}$.

In case of the transverse thrust action: $\frac{d_{max}}{b} / \frac{\sigma_Y}{E} = \frac{\varepsilon_y}{\varepsilon_Y}$. The parameters a and b represent the length and the breadth of the plate respectively, and the values $\varepsilon_x/\varepsilon_Y$ and $\varepsilon_y/\varepsilon_Y$ correspond to the maximum average strain value, which is expected to be on the average stress-average strain diagram. Strain rate values $\dot{\varepsilon}$ can be also calculated for longitudinal $\dot{\varepsilon} = V/a$ and transverse $\dot{\varepsilon} = V/b$ thrust application.

The results of the dynamic analysis of the 4-node ISUM element are presented in Figure 24 for two applied edge velocity values. The curves, corresponding to the force control load application were already shown in subchapter 4.3, Figure 22. Here, they get the additional description FC, which means force control, ISUM NMK FC and ISUM CDM FC. The newest results, obtained using the implicit and explicit time integration schemes and considering the external thrust applied by displacements are given by two curves respectively ISUM NMK DC and ISUM CDM DC.



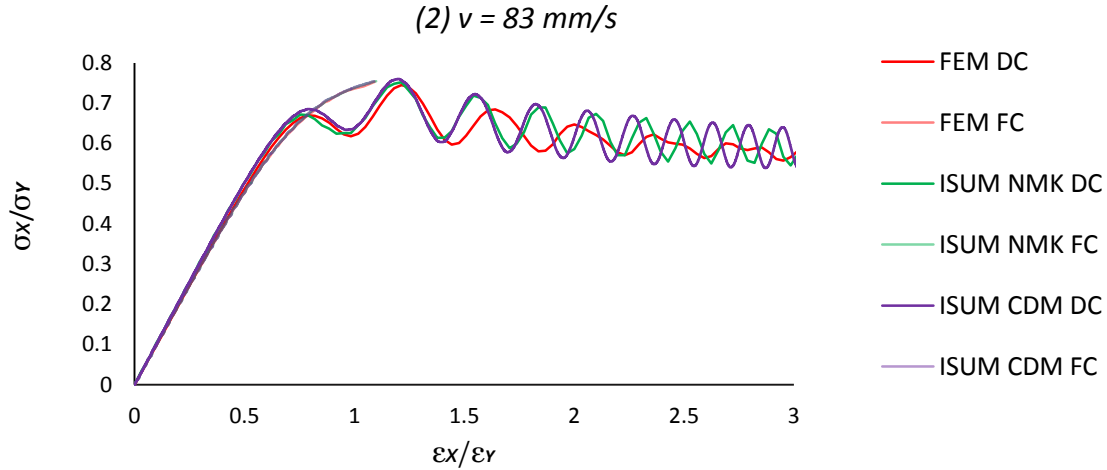


Figure 24 (1),(2): Displacement control vs. force control on example of the dynamic collapse analysis of the 4-node ISUM element

Analyzing the results presented in the Figure 24 (1)-(2) one can make three important conclusions:

1. The displacement control load application is more suitable for the dynamic collapse analysis of the plate panels than the force control load application. As one can see, the curves FEM DC, ISUM NMK DC and ISUM CDM DC describe also the post-buckling behavior of ISUM element, which is missing in case of the force control thrust application, since the curves FEM FC, ISUM NMK FC and ISUM CDM FC terminate reaching the ultimate strength value.
2. The explicit central difference and implicit Newmark's time integration schemes implemented in the Idealized Structural Unit Method, adjusted to the enforced motion technique, supply reliable results. The corresponding curves ISUM CDM DC and ISUM NMK DC just slightly differ from each other in the post-buckling regime and follow quite well the finite element solution FEM DC.
3. Leaving the range of elastic deformations behind, the solution starts to oscillate and the amplitudes of the oscillations depend on the edge velocity – with the increase of the applied edge velocity values, or in other words decreasing the time of the thrust-application, the amplitudes of the oscillations also increase due to the growth of the inertia effects.

In addition one can see from the presented graphs that the amplitudes of the ISUM CDM DC and ISUM NMK DC curves are higher than the amplitudes of the FEM DC curves. The difficulty is that we consider the nonlinear dynamic problem and the numerical solution can even become unstable especially for large deformations. To avoid this undesirable event or to increase accuracy of the numerical integration schemes the physical damping should be added to ISUM model.

5.5 Concluding Remarks

In Chapter *Application of the Displacement Control Procedure to the Direct Time Integration Methods* the following subjects were highlighted and discussed:

- Formulation of the enforced motion method: the subdivision of the matrix dynamic equation of motion is performed in terms of the “enforced” and “free” degrees of freedom, [55].
- Application of the enforced motion technique to the explicit and implicit time integration methods: the corresponding numerical schemes are adjusted to the enforced motion technique by rewriting them according to the considered formulation. These transformations bring the additional difficulties in terms of the computational costs, since not only the displacement vector, but also the applied load vector should be updated. This remark mainly concerns the Newmark’s implicit time integration method, where the updating carries the iterative character for the nonlinear analysis.
- Implementation of the explicit central difference and implicit Newmark’s time integration schemes to the Idealized Structural Unit Method: validation was performed on an example of the 4-node ISUM element, uniaxial-loaded by displacements with two different edge velocities. The results of the dynamic collapse analysis under assumption of the external thrust applied by displacements (enforced motion or displacement control) are presented by the average stress-average strain curves and compared with the results of the dynamic collapse analysis of the 4-node ISUM element, uniaxial-loaded by forces (force control), subchapter 4.3.
- The enforced motion technique applied to the explicit and implicit time integration methods provides desirable results, since the total buckling behavior of the plate structure can be obtained in contrast to the previous formulation, which considers the thrust applied by forces.
- The correctness of the applied enforced motion technique is proved by the finite element results, since the obtained ISUM average stress-average strain curves for both implicit and explicit time integration methods follow the FEM-solution very well. The differences in the oscillation amplitudes between ISUM and FEM curves can be avoided by addition of the physical damping properties to the ISUM formulation.

6 Dynamic Collapse Analyses of ISUM Plate Panels

Based on the results of the previous Chapter the explicit central difference and the implicit Newmark's time integration methods with the enforced motion formulation will be used for further investigations on the dynamic collapse analysis of the ISUM plate panels. The present Chapter will give answers to the following questions:

1. What is the typical dynamic collapse behavior of ISUM plate panels under longitudinal and transverse thrust?
2. How does buckling behavior change with increasing velocity of the applied displacements?
3. Is it possible to make an unambiguous conclusion that one numerical time integration scheme is superior?

As it was already mentioned, addition of physical damping to ISUM model could increase the accuracy of the numerical integration schemes. That is why the subchapter 6.1 is dedicated to the building of the damping models. The subsequent sections 6.2 – 6.5 present the results of the dynamic collapse analysis of ISUM plate panels.

The following conditions are the same for all test cases:

- validation of the obtained ISUM results is based on a comparison with the FE-solution, provided by the program complex "ANSYS 15.0", [55];
- static solutions are obtained from FEA performed with program complex "ANSYS 15.0" and are shown to assess the significance of dynamic effects. Results of static collapse analyses of rectangular plates with ISUM are widely represented in [36];
- external dynamic thrust is applied by displacements with a prescribed edge velocity;
- spread of yielding in images of collapse modes corresponds to the middle layer of plate material and is presented in percent by color gradient from dark blue (zero plasticity) to bright red (full plasticity);
- principal dimensions, FE-discretization and material properties of examined plates are pointed out in Table 6;
- solutions are presented according to the undamped ($\xi = 0$, marked with odd numbers) and damped ($\xi \neq 0$, marked with even numbers) test cases;
- Newmark's time integration parameters α and β are equal to 1/4 and 1/2 respectively.

The following conditions are unique for each test case and are given in the corresponding paragraphs:

- consistent mass matrix for each plate panel;
- obtained for each test case collapse modes, corresponding to ultimate and post-ultimate stress states;
- initial deflection values of FE- and ISUM-models;
- time step values.

Table 6: Properties of the examined plate panels

Plate number	Dimension	FE-discretization, ISUM/FEM		
	$L \times B \times T$, [mm]	Longitud. thrust	Transverse thrust	Biaxial thrust
plate 1	1000 x 1000 x 15.5	1/50 x 50	-	-
plate 2	2400 x 835 x 15	3/10 x 30	3/10 x 30	-
plate 3	4200 x 835 x 13	5/10 x 70	3/10 x 70	-
plate 4	4200 x 835 x 22	7/10 x 70	3/10 x 70	9/10 x 70
Material properties for all plate panels:	yield strength	σ_Y	313.6	MPa
	young's modulus	E	205.8	MPa
	density	ρ	7850	kg/m ³
	poisson's ratio	ν	0.3	-

Subjected to axial compressive loads rectangular plate panels buckles into several number of half waves, [20]. As discussed in Chapter 2, buckling modes can be sinusoidal with a distinct plasticity localization zone (under longitudinal loading) or cylindrical (under transverse loading) according to the direction of applied thrust, Figure 8. The number of buckling half waves under longitudinal thrust depends on dimensions and material properties of plates: if a theoretical buckling strength exceeds the yield strength, plastic buckling occurs and the aspect ratio of each buckling half wave tends to 0.7. Otherwise, elastic buckling with aspect ratios around 1.0 per half wave takes place, [36]. Thus, due to the high thickness and therefore increased strength margin, plate 4 has more buckling half waves than plate 3. Number of ISUM elements must be equal to the number of buckling half waves. At transverse thrust, for the shape function reflecting the cylindrical collapse mode an mesh with three ISUM elements is required, [36]. For plate panels subjected to the biaxial thrust, a combination of two meshes (for longitudinal and transverse thrust) is needed, [36]. ISUM-discretization is presented in Table 6 and visualized in Figure 25:

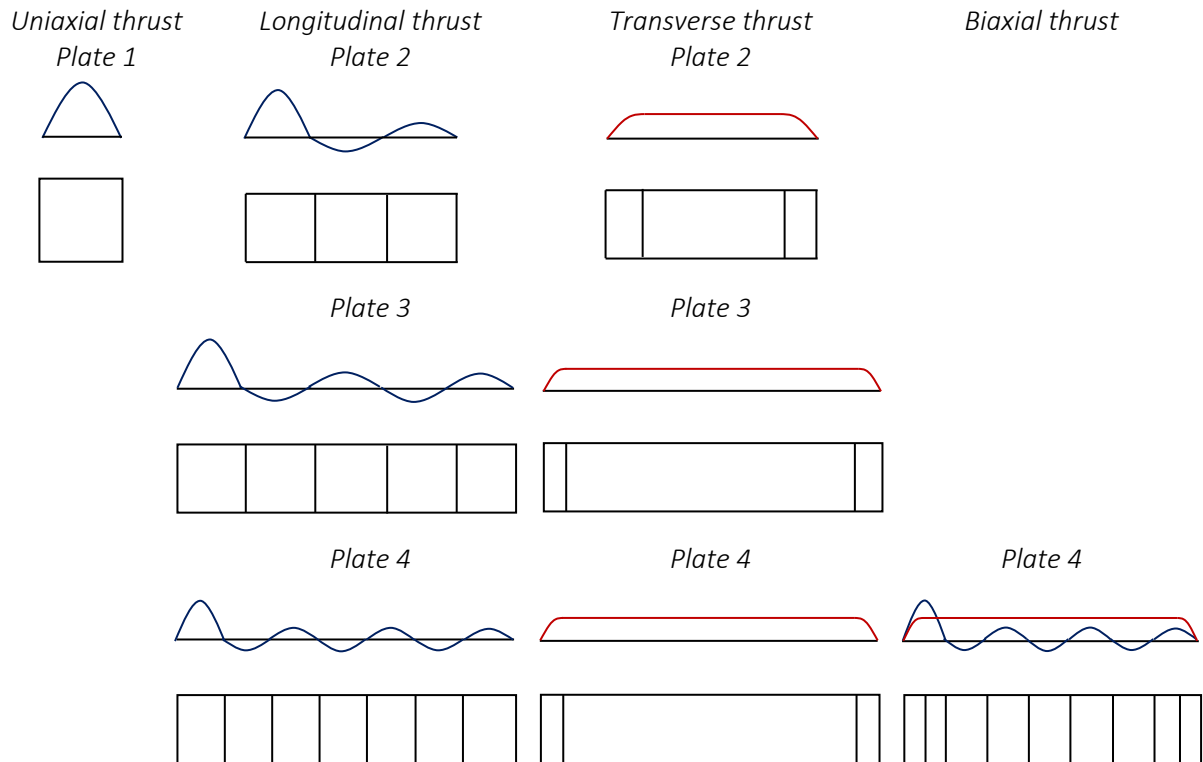


Figure 25: ISUM-discretization for rectangular plate panels

6.1 Rayleigh Damping Model

Damping can be introduced as a physical process, which represents the dissipation of the mechanical energy stored in the oscillations. As a result, damping leads to reducing or preventing of the oscillations. Since this phenomenon is directly connected with vibration and oscillation, it makes sense to introduce the finite element equilibrium equation of motion on the basis of the eigenvectors:

$$\{\ddot{X}(t)\} + [\Phi]^T [C] [\Phi] \{\dot{X}(t)\} + [\Omega^2] \{X(t)\} = [\Phi]^T \{R(t)\} \quad (83)$$

Here, the nodal point displacements are transformed so that $\{\hat{d}(t)\} = [\Phi] \{X(t)\}$, [56]. The transformation matrix $[\Phi]$ is represented by eigenvectors ϕ_i ; vector $\{X(t)\}$ contains the generalized displacements; diagonal matrix $[\Omega^2]$ stores the eigenvalues ω_i^2 . Unfortunately the damping matrix $[C]$ cannot be constructed from element damping matrices, as it is performed for the mass and stiffness matrices of the element assemblage. To approximate the overall energy dissipation it is assumed that damping represents a linear combination of the stiffness and mass matrix parameters. This formulation corresponds to the Rayleigh damping with the unknown constants α and β :

$$[C] = \alpha[M] + \beta[K] \quad (84)$$

On the other hand, damping depends on the damping ratio $\{\xi\}$ and angular frequency $\{\omega\}$:

$$[\Phi]^T [C] [\Phi] = 2\{\omega\}\{\xi\} \quad (85)$$

Using the above given Eq. 84 and Eq. 85 one obtains:

$$[\Phi]^T (\alpha M + \beta K) [\Phi] = 2\{\omega\}\{\xi\}, \text{ or} \quad (86)$$

$$\alpha + \beta \omega_i^2 = 2\omega_i \xi_i$$

Having defined two damping ratios ξ_i (can be also equivalent) and having chosen two modes, according to the typical or expected collapse behavior, with the corresponding angular frequencies ω_i , the damping parameters α and β can be obtained from:

$$\alpha = 2\omega_1\omega_2 \frac{\xi_1\omega_2 - \xi_2\omega_1}{\omega_2^2 - \omega_1^2} \quad (87)$$

$$\beta = 2 \frac{\xi_2\omega_2 - \xi_1\omega_1}{\omega_2^2 - \omega_1^2}$$

The damping ratio ξ determines behavior of the system and can be understood as the level of damping in a system relative to critical damping. According to this definition, one can classify the system as:

- undamped, $\xi = 0$: the motion is periodic, system oscillates with constant amplitude;
- underdamped, $0 < \xi < 1$: the system oscillates with a slightly different frequency than in the undamped case with the amplitude gradually decreasing to zero. The angular frequency of the underdamped harmonic oscillator is given by $\omega = \omega_0 \sqrt{1 - \xi^2}$, where ω_0 represent the undamped angular frequency of the oscillator;

- critically damped, $\xi = 1$: the system returns to equilibrium state as quickly as possible without oscillating. This is the border between the overdamped and underdamped cases, which is often desired in many cases where engineering design of a damped oscillator is required;
- overdamped, $\xi > 1$: the system exponentially decays to equilibrium state without oscillating. The larger the values of damping ratio ξ are, the slower the system returns to its steady state.

Material damping depends on many factors such as type of material, stress amplitude, internal forces, size of geometry, the quality of surface and temperature. For steel structures, the typical range of damping ratio is 0.02 – 0.05. However, it is possible to consider for structures with joints higher values of damping ratio up to 0.1, [57].

To determine the damping parameters α and β for the four examined plate panels, modal analysis was performed with the program complex “ANSYS 15.0”. Two required angular frequencies ω_i are extracted according to the expected buckling behavior. For each plate, Table 7, the first undamped angular frequency ω_{0_1} is obtained for the vibration mode with one half wave. The second value ω_{0_2} corresponds to the vibration mode with a number of half waves equivalent to the number of buckling half waves (also ISUM elements) under longitudinal loading. For the square panel (plate 1) ω_{0_2} is calculated for three vibrational half waves.

Table 7: Damping parameters for the examined plate panels

<i>plate 1</i>	ω_{0_1}	ω_{0_2}	α	β	<i>plate 3</i>	ω_{0_1}	ω_{0_2}	α	β
$\xi=0.02$	478	2365	15.905	$1.407 \cdot 10^{-5}$	$\xi=0.02$	309	580	8.066	$4.499 \cdot 10^{-5}$
$\xi=0.05$			39.763	$3.517 \cdot 10^{-5}$	$\xi=0.05$			20.164	$1.125 \cdot 10^{-4}$
$\xi=0.10$			79.527	$7.034 \cdot 10^{-5}$	$\xi=0.10$			40.329	$2.250 \cdot 10^{-4}$
<i>plate 2</i>	ω_{0_1}	ω_{0_2}	α	β	<i>plate 4</i>	ω_{0_1}	ω_{0_2}	α	β
$\xi=0.02$	410	718	10.454	$3.543 \cdot 10^{-5}$	$\xi=0.02$	507	1422	14.954	$2.073 \cdot 10^{-5}$
$\xi=0.05$			26.135	$8.857 \cdot 10^{-5}$	$\xi=0.05$			37.384	$5.182 \cdot 10^{-5}$
$\xi=0.10$			52.271	$1.771 \cdot 10^{-4}$	$\xi=0.10$			74.768	$1.036 \cdot 10^{-4}$

According to the assumed damping ratios ($\xi = 0.02, 0.05$ and 0.10), validation of damping models is presented on an example of the square plate panel (*plate 1*), with the high-applied edge velocity of 100 mm/s . The Rayleigh damping is used within the FEA and ISUM to include the damping forces to the nonlinear differential equation of motion. Time step $\Delta t = 5 \cdot 10^{-4} \text{ s}$ is assumed for FEM and ISUM NMK, and $\Delta t = 5 \cdot 10^{-5} \text{ s}$ for ISUM CDM. Corresponding results are presented on Figure 26. The third damping model with the damping ratio $\xi = 0.10$ provides minimal difference between the obtained ISUM and FEM results. The ISUM CDM curve shows very good agreement with the FEM curve and becomes smooth in the post-buckling range. The ISUM NMK has in general the similar behavior as ISUM CDM, but at the same time, the implicit solution provides the additional tiny oscillations, which come up during the whole calculation period. The first damping model with damping ratio $\xi = 0.02$ does not supply the desired damping level so that the ISUM and FEM curves would get closer to each other.

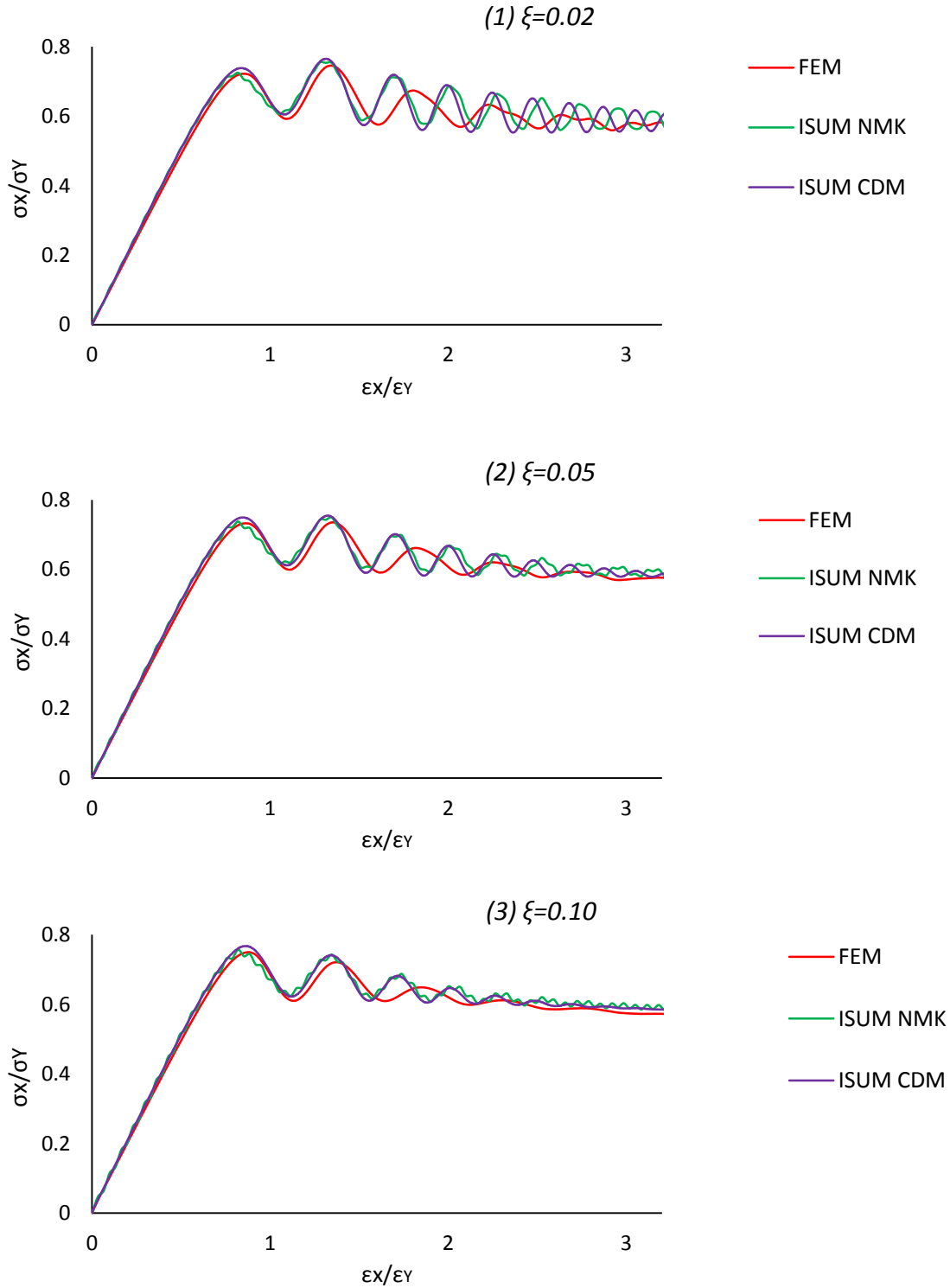


Figure 26 (1)-(3): Dynamic collapse behavior of 15 mm square plate with different damping models

The second damping model with the damping ratio $\xi = 0.05$ provides a sufficient matching between FEM and ISUM results. ISUM NMK and ISUM CDM coincide with each other very well and follow the FEA solution, gradually reducing the amplitude of oscillations. Having considered the fact that the damping ratio $\xi = 0.10$ is rather an exception for steel structures, the damping ratio $\xi = 0.05$ and the corresponding damping parameters α and β will be used for further investigations of all plate types, unless damping is specifically not considered.

6.2 Dynamic Collapse Analyses of Square Panels under Uniaxial Thrust

Dynamic collapse behavior of the square plates with different thickness values is presented in Figures 26-28. Time step $\Delta t = 5 \cdot 10^{-4}$ s is assumed for FEM and ISUM NMK, and $\Delta t = 5 \cdot 10^{-5}$ s for ISUM CDM. Consistent mass matrix is obtained from Eq. (65 with appropriate shape functions, Eq. (70). The influence of damping is not considered for this basic examples.

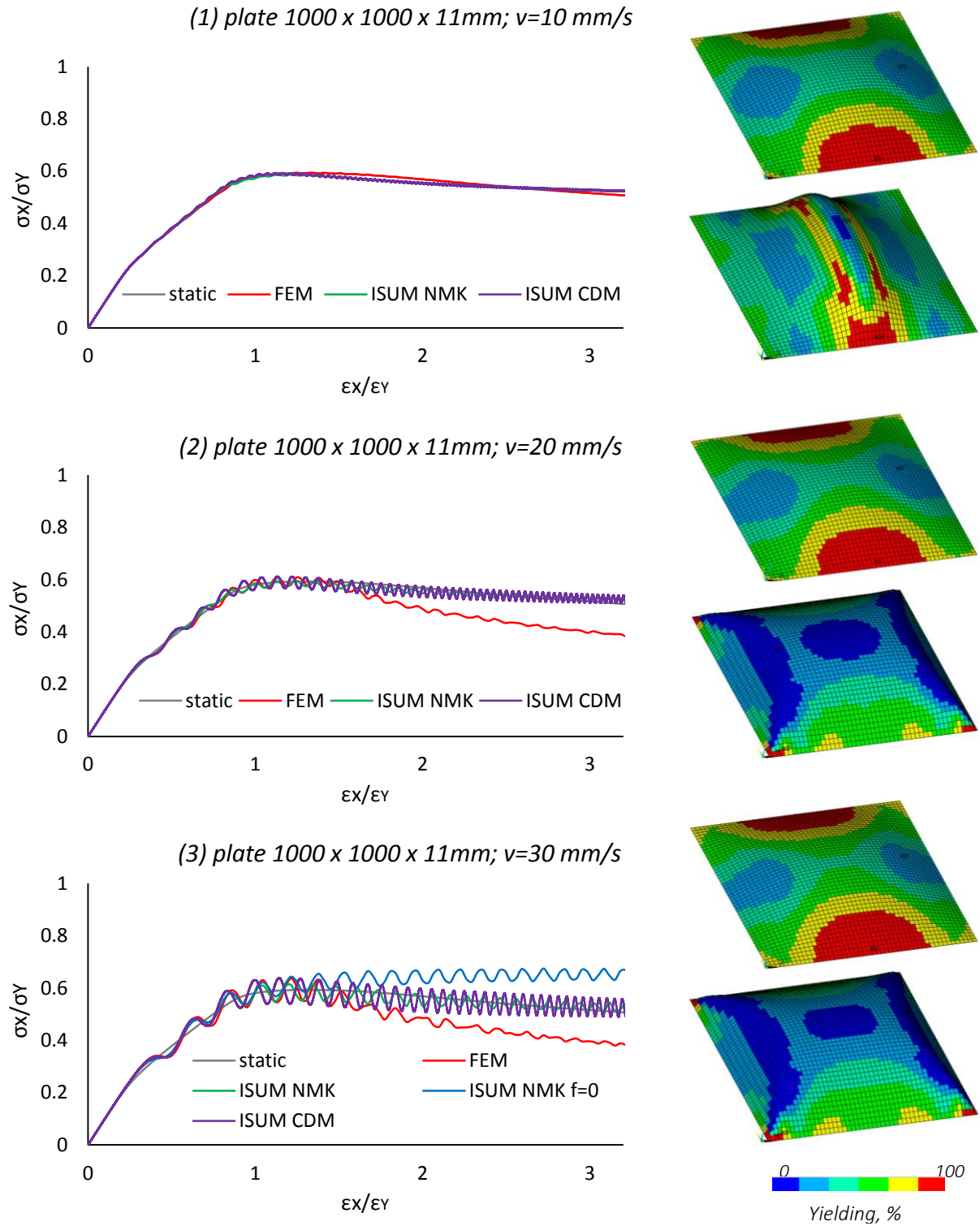
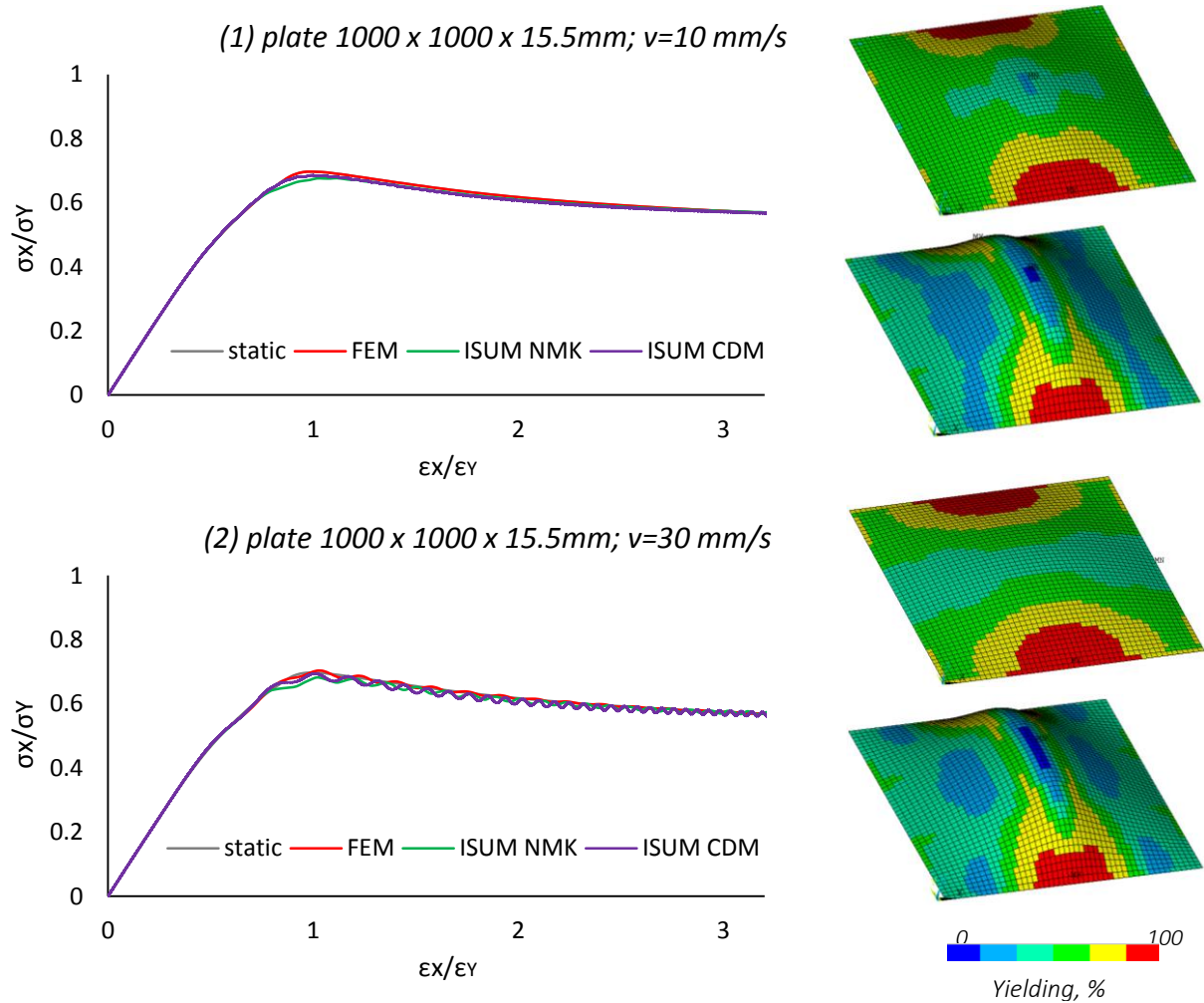


Figure 27 (1)-(3): Dynamic collapse behavior of the 11 mm square plate under uniaxial thrust

For three applied edge velocities each average stress-average strain diagram is supported by two images of the collapse modes, which corresponds to the ultimate (top image) and to the post-ultimate ($\epsilon_x/\epsilon_Y = 3$, bottom image) stress states. Performed investigations on the dynamic collapse behavior provided the interesting results: collapse modes and the corresponding stress-strain relationships of the thin plate, Figure 27 (2), (3), differ from the typical buckling behavior. Indeed, the square plate with thickness of 11 mm and slenderness ratio $\beta = 3.5$ tends to build a plateau in loading direction in the post-buckling regime instead of the expected roof shape. Moreover, this tendency depend on the applied velocity values: before reaching the certain “critical” velocity, the examined 11 mm square plate shows the classical roof mode (here at applied velocity of 10 mm/s). Increasing the applied velocity up to 20 mm/s, the collapse mode changes from the roof mode to the plateau that provides the decrease of the load-carrying capacity (see the corresponding average stress-average strain curves). Therefore, the ISUM NMK and ISUM CDM curves differ from the FEM curve in the post-ultimate strength range, since the implemented ISUM parameter f , which is responsible for the current shape function representation, see Eq. 6, is tuned for the formation of the roof mode in the post-buckling regime, [18]. Setting the parameter f zero does not provide any positive changes, (see curve ISUM NMK $f = 0$, Figure 27 (3)). The other examined 15.5 and 19 mm square plates with slenderness ratios $\beta = 2.5$ and 2 respectively do not show any changes in the collapse modes even at the high applied velocity of 100 mm/s. ISUM NMK and ISUM CDM curves follow the FEM solution very well, Figures 28 and 29.



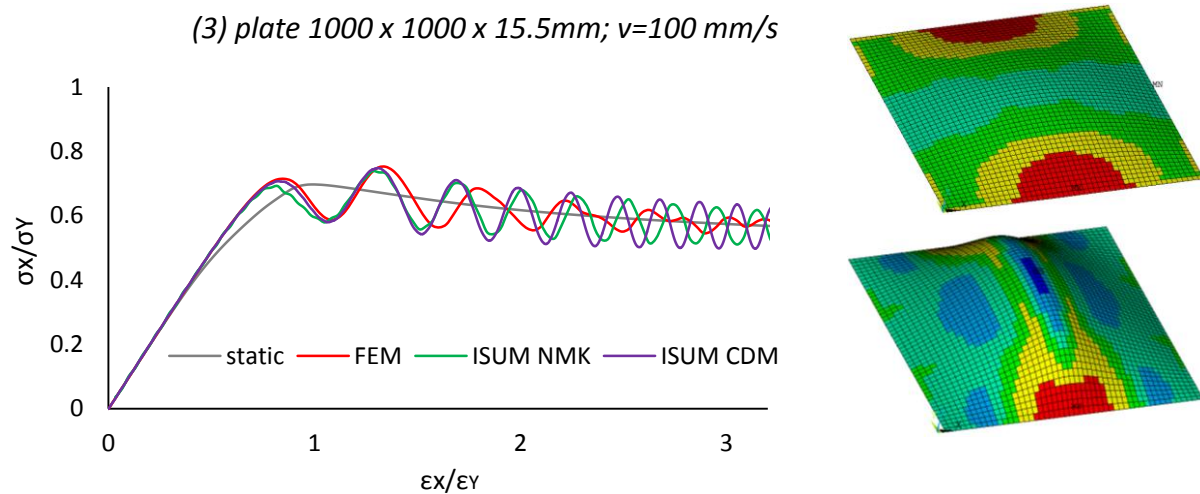
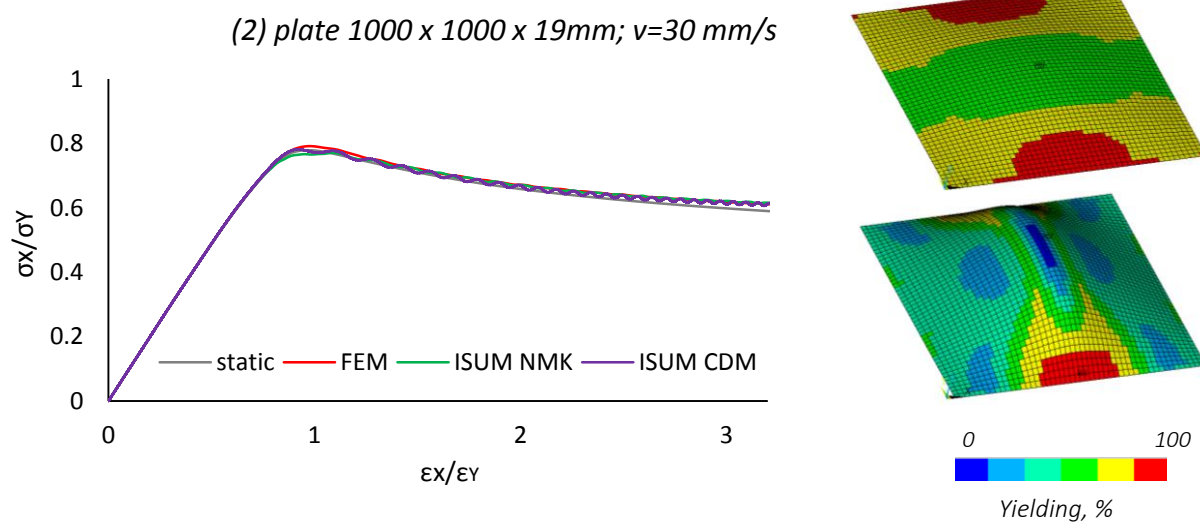
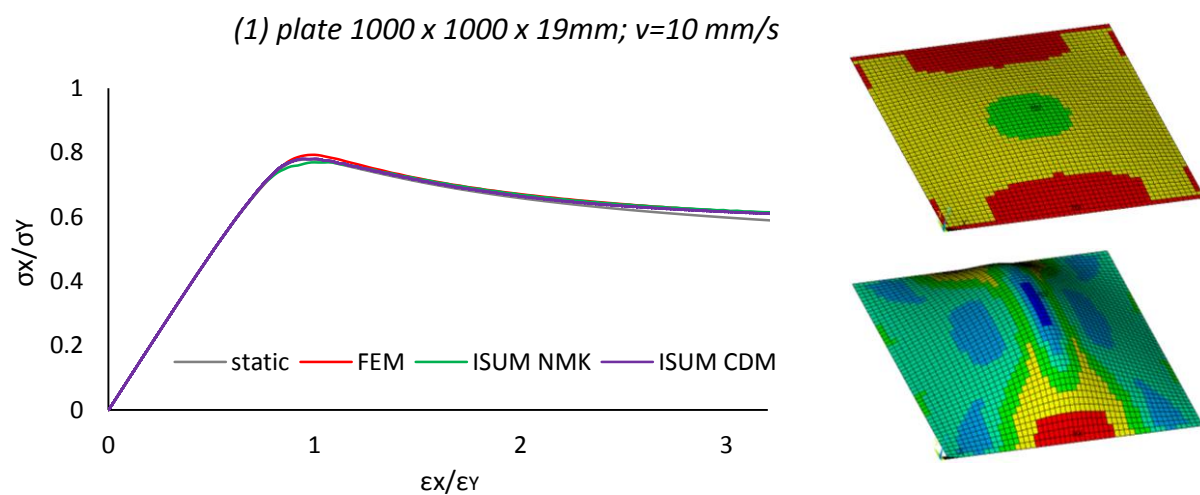


Figure 28 (1)-(3): Dynamic collapse behavior of the 15.5 mm square plate under uniaxial thrust



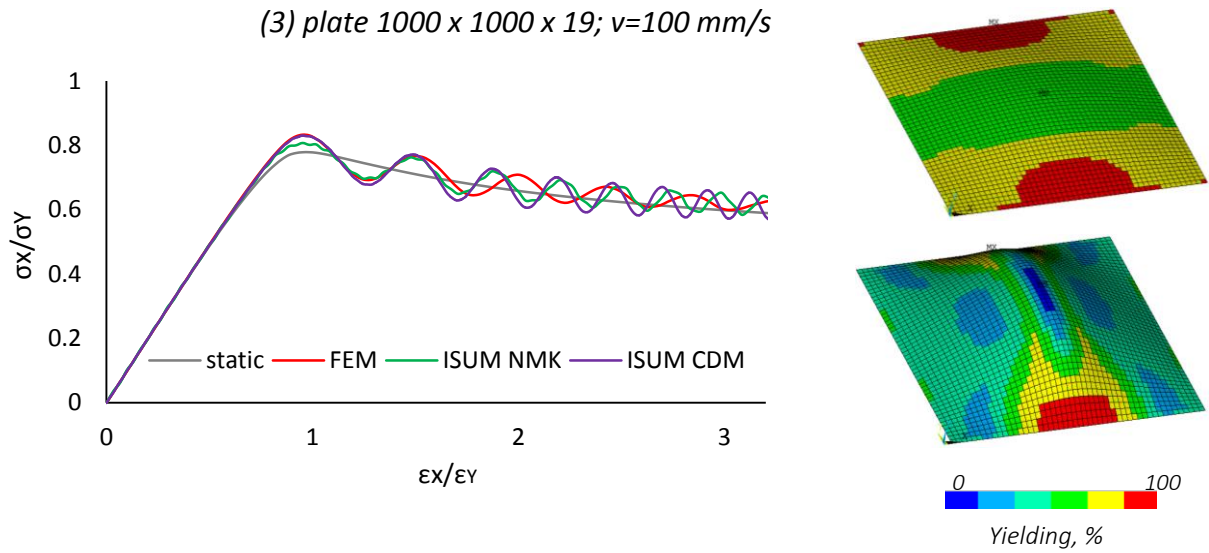


Figure 29 (1)-(3): Dynamic collapse behavior of the 19 mm square plate under uniaxial thrust

At the high applied edge velocity of 100 mm/s the average stress - average strain curves oscillate with a significant amplitude around the static solution. Therefore, the maximum applied dynamic thrust that the prescribed structure can withstand turns to be 12% higher (for 15 mm square plate) than in case of the static load application. The ISUM NMK and ISUM CDM solutions predict this ultimate strength level with a great accuracy; at the high applied edge velocities one can distinguish that the ISUM NMK and ISUM CDM curves slightly overtake the FEM curve, starting from the average strains $\epsilon_x/\epsilon_Y < 1.5 \div 2$.

Summarizing the presented results one can conclude that the dynamic collapse behavior of the square plate panels with the slenderness ratio $\beta < 3$ can be unrestrictedly analyzed using the Idealized Structural Method. Square plate panels with the slenderness ratio $3 \leq \beta \leq 3.5$ belong to the intermediate category and the simulation of the dynamic collapse behavior within the up to date ISUM provides reliable results only for low applied edge velocity values. For thin square plate panels with the slenderness ratio $\beta > 3.5 \div 3.7$ the roof mode does not take place at any applied velocity since even performing the static analysis other complicated collapse modes come up, [29].

6.3 Dynamic Collapse Analyses of Rectangular Panels under Longitudinal Thrust

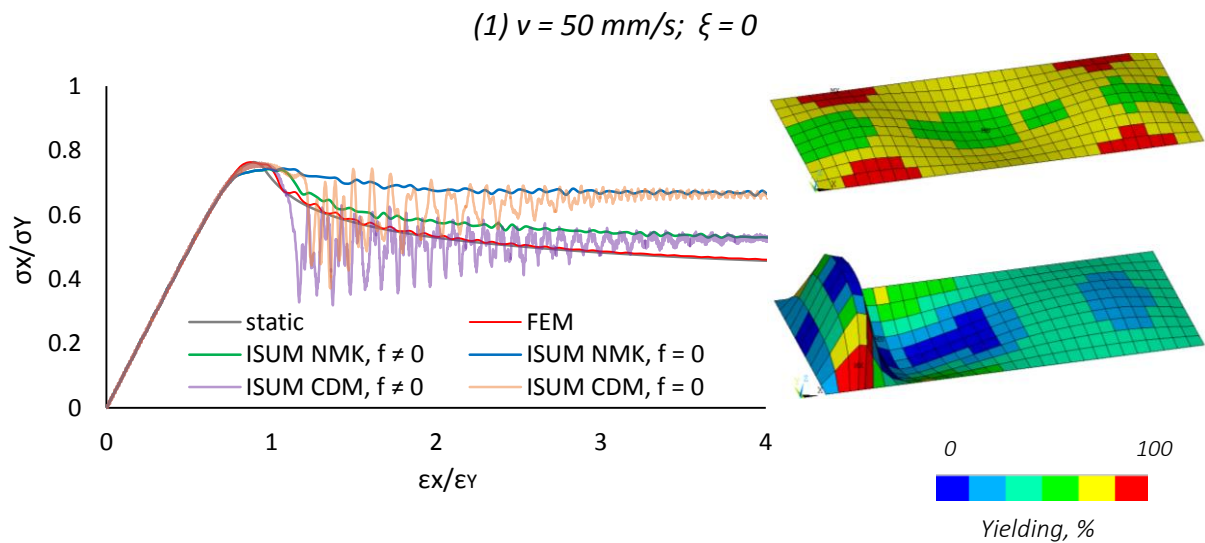
The rectangular plate panel is a common structural member of a ship. It is part of the bottom, side and deck plating, stiffened by framing for collapse prevention. According to the Common Structural Rules, [4], if a ship's length exceeds 120 m, it is preferable to adopt a longitudinal frame system. Besides, tankers greater than 200 m in length must be framed longitudinally. In this case, performance of the structural analysis of the deck and bottom plating subjected to the compressive stresses represents the analysis of the rectangular plate panels under longitudinal thrust. Within the present subchapter, the dynamic collapse behavior of three rectangular plate panels is considered.

6.3.1 Plate Panel 2400 x 835 x 15 mm

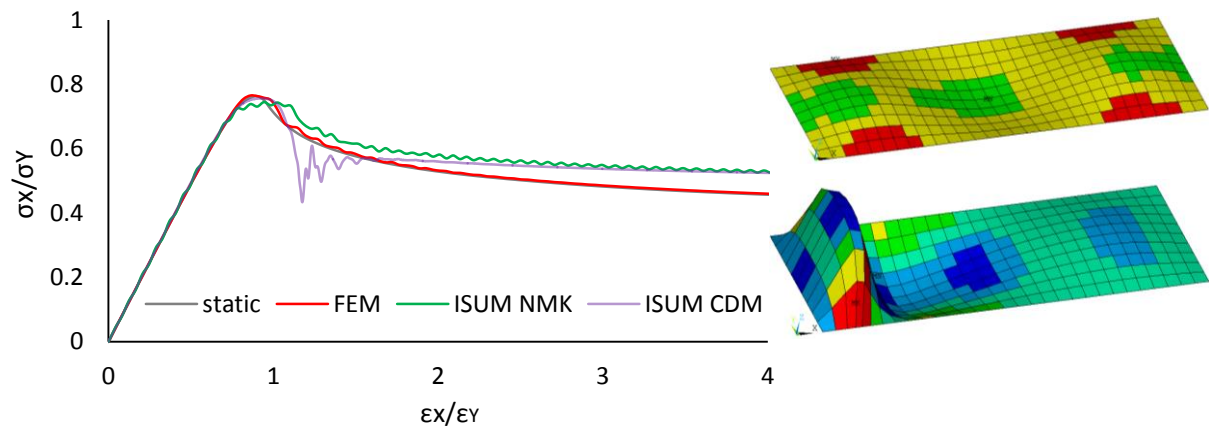
Dynamic collapse behavior of the rectangular plate is presented in Figure 30 (1)-(6). Analogously to the previous subchapter, the given images of the collapse modes correspond to the ultimate (top image) and to the post-ultimate ($\varepsilon_x/\varepsilon_Y = 4$, bottom image) stress states. The initial deflection values of the FE-model are presented in Table 3. Consistent mass matrix is obtained from Eq. 65 with appropriate shape functions, Eq. 70. Time step values Δt for each test case are assumed as follows:

applied edge velocity	ISUM NMK	ISUM CDM	FEM
50 mm/s	$3.0 \cdot 10^{-3}$	$3.0 \cdot 10^{-5}$	$3.0 \cdot 10^{-3}$
100 mm/s	$1.5 \cdot 10^{-3}$	$1.5 \cdot 10^{-5}$	$1.5 \cdot 10^{-3}$
200 mm/s	$7.5 \cdot 10^{-4}$	$7.5 \cdot 10^{-6}$	$7.5 \cdot 10^{-4}$

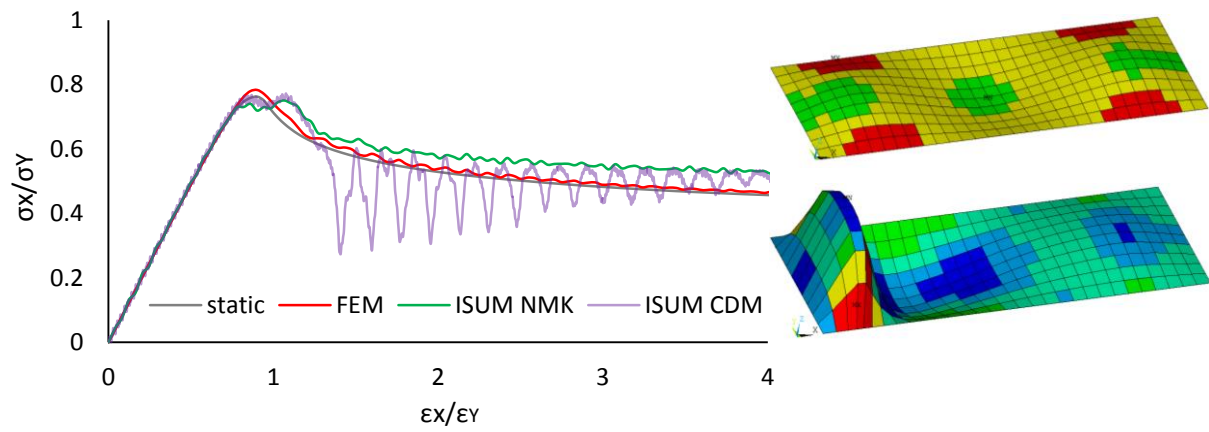
For all applied edge velocity values of 50 mm/s, 100 mm/s and 200 mm/s the ISUM CDM solution supplies high, frequent oscillation of the average stress-average strength curve, which starts from the ultimate strength and goes through the whole post-buckling range. To check the influence of the specially developed shape function, which enables the transformation of the buckling mode from sinusoidal to the roof mode within one half-wave [18], the parameter f was set on zero, Figure 30 (1). In this case, all three half-waves of ISUM plate model have the same amplitude A_l . As one can see, the ISUM CDM $f = 0$ and the ISUM CDM $f \neq 0$ curves have the similar behavior, featuring significant oscillations. This fact excludes the possible influence of the shape-parameter f on the heightening of the oscillations, performing the explicit time integration scheme.



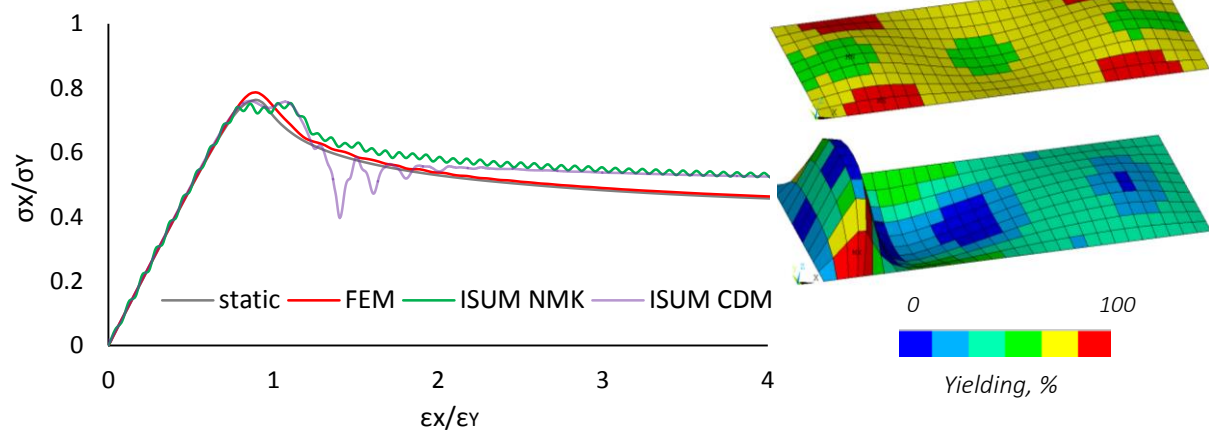
(2) $v = 50 \text{ mm/s}$; $\xi = 0.05$



(3) $v = 100 \text{ mm/s}$; $\xi = 0$



(4) $v = 100 \text{ mm/s}$; $\xi = 0.05$



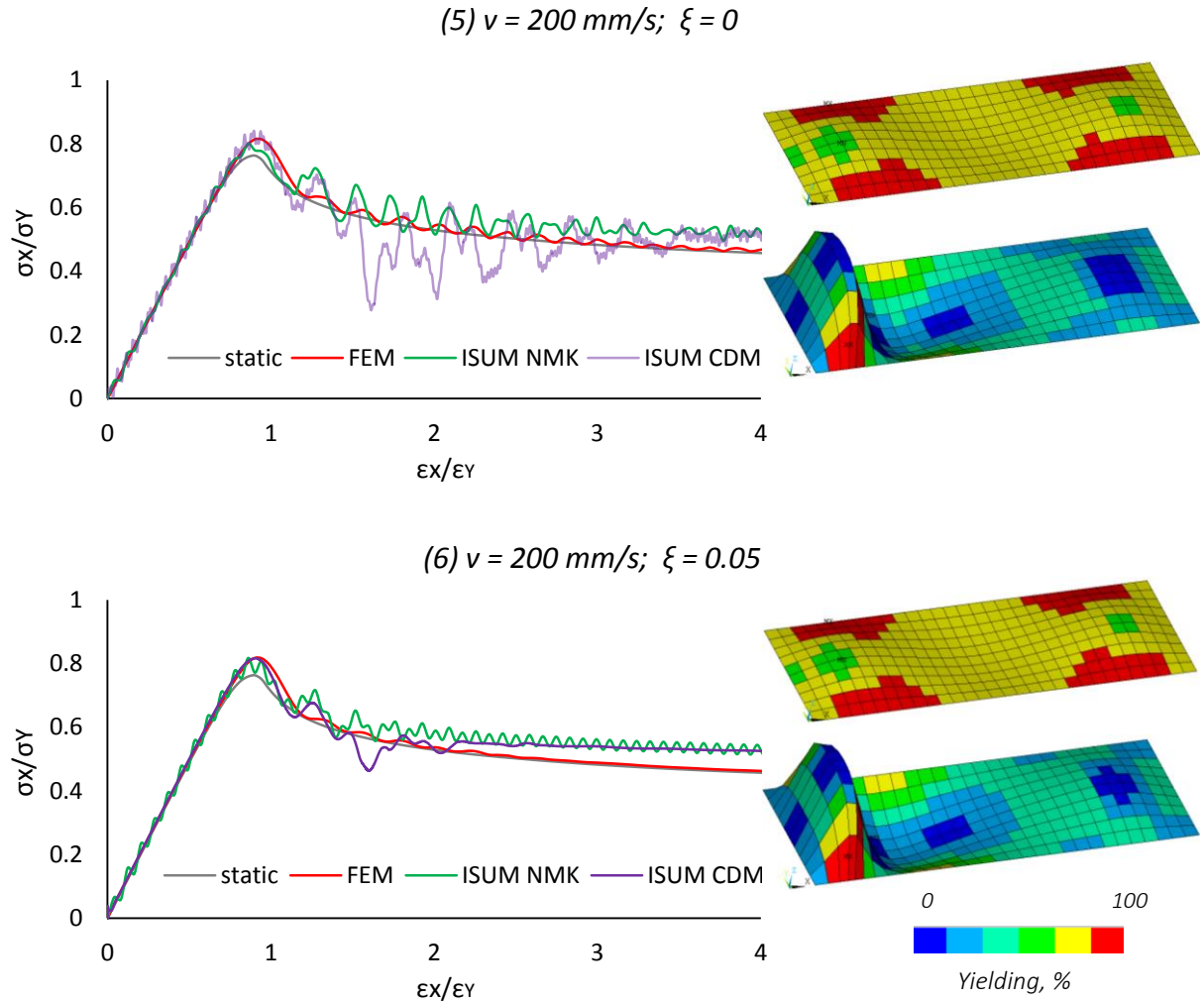


Figure 30 (1)-(6): Dynamic collapse behavior of longitudinally loaded plate 2400 x 835 x 15 mm

The consideration of the damping forces helps to avoid the excessive oscillations of the ISUM CDM solution. In this case, for all applied edge velocities one can distinguish one major peak direct after the ultimate strength, but then the solution stabilizes, Figure 30 (2), (4). Even for the highest applied edge velocity of 200 mm/s one cannot observe such an apparent oscillative manner of the average strength-average strain curve as in case of the square plate. Nevertheless, the 6.7 % rise of the ultimate strength is detected compared with the static load application case.

Having performed the dynamic collapse analysis of the rectangular plate panel one can conclude that the ISUM NMK and ISUM CDM results are very similar to the FEM solution for all applied velocities. Buckling behavior stays invariant to the increase of the applied edge velocity and remains as it was by the static calculations: one half-wave collapses and the rest of the plate unloads. However, rise of the applied edge velocity leads to the increase of the ultimate strength. This can be seen from the average stress-average strength curve and from the figures, which show the spread of yielding at the middle surface of the plate panel. The excessive implausible oscillations, which come up performing the explicit time integration (see ISUM CDM curve), can be prevented taking damping into account. The explicit solution can be very effectively damped so that any oscillations disappear in the post-buckling range. Unfortunately, the same conclusion cannot be made relative to the implicit scheme, since the tiny frequent oscillations stay in spite of the employed damping.

Trying to avoid the oscillations of the explicit solution (without considering of damping, $\xi = 0$) and of the implicit solution (with presence of damping, $\xi = 0.05$), it was decided to reduce the integration time step Δt for the both methods. Exemplary, the dynamic buckling behavior of the rectangular plate panel under the applied velocity of 200 mm/s is considered, Figure 31. The prescribed attempt does not supply any qualitative changes, since the oscillations are still present on the diagram. In case of the implicit time integration scheme, the oscillations have even become more frequent.

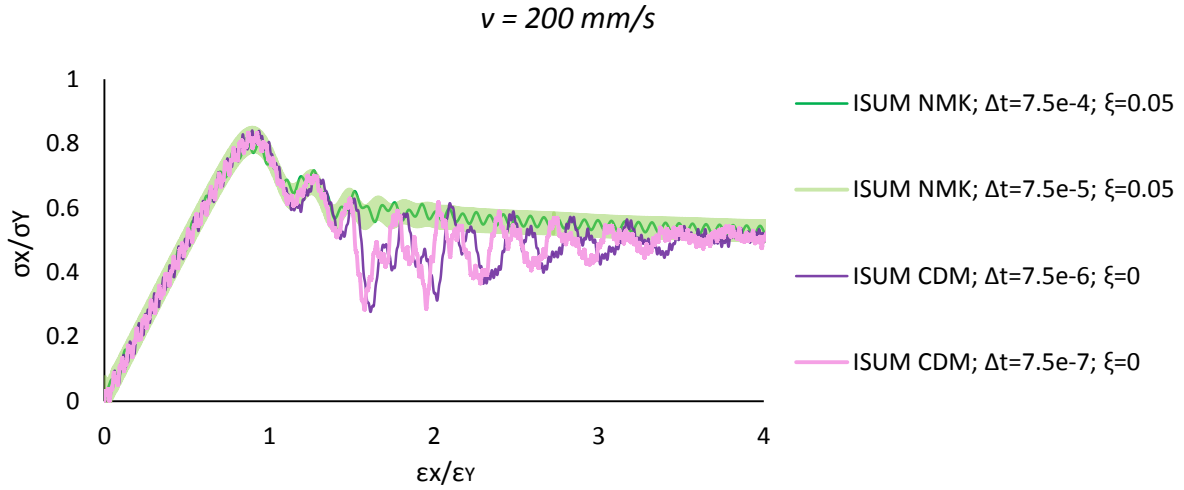


Figure 31: Influence of the reduced time step on the ISUM NMK and ISUM CDM oscillations

6.3.2 Plate Panel $4200 \times 835 \times 13 \text{ mm}$

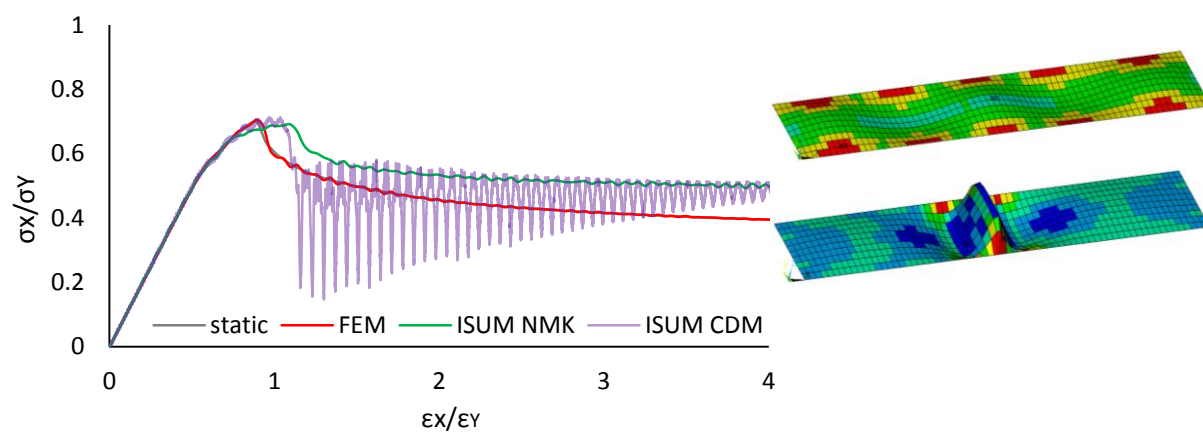
Dynamic collapse behavior of the rectangular plate is presented in Figure 32 (1)-(6). Analogously to the previous subchapter, the given images of the collapse modes correspond to the ultimate (top image) and to the post-ultimate ($\varepsilon_x/\varepsilon_y = 4$, bottom image) stress states. Consistent mass matrix is obtained from Eq. 65 with appropriate shape functions, Eq. 70. The initial deflection values of the FE-model are presented in Table 8. Time step values Δt for each test case are assumed as follows:

applied edge velocity	ISUM NMK	ISUM CDM	FEM
50 mm/s	$5.2 \cdot 10^{-3}$	$5.2 \cdot 10^{-5}$	$5.2 \cdot 10^{-3}$
100 mm/s	$2.6 \cdot 10^{-3}$	$2.6 \cdot 10^{-5}$	$2.6 \cdot 10^{-3}$
200 mm/s	$1.3 \cdot 10^{-4}$	$1.3 \cdot 10^{-6}$	$1.3 \cdot 10^{-4}$

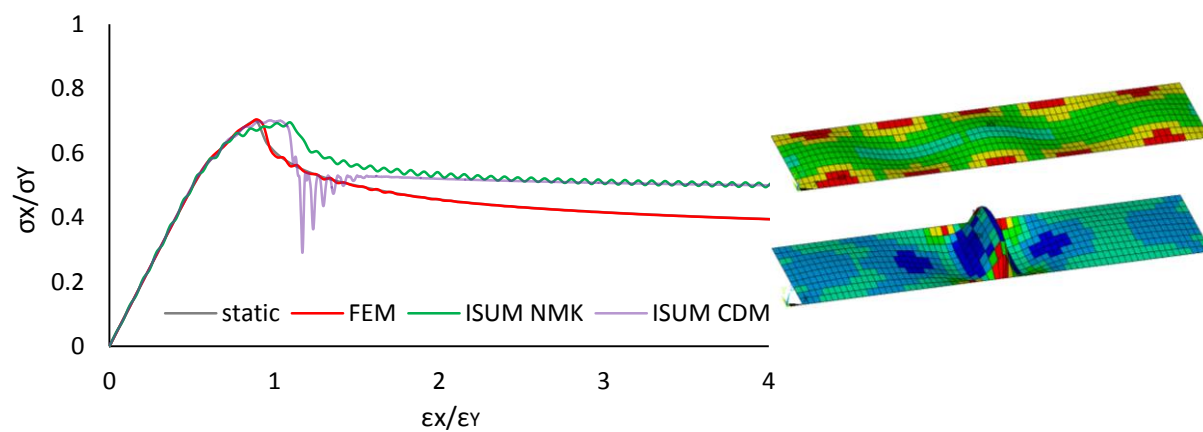
Table 8: Coefficients A_{0i} , [mm] for initial deflection definition of rectangular plate $4200 \times 835 \times 13 \text{ mm}$

A_{01}	A_{02}	A_{03}	A_{04}	A_{05}	A_{06}	A_{07}	A_{08}	A_{09}	A_{010}	A_{011}
1.862	0.3439	1.0984	0.3603	0.5491	0.2338	0.1545	0.0026	0.164	-0.0081	-0.0597

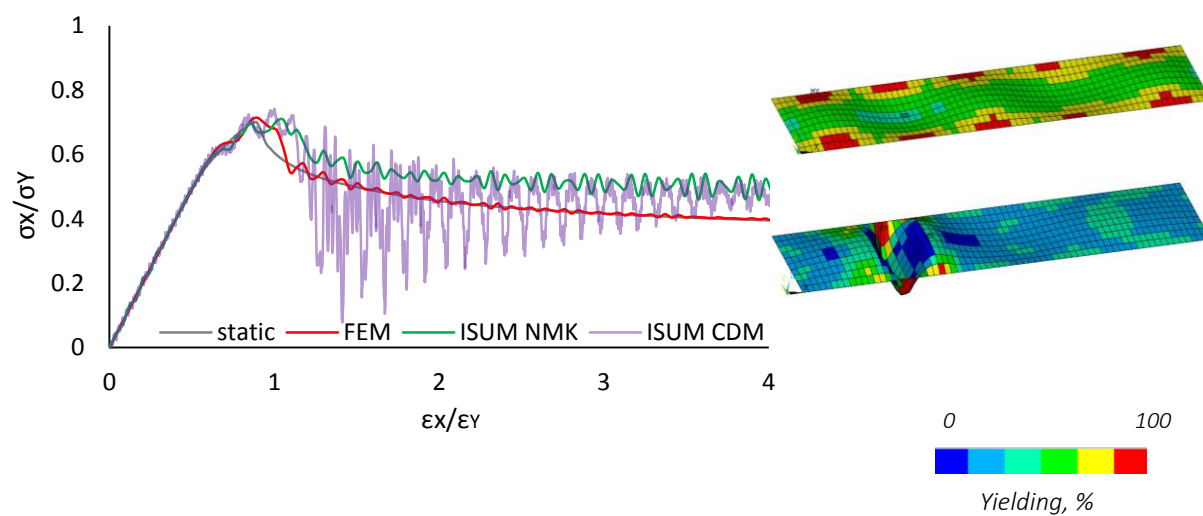
(1) $v = 50 \text{ mm/s}$; $\xi = 0$



(2) $v = 50 \text{ mm/s}$; $\xi = 0.05$



(3) $v = 100 \text{ mm/s}$; $\xi = 0$



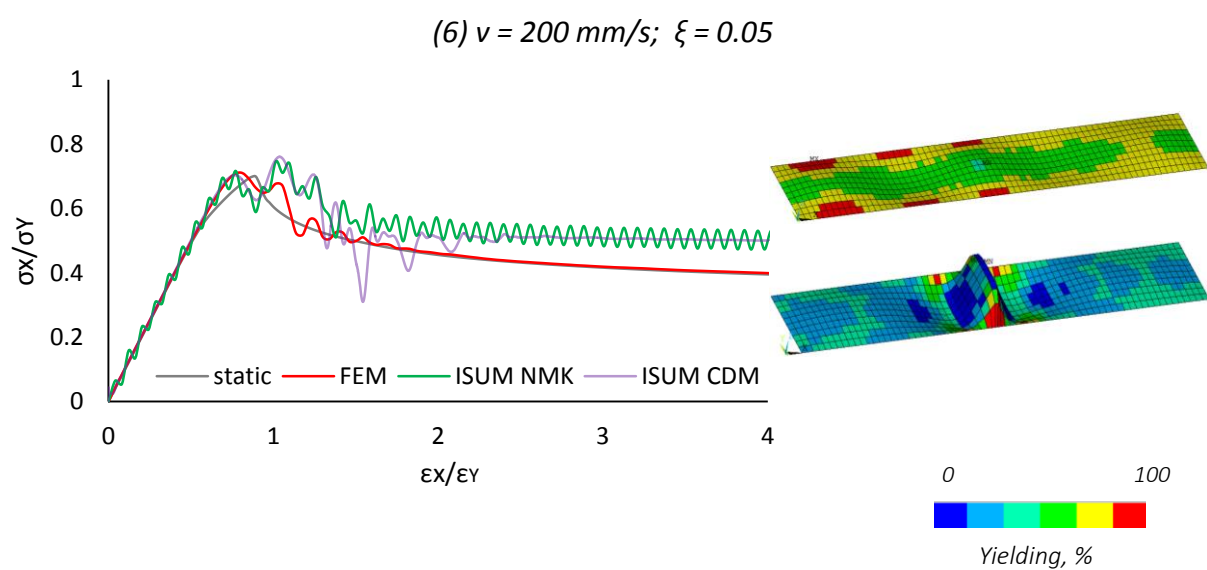
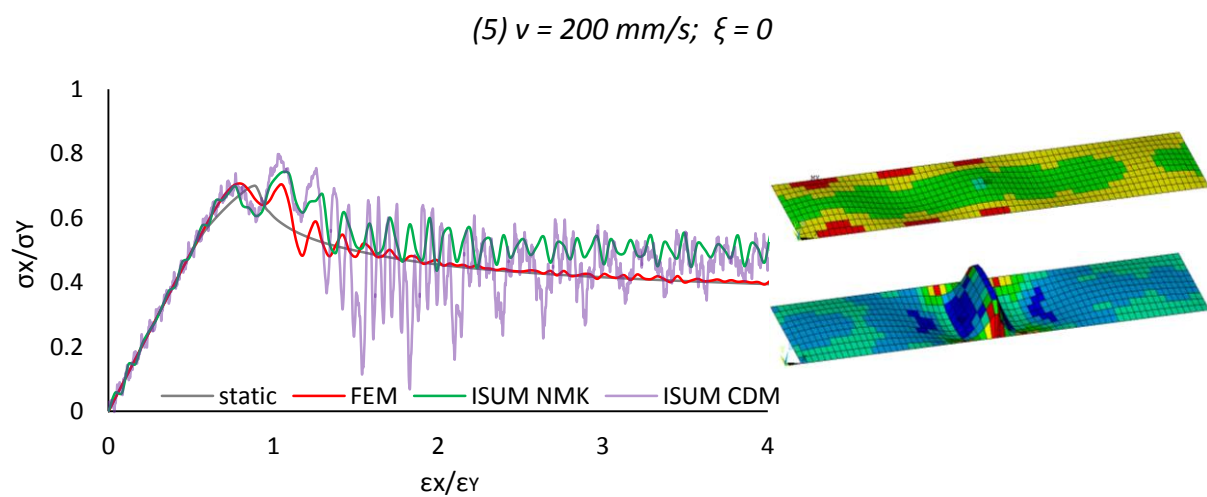
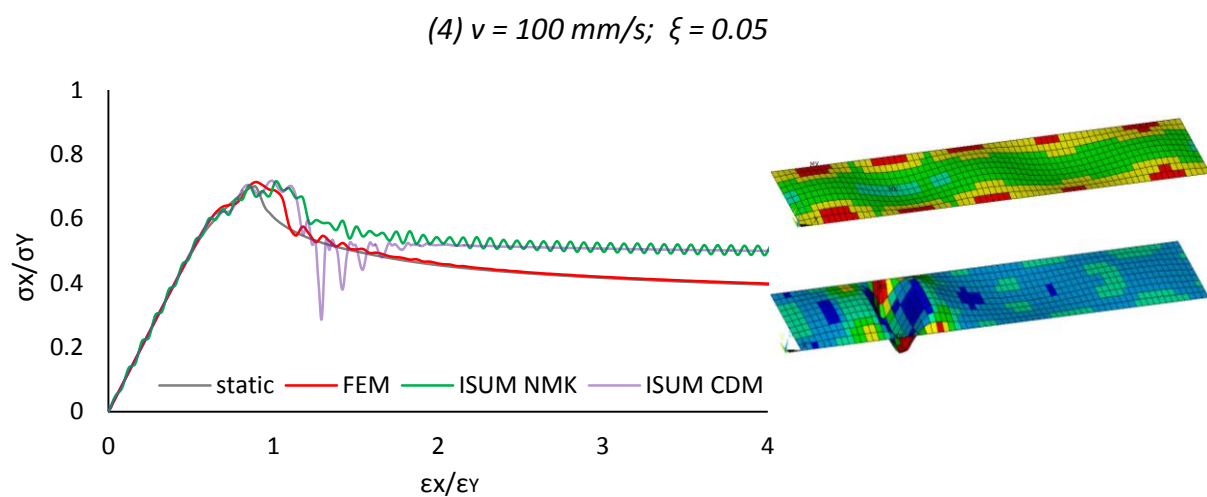


Figure 32 (1)-(6): Dynamic collapse behavior of longitudinally loaded plate 4200 x 835 x 13 mm

The dynamic collapse behavior of the presented rectangular plate is very similar to the dynamic collapse behavior of the rectangular plate, examined in the previous subchapter (2400 x 835 x 15 mm). For all applied edge velocity values of 50 mm/s, 100 mm/s and 200 mm/s the ISUM CDM solution provides strong oscillations of the stress-strain curve, which can be avoided by including the damping effects. At the applied velocity of 50 mm/s the middle half-wave starts its transformation from the sinusoidal to the roof mode at the post-buckling regime that causes the loss of the load-carrying capacity, Figure 32 (1), (2).

At the applied velocity of 100 mm/s the collapsing half-wave is no more in the middle of the rectangular plate, in comparison with the other test cases (50 mm/s, and 200 mm/s). It develops within the second half-wave, near to the left edge. However, this difference in direction and location of the collapsing half-wave does not influence on the average stress-average strain relationship, Figure 32 (3), (4).

At the applied velocity of 200 mm/s one can observe the significant oscillations of the average stress-average strain curves at the ultimate strength and direct after it. These oscillations lead to a relocation of the stresses, slightly modifying the buckling mode: the right-hand side of the rectangular plate unloads at ultimate strength, Figure 32 (5), (6).

Although the slenderness ratio of $\beta = 2.5$ is in the range of suitable values for the ISUM formulation, subchapter 6.2, for the considered rectangular plate panel one can notice that the ISUM NMK and ISUM CDM solutions start to depart from the FEM curve at the ultimate strength, and then, with the growth of the deformations this difference becomes significant (up to 28 % at the average strength $\varepsilon_x/\varepsilon_y = 4$). The same phenomenon was observed during the investigations on the dynamic collapse behavior of 11 mm square plate with the slenderness ratio $\beta = 3.5$. This means that the ISUM overestimates the stresses, which the prescribed thin plates can withstand. Thereby, further improvements of the shape function may be performed to enable the dynamic collapse analysis of thin plate panels.

6.3.3 Plate Panel 4200 x 835 x 22 mm

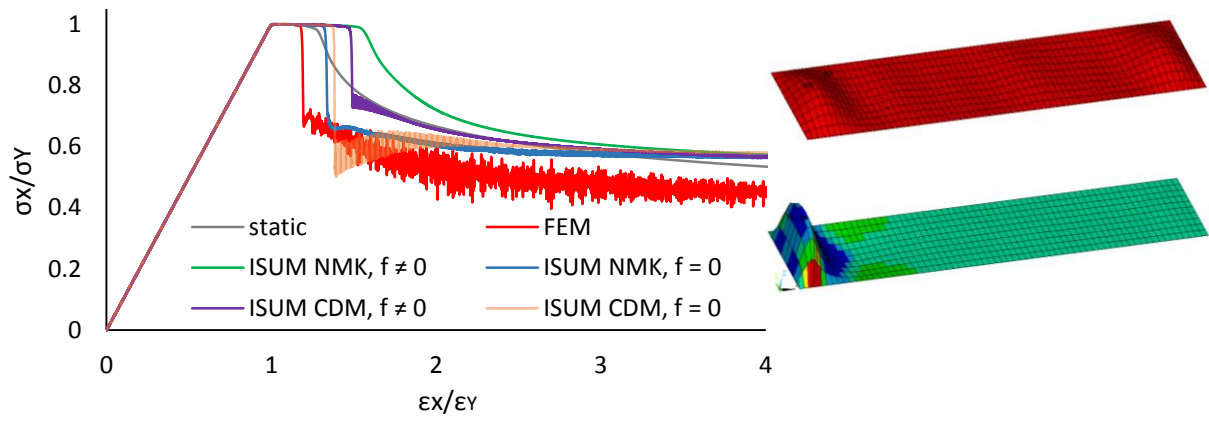
Dynamic collapse behavior of the rectangular plate is presented in Figure 33 (1)-(6). Introduced collapse modes correspond to the ultimate (top image) and to the post-ultimate ($\varepsilon_x/\varepsilon_y = 4$, bottom image) stress states, except for Figure 33 (5). Consistent mass matrix is obtained from Eq. 65 with appropriate shape functions, Eq. 70. The initial deflection values of the FE-model are presented in Table 9. Time step values Δt for each test case are assumed as follows:

<i>applied edge velocity</i>	<i>ISUM NMK</i>	<i>ISUM CDM</i>	<i>FEM</i>
10 mm/s	$2.6 \cdot 10^{-4}$	$2.6 \cdot 10^{-5}$	$2.6 \cdot 10^{-4}$
50 mm/s	$5.2 \cdot 10^{-4}$	$2.6 \cdot 10^{-5}$	$5.2 \cdot 10^{-4}$
100 mm/s	$2.6 \cdot 10^{-4}$	$2.6 \cdot 10^{-5}$	$2.6 \cdot 10^{-4}$

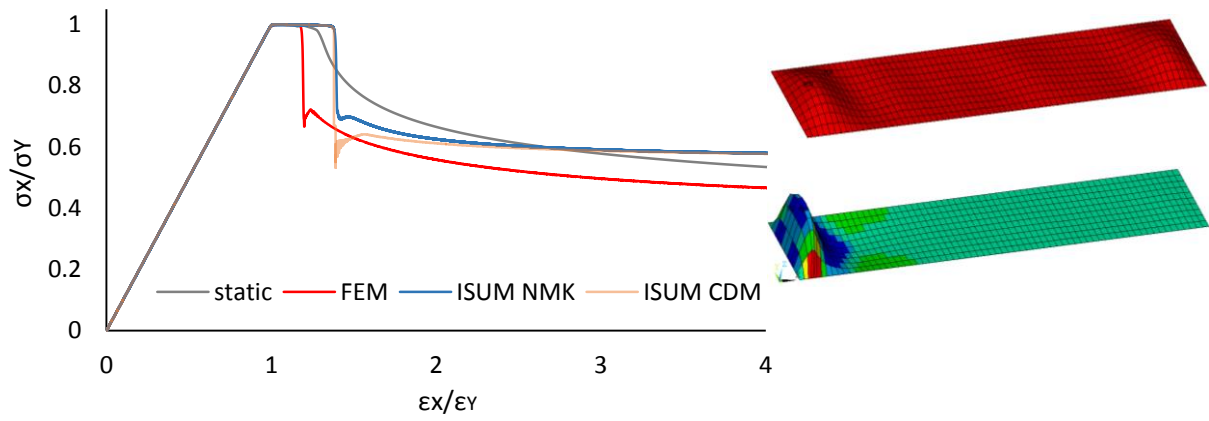
Table 9: Coefficients A_{0i} , [mm] for initial deflection definition of rectangular plate 4200 x 835 x 22 mm

A_{01}	A_{02}	A_{03}	A_{04}	A_{05}	A_{06}	A_{07}	A_{08}	A_{09}	A_{010}	A_{011}
0.4787	-0.04	0.1955	0.0585	0.1073	-0.0214	0.1294	0.026	0.0985	0.0285	0.0897

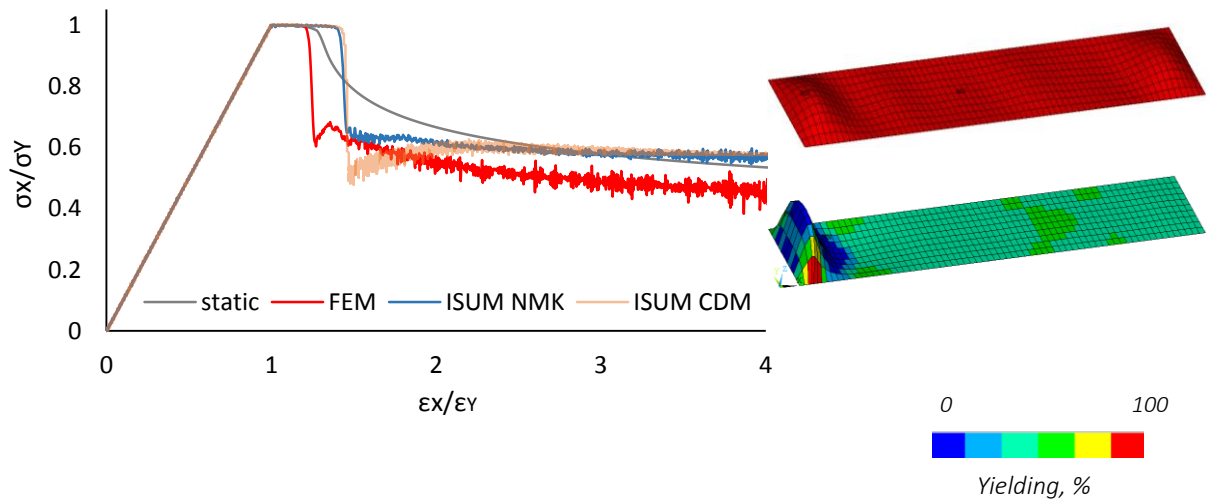
(1) $v = 10 \text{ mm/s}$; $\xi = 0$



(2) $v = 10 \text{ mm/s}$; $\xi = 0.05$



(3) $v = 50 \text{ mm/s}$; $\xi = 0$



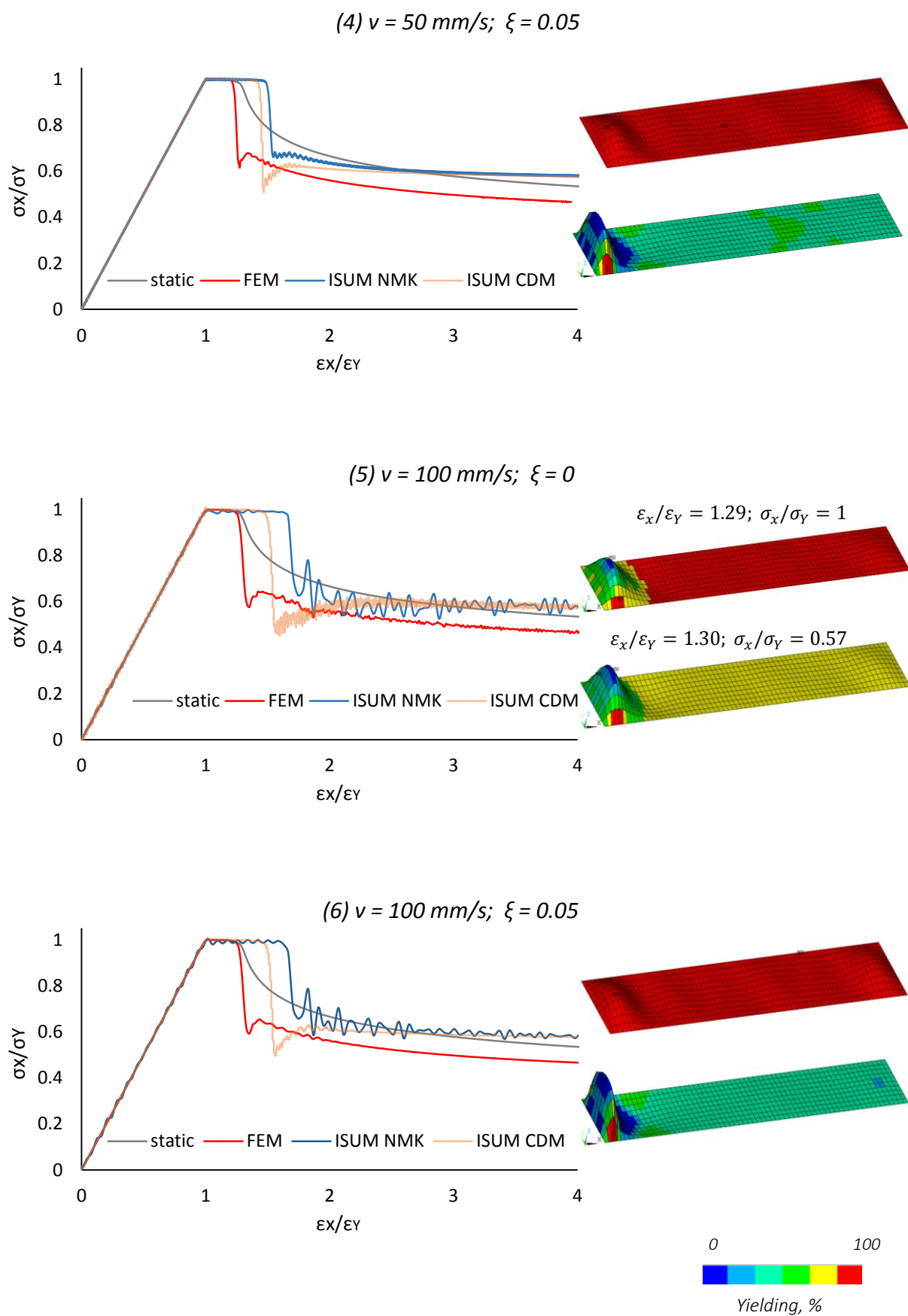


Figure 33 (1)-(6): Dynamic collapse behavior of longitudinally loaded plate 4200 x 835 x 22 mm

In the presented diagrams one can see that for all applied velocities of 10 mm/s, 50 mm/s and 100 mm/s the examined 22 mm rectangular plate panel undergoes plastic buckling. The collapsing half-wave starts its' transformation into the roof mode slightly beyond the ultimate strength, $\varepsilon_x/\varepsilon_Y \cong 1.3$. Then, the abrupt loss of the load-carrying capacity takes place and the rest of the plate unloads within a short period of time, Figure 33 (5). For the plate panels with an aspect ratio $a/b < 0.8$ per element (as the examined one) it may be better to use the old shape function, with the parameter f set to zero, Eq. 5, [36]. Indeed, for the ISUM solutions the parameter f set to zero provide better results as with non-zero parameter f , since the ISUM NMK $f = 0$ and ISUM CDM $f = 0$ curves are shifted closer to the FEM solution as the ISUM NMK $f \neq 0$ and ISUM CDM $f \neq 0$ curves, Figure 33 (1). The corresponding results with $f = 0$ are presented in the diagrams, Figure 33 (2)-(6). Nevertheless, there is a gap between the ISUM and FEM results at the ultimate strength region meaning that the ISUM solutions overestimate the load-carrying capacity of the examined plate panel. Consideration of the damping forces helps to avoid the additional oscillations of the stress-strain curves, Figure 33 (2), (4), (6). It is necessary to notice, that ISUM NMK curve lies closer to FEM solution than ISUM CDM curve for applied velocity $V = 10$ mm/s and $V = 50$ mm/s, Figure 33 (1)-(4). But at the higher applied velocity $V = 100$ mm/s the central difference method (ISUM CDM) supplies better results than Newmark's method (ISUM NMK), being closer to FEM and providing less oscillations, Figure 33 (5),(6). Therefore, one can make a conclusion that the explicit solver is more suitable for dynamic scenario with high frequent forces applied: impact loading caused by slamming, earthquake and crash simulations etc.

6.4 Dynamic Collapse Analyses of Rectangular Panels under Transverse Thrust

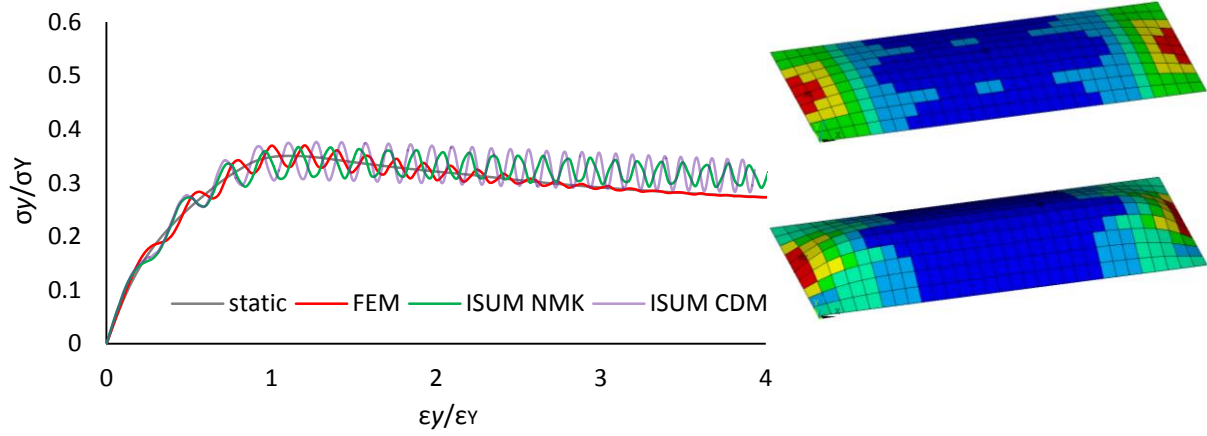
As it was mentioned in the previous subchapter, rectangular plate panel is an essential element of any shipbuilding structure. Plates of double bottom in longitudinal framing are subjected to compressive stresses under transverse bending, which includes hydrostatic pressure on the outer shell, weight of cargo load acting on the bottom structure, ballast water pressure inducing deformation of ballast tanks, etc. Thus, the dynamic collapse behavior of the three rectangular plate panels under transverse thrust is investigated within the present subchapter.

6.4.1 Plate Panel 2400 x 835 x 15 mm

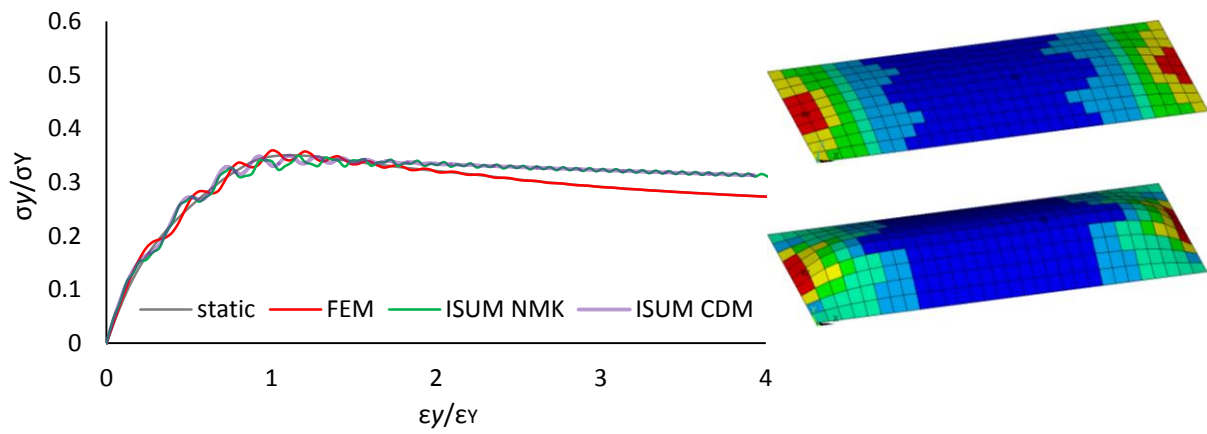
Dynamic collapse behavior of the rectangular plate is presented in Figure 34 (1)-(6). Analogously to the previous subchapter, the given images of the collapse modes correspond to the ultimate (top image) and to the post-ultimate ($\varepsilon_y/\varepsilon_Y = 4$, bottom image) stress states, except for Figure 34 (5). Consistent mass matrix is obtained from Eq. 65 with appropriate shape functions, Eq. 71. The initial deflection values of the FE-model are presented in Table 3. Time step values Δt for each test case are assumed as follows:

<i>applied edge velocity</i>	<i>ISUM NMK</i>	<i>ISUM CDM</i>	<i>FEM</i>
35 mm/s	$1.5 \cdot 10^{-3}$	$1.5 \cdot 10^{-5}$	$1.5 \cdot 10^{-3}$
50 mm/s	$1.0 \cdot 10^{-3}$	$1.0 \cdot 10^{-5}$	$1.0 \cdot 10^{-3}$
80 mm/s	$6.4 \cdot 10^{-4}$	$6.4 \cdot 10^{-6}$	$6.4 \cdot 10^{-4}$

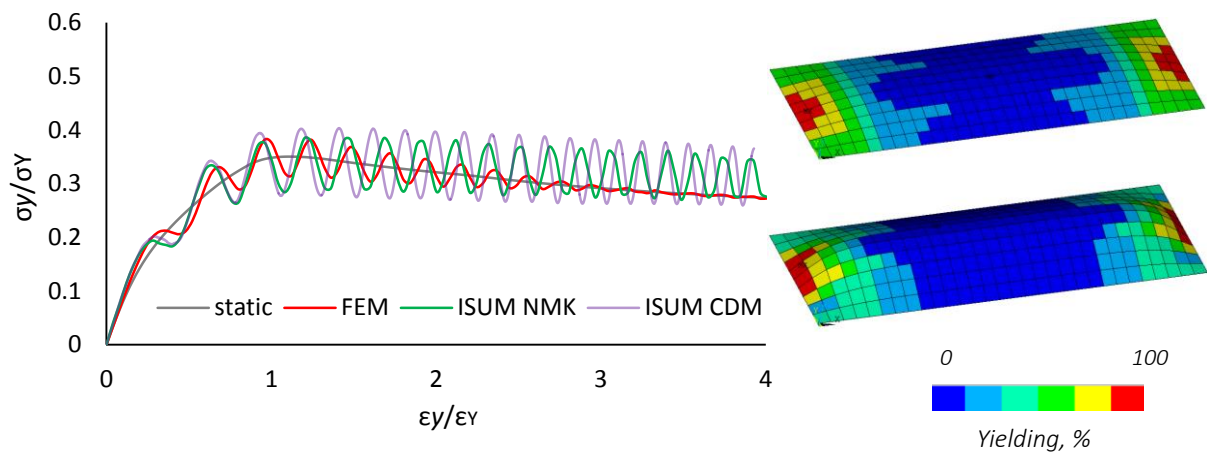
(1) $v = 35 \text{ mm/s}$; $\xi = 0$



(2) $v = 35 \text{ mm/s}$; $\xi = 0.05$



(3) $v = 50 \text{ mm/s}$; $\xi = 0$



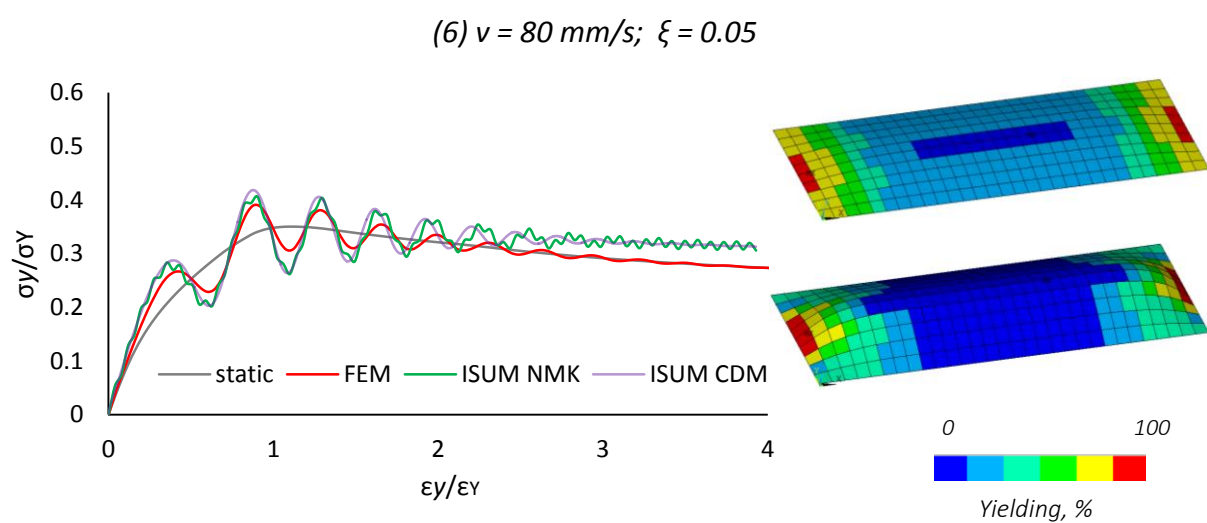
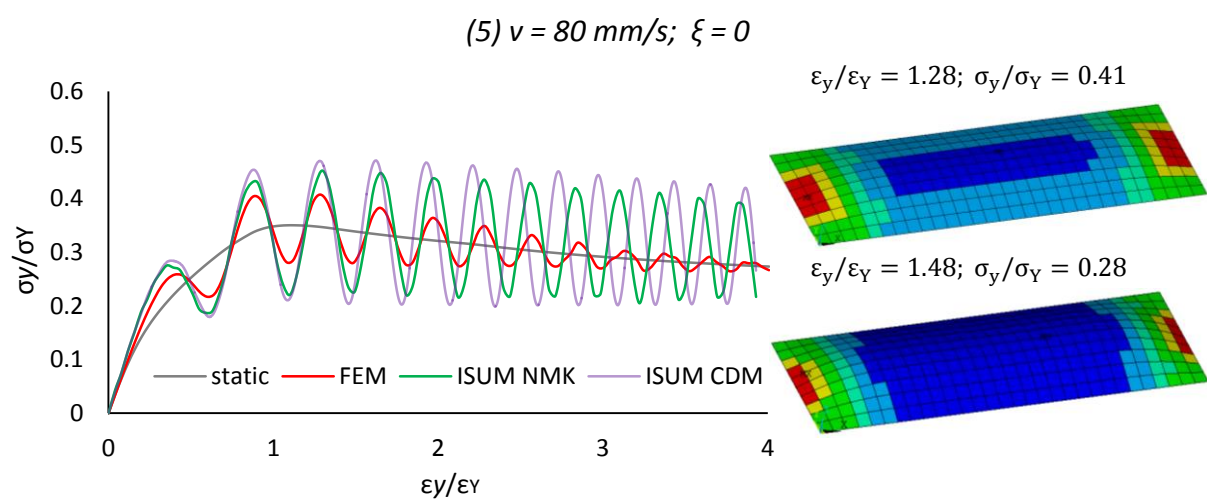
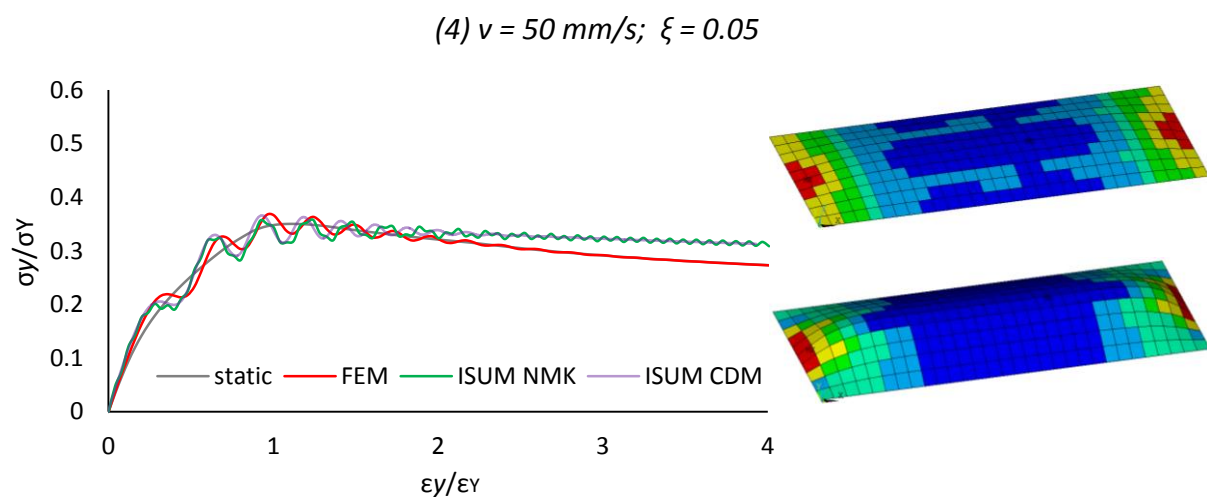


Figure 34 (1)-(6): Dynamic collapse behavior of transversely loaded plate 2400 x 835 x 15 mm

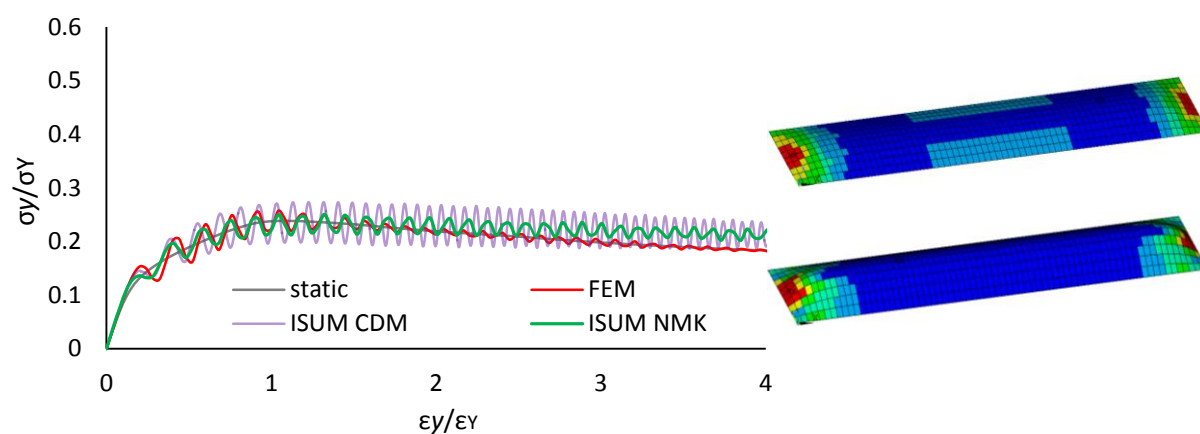
The first thing that catches the eye is that the load-carrying capacity of the examined rectangular plate panel under dynamic transverse thrust is significantly lower as in case of the dynamic longitudinal loading. Thus, the ultimate strength values of the analogous rectangular plate under dynamic longitudinal thrust are approximately two times higher than under dynamic transverse thrust. Nevertheless, one can see an apparent decrease of the load-carrying capacity of plates under longitudinal thrust: $\frac{\sigma_x|_{\varepsilon_x/\varepsilon_Y=1}}{\sigma_x|_{\varepsilon_x/\varepsilon_Y=4}} \approx 0.6$, while under transverse thrust the decrease of the load-carrying capacity is less distinct: $\frac{\sigma_y|_{\varepsilon_Y/\varepsilon_Y=1}}{\sigma_y|_{\varepsilon_Y/\varepsilon_Y=4}} \approx 0.8$. For all applied edge velocity values of 35 mm/s, 50 mm/s and 80 mm/s, buckling modes at the ultimate strength are represented by the cylindrical middle part and by the collapsing end parts, which behave as half of a square plate each. Beyond the ultimate strength, the roof-like mode develops due to the straightening in loading direction. Since the same collapse modes were introduced performing the static analysis of the rectangular plate panels [18], Figure 9, one can conclude that the transient effects do not influence the typical buckling modes of rectangular plates under transverse thrust. The strong oscillations of the average stress-average strength curve around the static solution provoke the reallocation of stresses; meanwhile the buckling shape stays invariant to the stress-jumps, Figure 34 (5). Compared with the static load application case, a 11 % rise of the ultimate strength of the prescribed rectangular plate is observed at the highest applied velocity of 80 mm/s. As for the reliability of the ISUM NMK and ISUM CDM results, one can see that the corresponding curves follow the FEM solution very well. The explicit ISUM CDM curve tend to overtake the ISUM NMK and FEM curves, which both represent implicit solutions. Nevertheless, the damping effects can be better introduced on an example of the explicit solution, since the ISUM CDM curve does not demonstrate any oscillation in the post-buckling regime.

6.4.2 Plate Panel 4200 x 835 x 13 mm

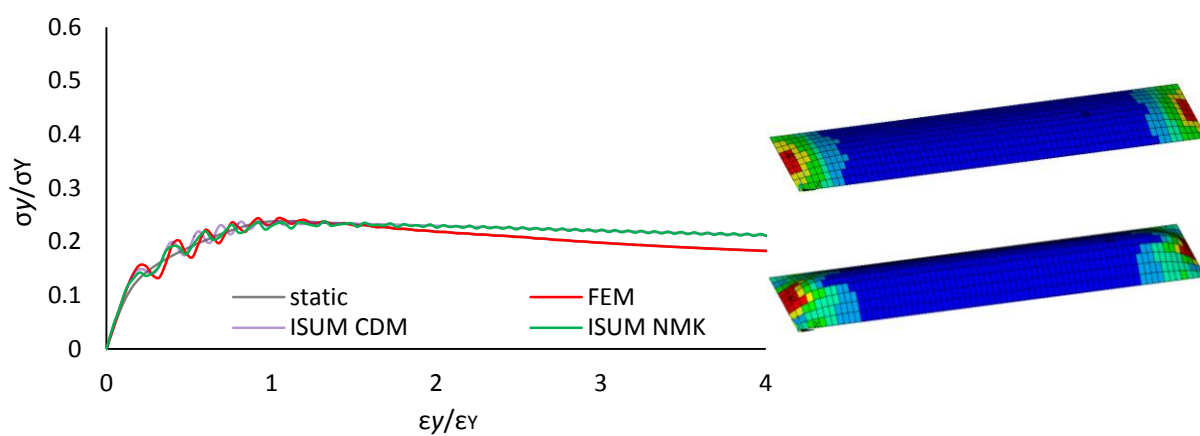
Dynamic collapse behavior of the rectangular plate is presented in Figure 35 (1)-(6). Images of the collapse modes correspond to the ultimate (top image) and to the post-ultimate ($\varepsilon_Y/\varepsilon_Y = 4$, bottom image) stress states. Consistent mass matrix is obtained from Eq. 65 with appropriate shape functions, Eq. 71. Initial deflection values of the FE-model are presented in Table 8. Time step values Δt for each test case are assumed as follows:

<i>applied edge velocity</i>	<i>ISUM NMK</i>	<i>ISUM CDM</i>	<i>FEM</i>
20 mm/s	$2.6 \cdot 10^{-3}$	$2.6 \cdot 10^{-5}$	$2.6 \cdot 10^{-3}$
50 mm/s	$1.0 \cdot 10^{-3}$	$1.0 \cdot 10^{-5}$	$1.0 \cdot 10^{-3}$
80 mm/s	$6.4 \cdot 10^{-4}$	$6.4 \cdot 10^{-6}$	$6.4 \cdot 10^{-4}$

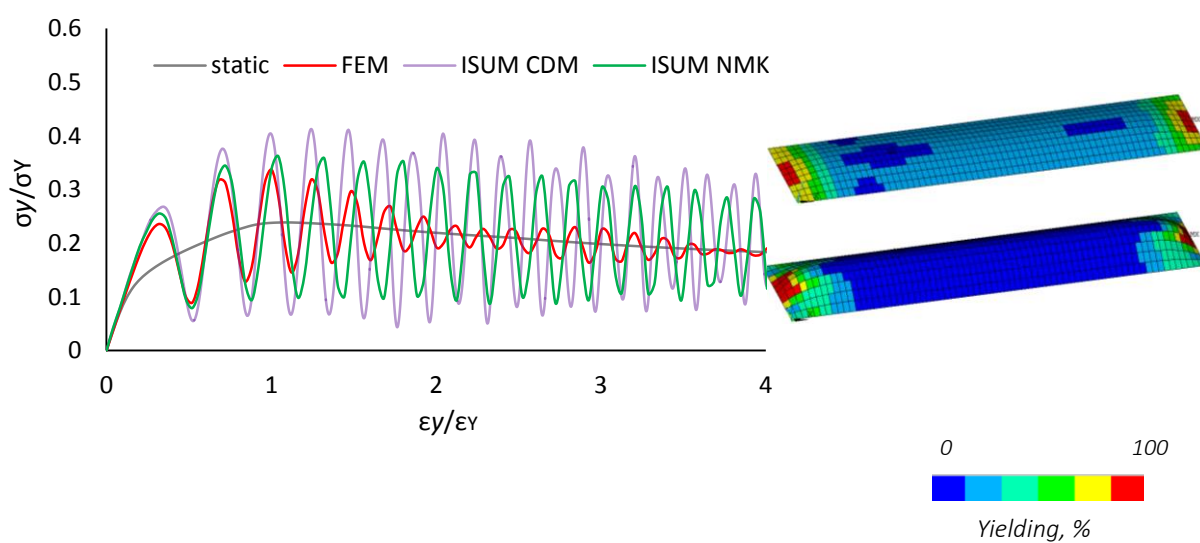
(1) $v = 20 \text{ mm/s}$; $\xi = 0$



(2) $v = 20 \text{ mm/s}$; $\xi = 0.05$



(3) $v = 50 \text{ mm/s}$; $\xi = 0$



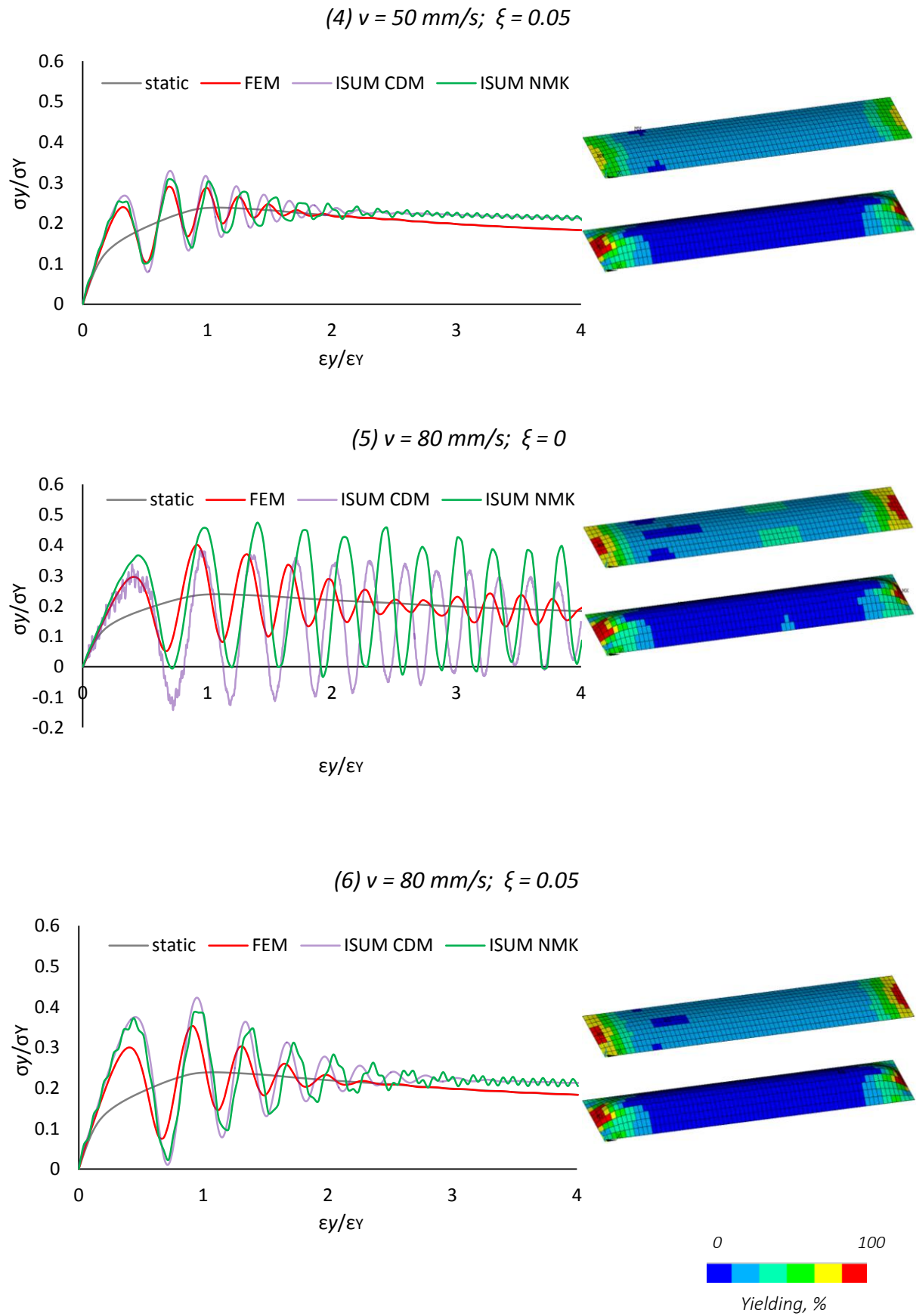


Figure 35 (1)-(6): Dynamic collapse behavior of transversely loaded plate 4200 x 835 x 13 mm

For the given 13 mm rectangular plate panel one can observe significant oscillations of the average stress-average strain curves around the static solutions. At the applied velocity of 80 mm/s, the ISUM CDM and ISUM NMK solutions even supply the negative average stress values meaning that the average stress is no more compressive, but tensile. To understand closer the nature of such a process let us consider the stress state of the prescribed plate panel under the applied velocity of 250 mm/s so that the FEM solution also goes to the negative range of the average stresses, Figure 36:

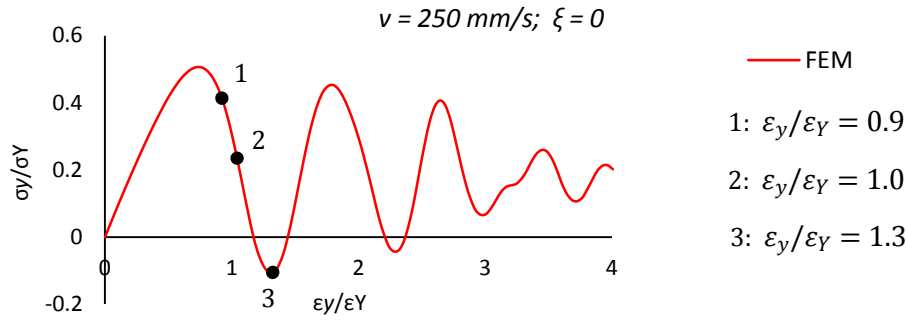


Figure 36: Collapse behavior of transversely loaded plate under high applied velocity of 250 mm/s

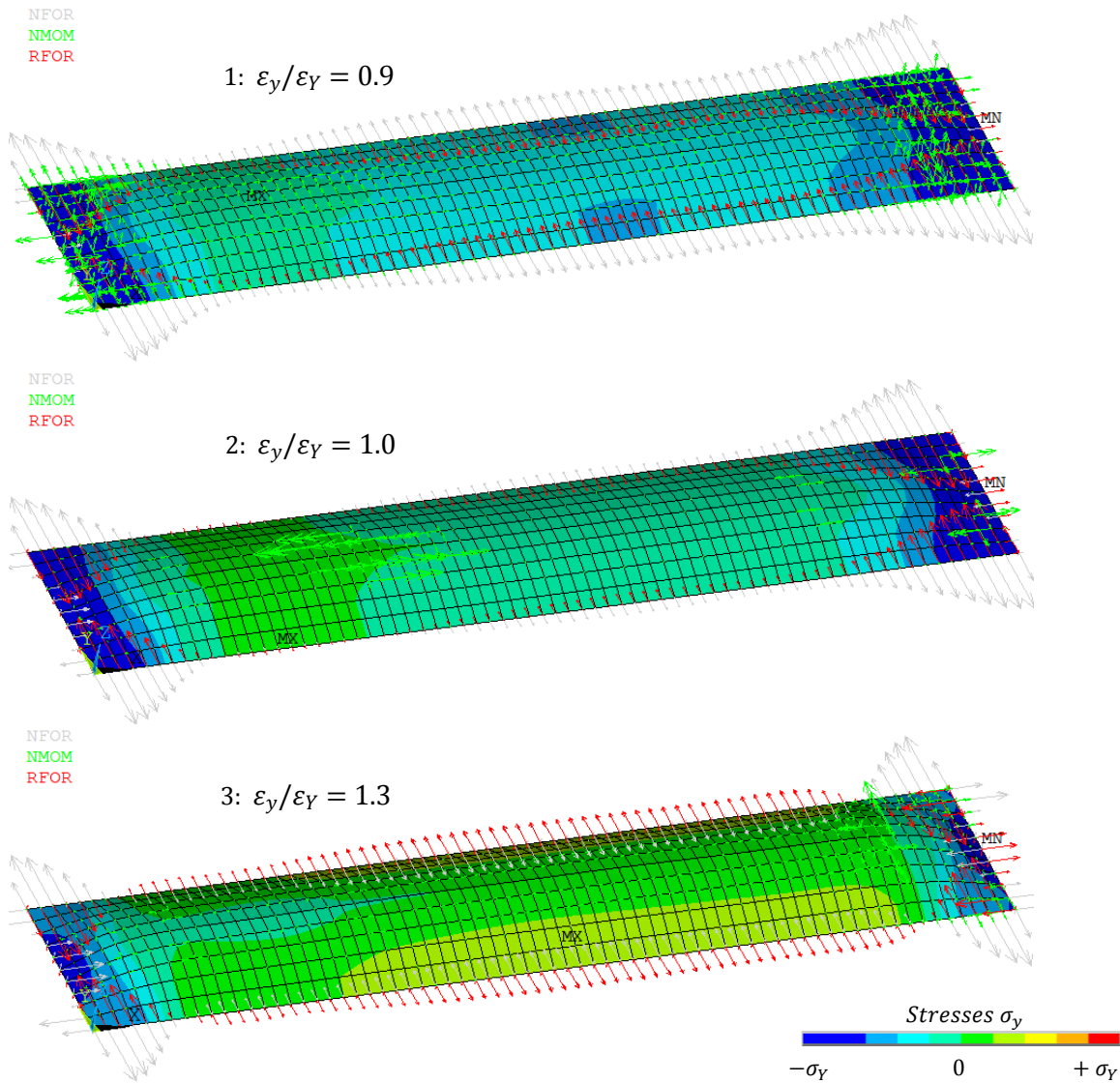


Figure 37: Collapse modes of transversely loaded plate under high applied velocity of 250 mm/s

At the average strain $\varepsilon_y/\varepsilon_Y = 0.9$, point 1 on the stress-strain diagram, the plotted in Figure 36 applied forces (red arrows) and the stresses σ_y are compressive. As the buckling develops and the prescribed plate straightens in loading direction, point 2 on the stress-strain diagram, a part of the forces changes the direction and becomes negative. Correspondingly, a zone with the tensile stresses develops on the left-hand side of the plate panel. Nevertheless, the sum of the total applied forces along the edge stays positive. At the average strain $\varepsilon_y/\varepsilon_Y = 1.3$, point 3 on the stress-strain diagram, a significant part of the forces becomes negative so that the sum of the total applied forces along the edge also becomes negative. In this case, the great part of the plate undergoes tension.

Coming back to the dynamic collapse analysis of the prescribed plate under applied velocities of 20 mm/s, 50 mm/s and 80 mm/s, the ISUM CDM and ISUM NMK solutions provide reliable results, when the damping forces are considered.

6.4.3 Plate Panel 4200 x 835 x 22 mm

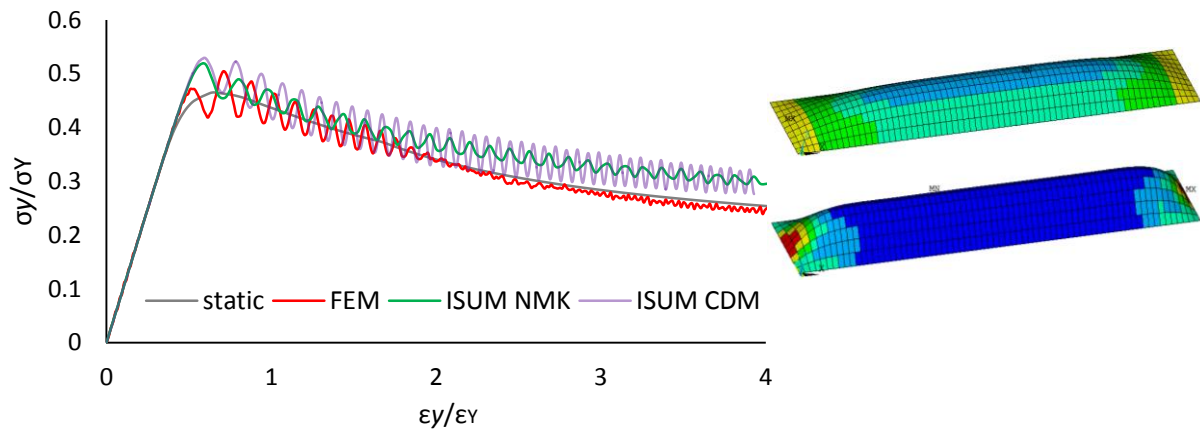
Dynamic collapse behavior of the rectangular plate is presented in Figure 38 (1)-(6). Images of the collapse modes correspond to the ultimate (top image) and to the post-ultimate ($\varepsilon_y/\varepsilon_Y = 4$, bottom image) stress states. Consistent mass matrix is obtained from Eq. 65 with appropriate shape functions, Eq. 71. Initial deflection values of the FE-model are presented in Table 9. Time step values Δt for each test case are assumed as follows:

<i>applied edge velocity</i>	<i>ISUM NMK</i>	<i>ISUM CDM</i>	<i>FEM</i>
20 mm/s	$2.6 \cdot 10^{-3}$	$2.6 \cdot 10^{-5}$	$2.6 \cdot 10^{-3}$
35 mm/s	$1.5 \cdot 10^{-3}$	$1.5 \cdot 10^{-5}$	$1.5 \cdot 10^{-3}$
50 mm/s	$1.0 \cdot 10^{-3}$	$1.0 \cdot 10^{-5}$	$1.0 \cdot 10^{-3}$

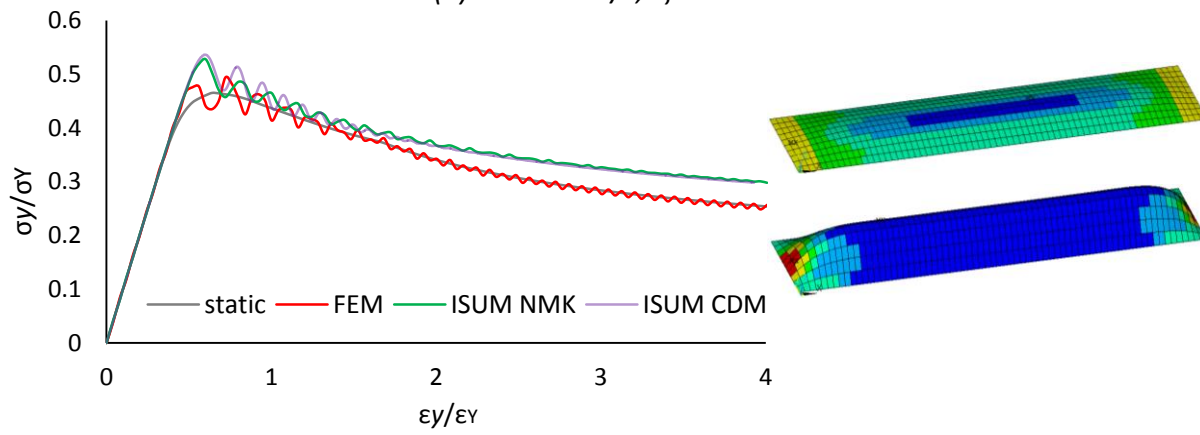
The ultimate strength of the examined thick plate panel is significantly higher compared with the above-considered rectangular plates under transverse thrust. The average stress-average strain curves oscillate around the static solution with a grate amplitude and therefore, the ultimate strength of the dynamically loaded plate panel is higher than in case of the static load application. The higher the applied edge velocity the greater is the load-carrying capacity of the plate. Thus, at the applied velocity of 50 mm/s the dynamic ultimate strength exceeds 30 % the corresponding static value. As mentioned in previous subchapters, covering the investigations on dynamic collapse behavior of rectangular plates under longitudinal thrust, ISUM NMK and ISUM CDM solutions start to depart from FEM curve at ultimate strength and further. Under applied transverse thrust one can see the same tendency. Nevertheless, the obtained dynamic solutions ISUM CDM and ISUM NMK oscillate around static ISUM curve, (as the FEM curve oscillates around static one), which is not shown in diagrams, but can be found in [36].

The collapse modes of the prescribed plate panel are the same as by the above-considered rectangular plates under transverse thrust. Due to the increased strength margin of the given plate, one can observe the more visible straightening of the plate in loading direction in the late post-buckling range. The ISUM CDM and ISUM NMK solutions provide very good results, especially when the damping forces are considered.

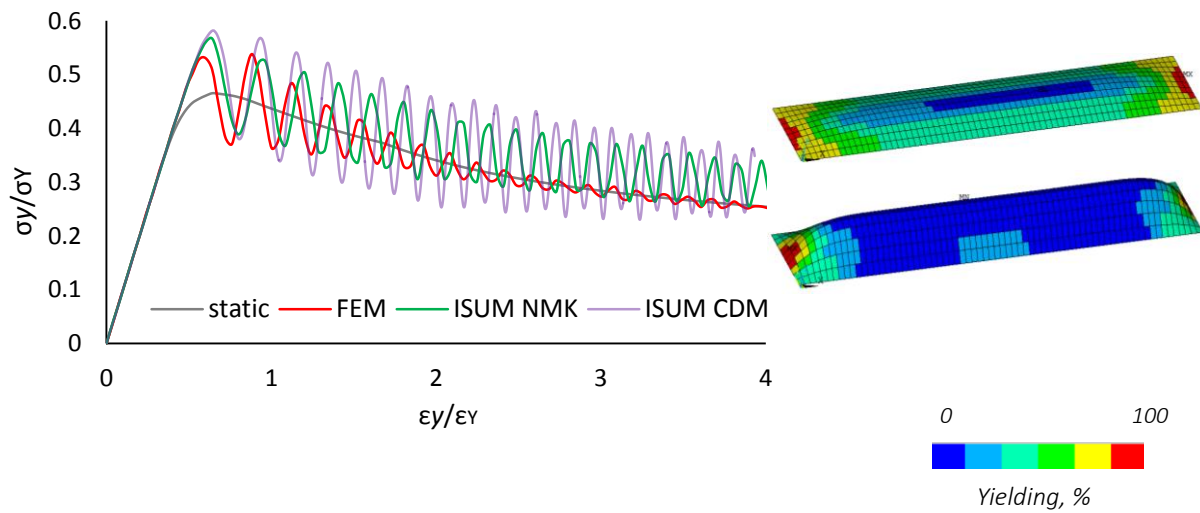
(1) $v = 20 \text{ mm/s}$; $\xi = 0$



(2) $v = 20 \text{ mm/s}$; $\xi = 0.05$



(3) $v = 35 \text{ mm/s}$; $\xi = 0$



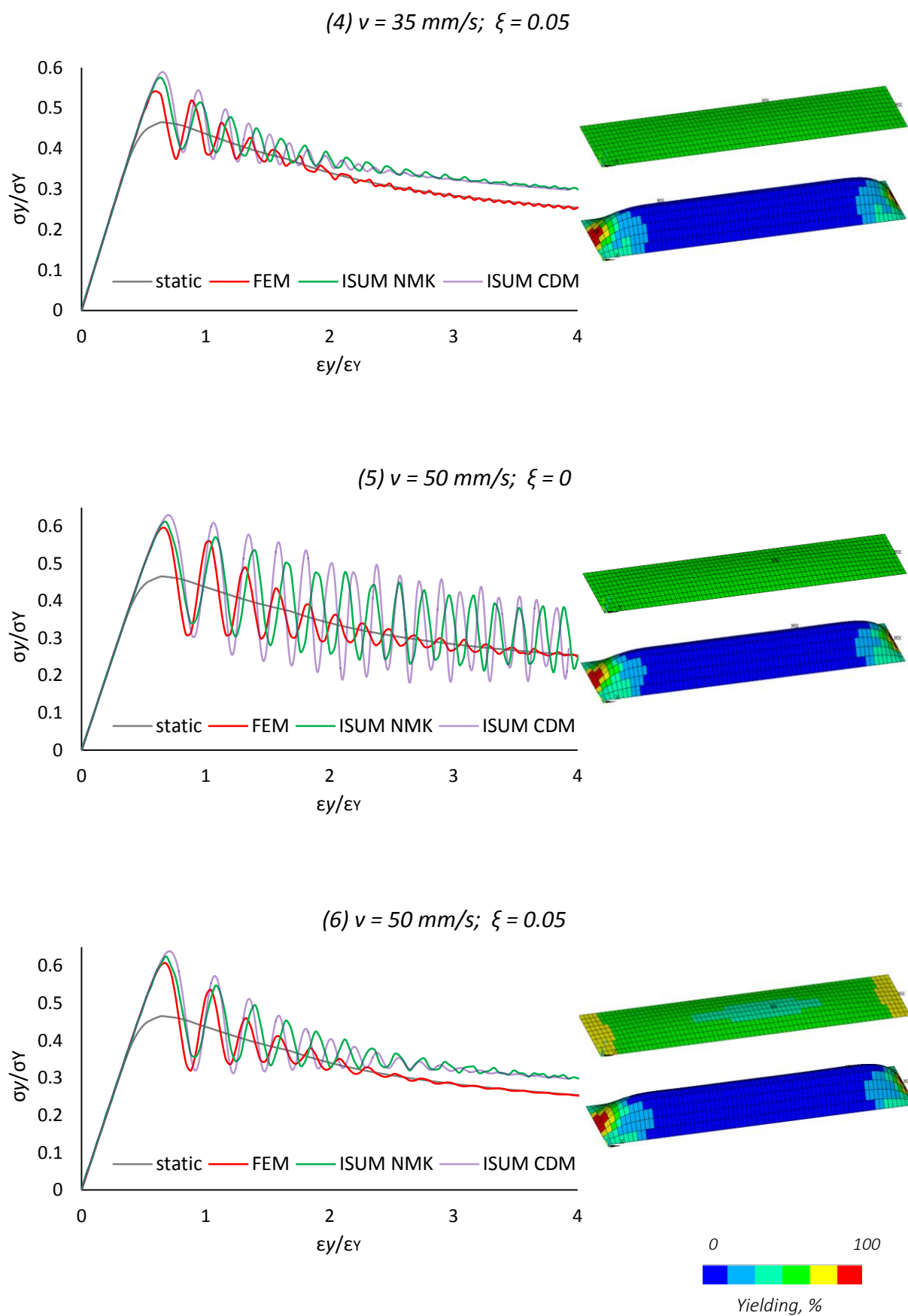


Figure 38 (1)-(6): Dynamic collapse behavior of transversely loaded plate 4200 x 835 x 22 mm

6.5 Dynamic Collapse Analyses of a Rectangular Panel under Biaxial Thrust

Within the latest test case we consider more complicated dynamic collapse analysis of the rectangular plate panel under biaxial thrust. As an example, the bottom plating experiences such a loading condition when the longitudinal compression from the hull bending together with the transverse compression from the bending of framing take place. Varying the constant ratios of applied transverse and longitudinal strains $\varepsilon_y/\varepsilon_x$, one can build an ultimate-strength interaction curve, which represents the relationship between the stresses σ_x and σ_y .

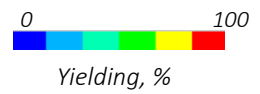
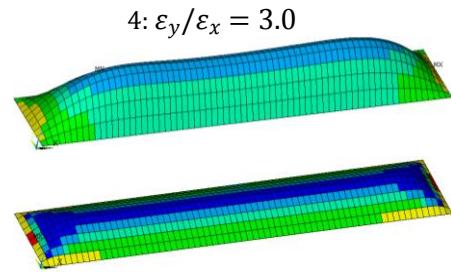
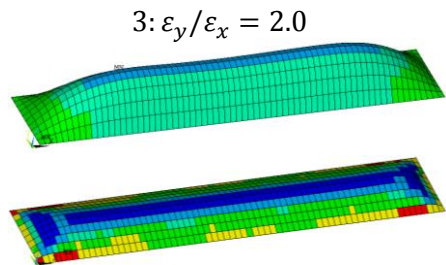
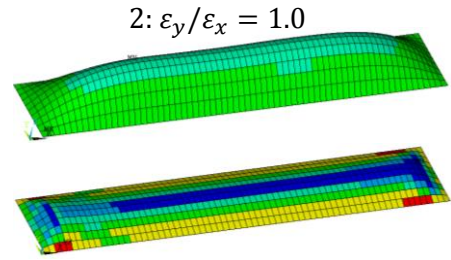
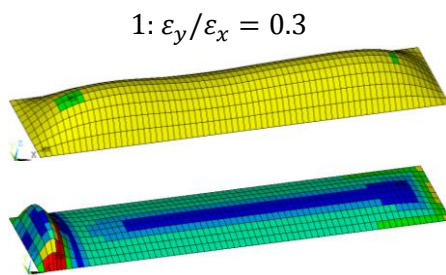
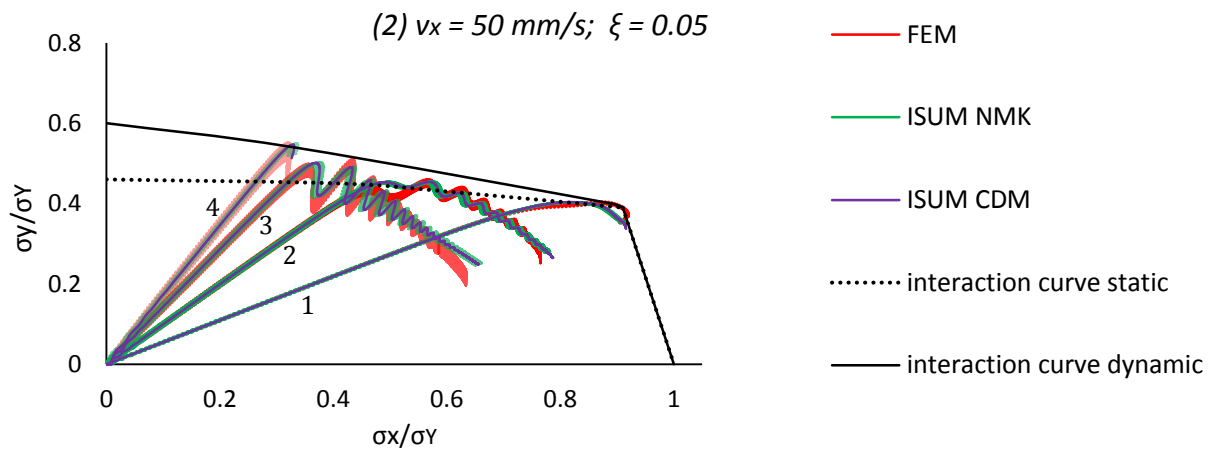
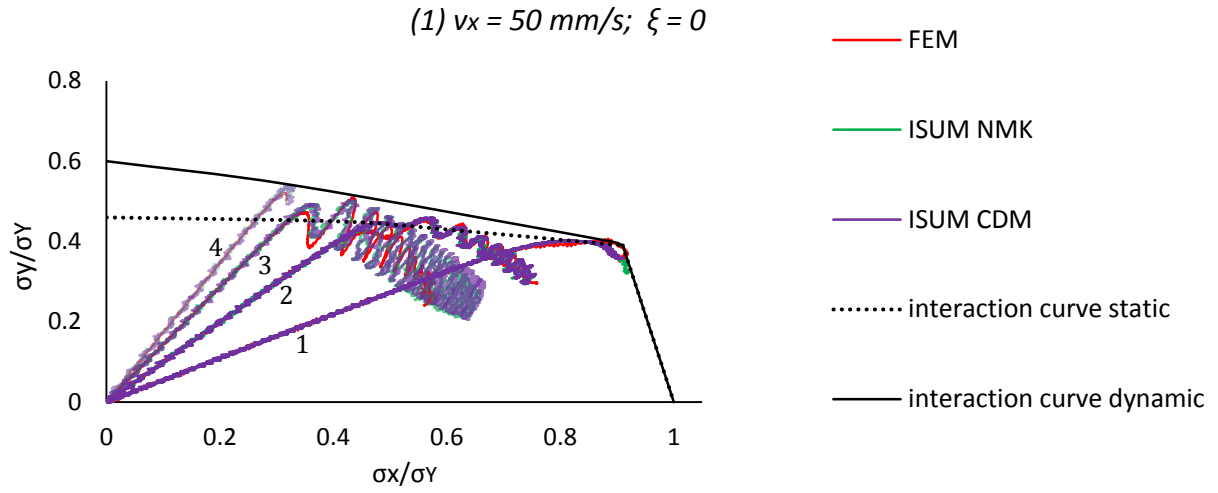
Dynamic collapse behavior of the rectangular plate is presented in Figure 39 (1)-(6). Consistent mass matrix is obtained from Eq. 65 with appropriate shape functions, Eqns. 70 and 71. The initial deflection values of the FE-model are presented in Table 9. Time step values Δt for each test case are assumed as follows:

<i>applied edge velocity</i>	<i>ISUM NMK</i>	<i>ISUM CDM</i>	<i>FEM</i>
$v_x = 50 \text{ mm/s}$			
$\varepsilon_y/\varepsilon_x = 0.3$	$4.4 \cdot 10^{-4}$	$2.2 \cdot 10^{-5}$	$4.4 \cdot 10^{-4}$
$\varepsilon_y/\varepsilon_x = 1.0$	$1.6 \cdot 10^{-4}$	$1.6 \cdot 10^{-5}$	$1.6 \cdot 10^{-4}$
$\varepsilon_y/\varepsilon_x = 2.0$	$1.4 \cdot 10^{-4}$	$1.4 \cdot 10^{-5}$	$1.4 \cdot 10^{-4}$
$\varepsilon_y/\varepsilon_x = 3.0$	$1.4 \cdot 10^{-4}$	$1.4 \cdot 10^{-5}$	$1.4 \cdot 10^{-4}$
$v_x = 100 \text{ mm/s}$			
$\varepsilon_y/\varepsilon_x = 0.3$	$2.2 \cdot 10^{-4}$	$2.2 \cdot 10^{-5}$	$2.2 \cdot 10^{-4}$
$\varepsilon_y/\varepsilon_x = 1.0$	$8.0 \cdot 10^{-5}$	$8.0 \cdot 10^{-6}$	$8.0 \cdot 10^{-5}$
$\varepsilon_y/\varepsilon_x = 2.0$	$7.0 \cdot 10^{-5}$	$7.0 \cdot 10^{-6}$	$7.0 \cdot 10^{-5}$
$\varepsilon_y/\varepsilon_x = 3.0$	$7.0 \cdot 10^{-5}$	$7.0 \cdot 10^{-6}$	$7.0 \cdot 10^{-5}$

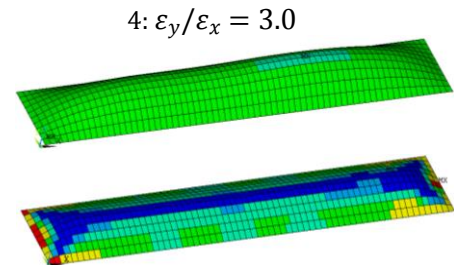
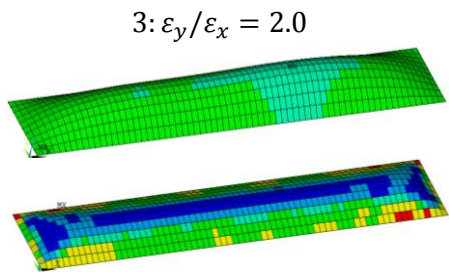
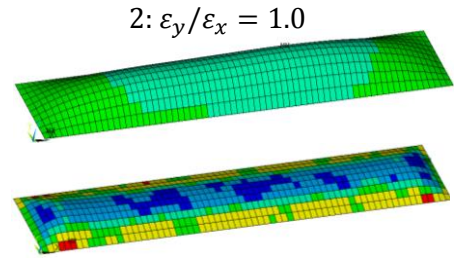
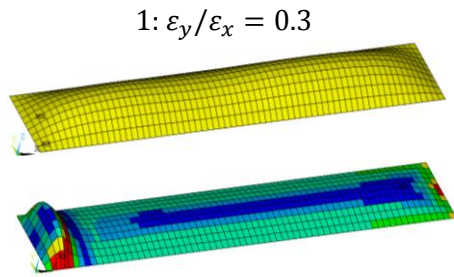
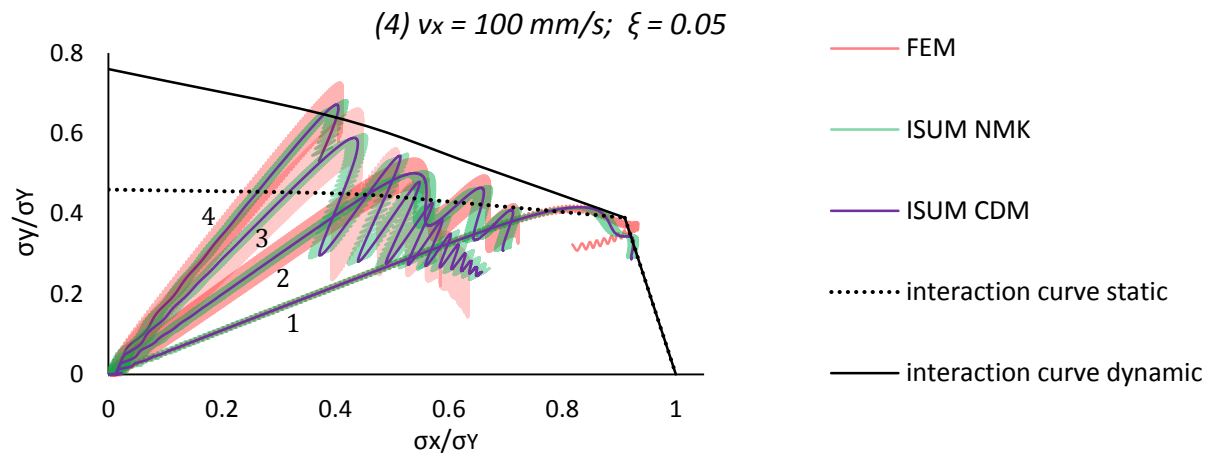
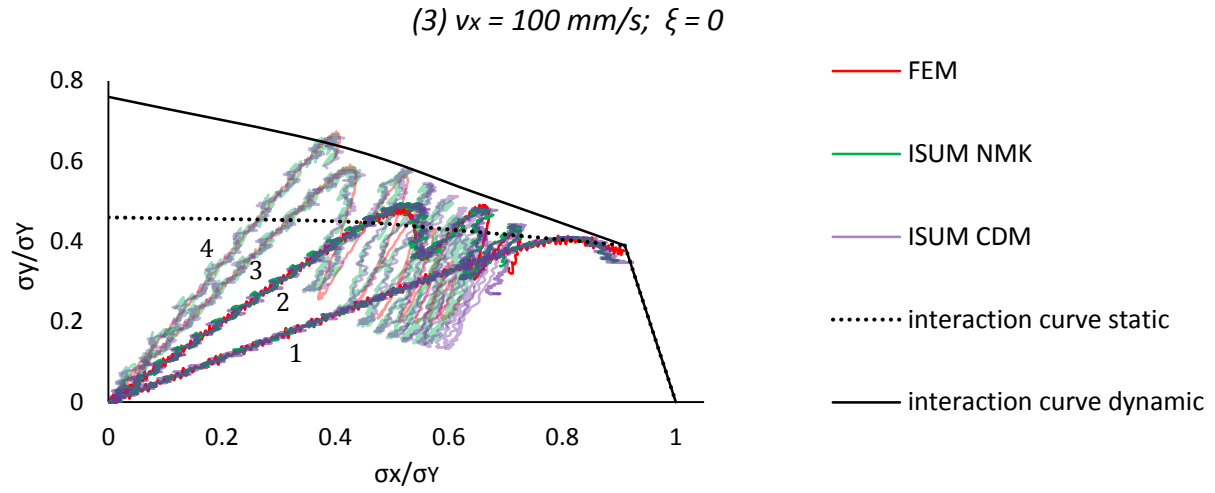
Presented in Figure 39 (1)-(6) envelope interaction curve is the boundary of static, [36], and dynamic solutions. Values, which lie on horizontal and vertical axis correspond to the maximum average-stress values σ_x/σ_Y and σ_y/σ_Y , obtained for longitudinal and transverse thrust applications respectively. For two applied edge velocity values $v_x = 50$ and 100 mm/s the comparison between static and dynamic interaction curves allows to make a conclusion that the transient effects (oscillation of the stress-strain curve and the corresponding rise of the load-carrying capacity) increase as the relation between the transverse and longitudinal strains $\varepsilon_y/\varepsilon_x$ grows. It is necessary to note that this difference becomes more significant with the growth of the applied velocity.

With the dominance of the applied transverse strains the total stress level, which correspond to the maximal applied average transverse stresses σ_y/σ_Y , decreases and the hungry-horse mode develops into the cylindrical buckling-mode like in case of the uniaxial transverse loading. Only for the first applied strain relation $\varepsilon_y/\varepsilon_x = 0.3$ the collapsing half wave can be observed as the average longitudinal stresses σ_x/σ_Y reach the maximum value.

The ISUM NMK and ISUM CDM solutions show very good agreement with the FEM results. Interesting to note that performing a dynamic collapse analysis of rectangular plate, ISUM CDM supplies the most reliable solution, since both ISUM NMK and FEM curves provide tiny, high frequent oscillations even within a damped analyses, Figure 39 (2), (4). The ISUM CDM solution can be in contrast very effectively damped.



For each of four test cases the above given collapse modes correspond to the maximum average transverse stresses σ_y/σ_Y (top image, deflection scale: 50) and to the maximum average longitudinal stresses σ_x/σ_Y (bottom image, deflection scale:



For each of four test cases the above given collapse modes correspond to the maximum average transverse stresses σ_y/σ_Y (top image, deflection scale: 50) and to the maximum average longitudinal stresses σ_x/σ_Y (bottom image, deflection scale: 50):

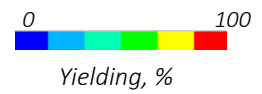


Figure 39 (1)-(4): Dynamic collapse behavior of rectangular plate 4200 x 835 x 22 mm under biaxial thrust

6.6 Concluding Remarks

In Chapter *Dynamic collapse analysis of the ISUM plate panels* the following subjects were highlighted and discussed:

- Determination of the damping parameters α and β for the four examined rectangular plate panels within the modal analysis, Table 7: based on the validation of the Rayleigh damping model on an example of the square plate panel, Figure 26, the damping ratio $\xi = 0.05$ is chosen for the dynamic collapse investigations of rectangular plate panels since this value provides a sufficient matching between FEM and ISUM results.
- Dynamic collapse behavior of the square plate panels with different slenderness ratio under uniaxial thrust without consideration of damping: both ISUM NMK and ISUM CDM solutions provide reliable results. Due to the oscillation of the average stress-average strain curves the load-carrying capacity turns to be higher (12% for the 15 mm square plate at the applied velocity of 100 mm/s) than compared with the static load application. For thin square plates with slenderness ratio $\beta > 3$, the collapse mode represents plateau in loading direction instead of the roof shape. Therefore, the shape function of ISUM plate element might be modified to enable the accurate dynamic collapse analysis of the thin square plates.
- Dynamic collapse behavior of rectangular plate panels under longitudinal thrust: plate panels with dimensions 2400 x 835 x 15 mm and 4200 x 835 x 13 mm were subjected to dynamic loading with edge velocity of 50 mm/s, 100 mm/s and 200 mm/s. The ISUM NMK and ISUM CDM solutions yield similar characteristics of the buckling behavior for both rectangular plates: the ISUM CDM solution supplies high, frequent oscillations of the average stress-average strength curve, which starts from the ultimate strength and goes through the whole post-buckling range. The consideration of the damping forces helps to avoid the excessive oscillations of the ISUM CDM solution, but as for the ISUM NMK solution, tiny oscillation are still present on the average stress-average strain diagram. Again, for the thin 13 mm rectangular plate panel the shape function of ISUM plate element might be modified, since the ISUM NMK and ISUM CDM solutions start to depart from the FEM curve at ultimate strength as for the thin square plate, and then, with the growth of the deformations this difference becomes significant (up to 28 %). Nevertheless, the ISUM NMK and ISUM CDM solutions predict the ultimate strength of prescribed rectangular plates with great accuracy.

Rise of the applied edge velocity leads to a slight increase of the ultimate strength. For the highest applied edge velocity of 200 mm/s one cannot observe such an apparent oscillative manner of the average strength-average strain curve as in case of the square plate. Nevertheless, the 6.7 % rise of the ultimate strength of the prescribed 15 mm rectangular plate is detected compared with the static load application case. Buckling behavior stays invariant to the increase of the applied edge velocity and remains as it was by the static calculations: one half-wave collapses and the rest of the plate unloads. For all applied edge velocities of 10 mm/s, 50 mm/s and 100 mm/s, the rectangular plate panel with dimensions 4200 x 835 x 22 mm undergoes plastic buckling. The ISUM NMK and ISUM CDM solutions follow the FEM results very well and depict the abrupt loss of the load-carrying capacity, which takes place slightly beyond the ultimate strength. As long as an aspect ratio per element $a/b < 0.8$, the old shape function with the parameter f set on zero yields better results.

- Dynamic collapse analysis of the rectangular plate panels under transverse thrust: the ISUM CDM and ISUM NMK solutions provide very good results for all panels, especially when damping is considered. The load-carrying capacity of all examined rectangular plate panels

under dynamic transverse thrust is significantly lower than in case of the dynamic longitudinal loading. Nevertheless, due to the strong oscillations of the average stress-average strain curves around the static solution, the ultimate strength of the dynamically loaded plate panel turns to be higher than in case of the static load application: for the rectangular plate panel with dimensions 2400 x 835 x 15 mm a 11 % rise of the ultimate strength is observed at the highest applied velocity of 80 mm/s; for the rectangular plate panel with dimensions 4200 x 835 x 22 mm this increase of the load-carrying capacity reaches 30 % at the applied velocity of 50 mm/s. The transient effects do not influence the typical buckling modes of rectangular plates under transverse thrust, since they are completely the same as the buckling modes, obtained from the static collapse analysis.

- Dynamic collapse analysis of the rectangular plate panel with dimensions 4200 x 835 x 22 mm under biaxial thrust: the ISUM NMK and ISUM CDM solutions show very good agreement with the FEM results and can be successfully used for the dynamic collapse analysis of plate panels under biaxial thrust. ISUM CDM supplies the most reliable solution, since both ISUM NMK and FEM curves provide tiny, high frequent oscillations even within a damped analyses. The ISUM CDM solution can be in contrast very effectively damped. With a growth of the relation between the applied transverse and longitudinal strains the dynamic effects also increase, producing stronger oscillations of the stress-strain curve and the rise of the load-carrying capacity. With the domination of the applied transverse strain the cylindrical collapse mode, as in the case of the pure transverse loading, takes place.
- Trying to conclude whether the implicit or explicit time integration method is more suitable for dynamic collapse analyses of rectangular plates with ISUM, it would be essential to take various aspects into account. In terms of reliability of the obtained results the explicit central difference method CDM would seem to be more effective if there were not the unrealistic oscillations, which come up during the longitudinal loading and do not disappear totally when damping effects are considered. Having noticed that CDM can be successfully damped in case of transverse and biaxial thrust application, one can presume that the complex longitudinal buckling mode should be additionally investigated in terms of possible shape function modification. This can be proved by the fact that CDM shows good results (without oscillations in damped case) for longitudinally loaded thick plate 4200 x 835 x 22 mm. Possessing the high strength margin this plate experience small deflections, and therefore, the influence of buckling mode on the solution decreases. The implicit Newmark's time integration scheme NMK provides reliable results in terms of ultimate strength prediction and supplies the correct behavior of stress-strain curve, but it cannot be properly damped: for all examined plates under uniaxial and biaxial thrust small oscillation are still present. From point of computational costs, implicit NMK seems to be more attractive than the explicit CDM method for the considered investigations. With the particular integration parameters the NMK method is unconditionally stable, and therefore, time increment values can be much higher that enables performing approximately 10^3 times less calculation steps than using CDM. Generally, explicit time integration scheme can be a very effective algorithm, since it does not require the calculation of inverse of stiffness matrix, itself being a function of unknown displacements. Moreover, solution is obtained for a current step without an iteration procedure. These advantages can be fully utilized only within a dynamic scenario, covering impact loading caused by slamming, earthquakes, crash simulations etc. ISUM was extended on transient analyses with a purpose to assess the dynamic load-carrying capacity and to get an insight into dynamic pre- and post-buckling behavior. Taking the up to date ISUM formulation together with its goals into account one can give a preference to the implicit time integration method.

7 Conclusions

Within the present thesis the extension of the Idealized Structural Unit Method to the dynamic collapse analysis has been performed. The thorough study of the transient processes helped to understand the nature of dynamic buckling behavior of plate structures and to develop a solution concept, which subsequently supplied reliable results.

The derivation and profound consideration of the linear and nonlinear dynamic equilibrium equations of motion led to a close insight into the dynamic problems. Consistent mass matrix, which reflects the inertial properties of the body, was implemented in ISUM using the shape functions developed for the static analysis, since no significant change between the static and dynamic buckling modes is observed. The damping effects are included in dynamic analysis by formation of the damping matrix according to Rayleigh formulation, which represents a linear combination of mass and stiffness matrices.

As solution procedures, the nonlinear explicit central difference scheme and the nonlinear implicit Newmark's scheme were implemented in ISUM for time integration. Validation was performed on an example of the 4-node ISUM element, uniaxially loaded by dynamic forces. This direct approach does not give the full picture of buckling behavior, as long as force control is used. Formulation of the enforced motion method in terms of the "enforced" and "free" degrees of freedom and application of this technique to the nonlinear explicit and implicit schemes let performing displacement control instead of force control. Due to this formulation, obtained stress-strain curves provide the desirable results, since total buckling behavior of the plate structure can be obtained by displacement control.

The included inertia and damping effects have a significant influence on the dynamic buckling behavior of rectangular plate panels. The inertial component provokes strong oscillations of the average stress-average strain curves around the static solution, especially when the rectangular plate is subjected to transverse and biaxial thrust. Moreover, the ultimate strength of the dynamically loaded plate panels under transverse and biaxial loading turns to be higher than in case of static load application. Nevertheless, the transient effects do not influence the typical buckling modes of rectangular plates, since they are completely the same as obtained from static collapse analysis.

Having noticed that the explicit central difference scheme can be successfully damped in case of transverse and biaxial thrust application, but provides the unrealistic oscillations of the average stress-average strain curve during the longitudinal loading one can presume that the complex longitudinal buckling mode should be additionally investigated in terms of possible shape function modification. This is especially true for the thin rectangular plate panels, since the ISUM implicit and ISUM explicit solutions start to depart from the FEM curve beyond ultimate strength. The implicit Newmark's time integration scheme provides reliable results in terms of ultimate strength prediction and supplies the correct behavior of stress-strain curve, but the tiny oscillation of the stress strain curve are still present even within the damped analyses.

In conclusion, it is shown that the explicit central difference and implicit Newmark's time integration methods newly implemented in the ISUM provide reliable results and can be used for dynamic collapse analysis of plate structures. Both time integration schemes have been successfully coupled with the enforced motion technic to allow for analyses under displacement control. Performance of the ISUM dynamic analysis is much less time consuming than by using common FEM. Although the nonlinear explicit central difference scheme requires neither the calculation of inverse of stiffness matrix nor an iterative solution search, the unconditionally stable Newmark's method takes less computational time in the application considered here and can be recommended for further investigations.

References

- [1] Paik, J.K, Thayamballi, A. K. **Ultimate Limit State Design of steel-plated Structures**, John Wiley and Sons, Chichester, 2003.
- [2] Marguerre, K. **Zur Theorie der gekrümmten Platte großer Formänderung**. Proc. of the Fifth Intern. Congr. for Appl. Mech., pp. 93–101. 1938.
- [3] Murray, N. W. **Introduction to the Theory of Thin-Walled Structures**. Clarendon Press, Oxf, 1986.
- [4] IACS, **Common Structural Rules for Bulk Carriers and Oil Tankers**, CSR, July 2012.
- [5] Smith, C.S. **Structural redundancy and damage tolerance in relation to ultimate ship-hull strength**. AMTE Dunfermline, UK 1983.
- [6] Clough, R. W. **The Finite Element Method in plane stress analysis**, Proc. American Society of Civil Engineers (2nd Conference on Electronic Computation, Pittsburg, USA), 1960, Vol. 23, P. 345-378.
- [7] Argyris, J. H. **Energy theorems and structural analysis**, Aircraft Engineering, 1954, Vol. 26, Part 1 (Oct. – Nov.), 1955, Vol. 27, Part 2 (Feb. – May).
- [8] Turner, M. J., Clough, R. W., Martin, H. C. and Topp, L. J. **Stiffness and deflection analysis of complex structures**, Journal of Aeronautical Science, 1956, Vol. 23, No. 9, P. 805-824.
- [9] Hrennikov, A. **Solution of problems in elasticity by the framework method**, Journal of Applied Mechanics, 1941, Vol. 8, P. 169-175.
- [10] Zienkiewicz, O. C. and Cheung Y. K. **The Finite Element Method in Structural and Continuum Mechanics**, McGraw-Hill: London, 1967.
- [11] Ueda, Y and Rashed. **The Idealized Structural Unit Method and Its Application to Deep Girder Structures**. Computers and Structures, Vol 18(2), pp 277-293, 1984.
- [12] Paik, JK and Che, JS. **Ultimate strength hulls under combined vertical bending, horizontal bending, and shearing forces**, Trans SNAME, 104, pp 31-59, 1996.
- [13] Paik, JK and Pedersen. **Ultimate strength of ship hulls under torsion**, Ocean Eng, 28, 2001
- [14] Paik, JK, Kim, BJ, Seo, JK. **Methods for ultimate limit state assessment of ships and ship-shaped offshore structures: Part III hull girders**, Ocean Eng., 35, pp 281-286, 2008.
- [15] Paik, J.K., Kim, B.J. **Progressive collapse analysis of thin-walled box columns**, Thin-Wall Structures, 46, pp 541-550, 2008.
- [16] Underwood, JM, Sobey, AJ, Blake, JIR, Shenoi, RA. **Ultimate collapse strength assessment of damaged steel-plated structures**, Eng Struct., 38, pp 1-10, 2012.
- [17] Masaoka, K, Okada, H, Ueda, Y. **A Rectangular Plate Element for Ultimate Strength Analysis**, 2nd Int Conf Thin-Walled Structures, pp 469-476, 1998.
- [18] Fujikubo, M and Kaeding, P. **New simplified approach to collapse analysis of stiffened plates**, Mar Struct, Vol 15, pp 251-283, 2002.
- [19] Fujikubo, M, Olaru, VD, Yanagihara, D and Setoyama, Y. **ISUM Approach for Collapse Analysis for Double-Bottom Structures in Ships**, Proc 12th Int Offshore and Polar Eng Conf, Kitakyushu, ISOPE, Vol 4, pp 644-651, 2002.

- [20] Kaeding, P, and Fujikubo, M. **New Simplified Model for Collapse Analysis of Stiffened Plates and its Application to Offshore Structures**, ISOPE, Vol 12, No 2, pp 126-133, 2002.
- [21] Kaeding, P, and Fujikubo, M. **Idealized Structural Unit Method for Collapse Analyses of Stiffened Plate Structures**, Ship Technology Research, Vol 50, pp 23-33, 2003.
- [22] Fujikubo, M, Kaeding, P, Pei, Z. **Idealized Structural Unit Method for Collapse Analysis of Stiffened Plate Structures**, Int Conf Comp Methods in Marine Eng, pp 385-394, 2005.
- [23] Kaeding, K, Olaru, VD, Fujikubo, M. **Development of ISUM Plate Element with Consideration of Lateral Pressure Effects and its Application to Stiffened Plates of Ships**, Proc 9th Symp Prac Design of Ships and Other Float Structures, Lübeck, PRDAS, Vol 1, pp 148-155, 2004.
- [24] Ishibashi, K, Fujikubo, M, Yao, T. **Development of ISUM Element for Rectangular Plate with Cutout**, Proc 16th Int Offshore and Polar Eng Conf, San Francisco, ISOPE, Vol 4, pp 339-346, 2006.
- [25] Pei, Z, Takami, T, Gao, C, Fu, J, Tanaka, Y, Iijima, K, Fujikubo, M, Yao, T. **Development of ISUM Shear Plate Element and Its Application to Progressive Collapse Analysis of Plates under Combined Loading**, Proc ISOPE, Beijing, Vol 4, pp 773-780, 2010.
- [26] Pei, Z, Ji, Y, Nakamura, K, Tanaka, S, Okazawa, S, Fujikubo, M, Yao, T. **Development of Isoparametric ISUM Plate Element**, Proc 20th Int Offshore and Polar Eng Conf, Beijing, ISOPE, Vol 4, pp 781-788, 2010.
- [27] Pei, Z, Gao, C, Tanaka, Y, Tanaka, S, Okazawa, S, Iijima, K, Fujikubo, M, Yao, T. **Collapse Analysis of Container Ship Model under Combined Bending and Torsion Applying Idealized Structural Unit Method**, Proc of the 21th Int Offshore and Polar Eng Conf, Maui, ISOPE, Vol 4, pp 894-901, 2011.
- [28] Gao, C, Pei, Z, Yasuoka A, Tanaka, S, Okazawa S, Alie ZM, Lijima K, Fujikubo M, Yao T. **Collapse Analysis of double Bottom Structures Considerind Shear, Lateral Pressure and Wwelding Residual Stress**, Proc. ISOPE, Maui, USA, Vol 4: 902-909, 2011.
- [29] Lindemann, T, Klostermann, J, Kaeding, P. **Approaches to the Improvement of the Applicability of the Idealized Structural Unit Method for Collapse Analysis of Plate Structures**. Proc 22th Int Offshore and Polar Eng Conf, Rhodes, ISOPE, Vol 4, pp 847-854, 2012.
- [30] Lindemann, T. **Idealized Structural Unit Method for Collapse Analyses of Plate Structures under Inplane and Lateral Loads**, Dissertation, Universität Rostock, 2015
- [31] Rashed, S. **ISUM – Its birth, growth and future**. Proceedings of the OMAE 2016 International Conference on Ocean, Offshore & Arctic Engineering, OMAE2016- 54479, 2016.
- [32] Lindemann, T, Backhaus, E, Ulbertus, A, Oksina, A, Kaeding, P. **Investigations on the Dynamic Collapse Behaviour of Thin-Walled Structures and Plate Panels for Shipbuilding Applications**, the 25th International Ocean and Polar Engineering Conference, Kona, Big Island, Hawaii, USA, 21–26 Juni, 2015.
- [33] Cowper, G.R., Simonds, P. S. **Strain-hardening and strain-rate effects in the impact loading of the cantilever beams**, technical report No. 28, Division of Applied Mathematics, Broun Univ. 1957.
- [34] Pei, Z, Iijima, K, Fujikubo, M. **Collapse Behaviour of Ship Hull Girder of Bulk Carrier under Alternative Heavy Loading Condition**. Proc. 22nd Int Offshore and Polar Eng Conf, Rhodes, Greece, ISOPE, 839-846, 2012.

- [35] Fujikubo, M, Kaeding, P, Pei, Z. **ISUM for collapse analysis of stiffened plate structures**. International Conference on Computational Methods in Marine Engineering, Barcelona, 2005.
- [36] Fujikubo M, Kaeding P, Yao T. **ISUM rectangular plate element with new lateral shape functions**, 1st Report Flongitudinal and transverse thrust. J Soc Naval Arch Japan; 187:209–19, 2000.
- [37] Ueda Y, Yao T. **The influence of complex initial deflection modes on the behaviour and ultimate strength of rectangular plates in compression**, J Const Steel Res; 5:265–302, 1985.
- [38] Kaeding, P. **Development of New Idealized Structural Unit Method for the Collapse Analysis of the Stiffened Plate Structures**, Dissertation, Graduate School of Engineering of Hiroshima University, 2001.
- [39] Washizu K. **Variational Methods in Elasticity and Plasticity**, 3rd Edition, Pergamon Press, 1982.
- [40] Timoshenko SP, Woinowsky-Krieger S. **Theory of Plates and Shells**, McGraw-Hill, 1959.
- [41] Timoshenko SP, Gere JM. **Theory of Elastic Stability**, 2nd Edition, McGraw-Hill, 1961.
- [42] Eggers H, Kröplin BH. **Yielding of Plates with Hardening and Large Deformations**, Int Journal for Num Meth Eng, Vol 12: 737-750, 1978.
- [43] Ipatovtsev Y, Korotkin Y. **Structural mechanics and strength of ship**, Leningrad, 1991.
- [44] Werkle H. **Finite Elemente in der Baustatik**, Friedr.Vieweg & Sohn Verlag, Wiesbaden 2008.
- [45] Bathe K.U. **Finite Element Procedures for solids and Structures – Linear Analysis**, MIT Center for Advanced Engineering study.
- [46] Kaeding P. **Finite-Elemente-Methode zur Berechnung maritimer Strukturen**, Lecture notes, Univ. Rostock, 2014.
- [47] Gang L. Wong. K. **Theory of Nonlinear Structural Analysis**, John Wiley & Sons, 2014.
- [48] Bathe K.U. **Finite Element Procedures**, Prentice hall, Upper Saddle River, New Jersey, 1996.
- [49] Süli E. and Mayers D. **Introduction to Numerical Analysis**, Cambridge University Press, 2003.
- [50] Reddy, J.N. **Energy Principles and Variational Methods in Applied Mechanics**, John Wiley, 2002.
- [51] Dvorkin E.N, Goldschmit M.B. **Nonlinear Continua**, Springer, 2006.
- [52] Irgens F. **Continuum Mechanics**, Springer, 2008.
- [53] Madenci E., Guven I. **The Finite Element Method and Applications in Engineering Using ANSYS®**, Springer, 2006.
- [54] Oksina, A, Lindemann, T, Kaeding, P, Fujikubo, M. **Idealized Structural Unit Method - A Review of the Current Formulation**, Proceedings of the OMAE 2016 International Conference on Ocean, Offshore & Arctic Engineering, OMAE2016-54186, 2016.
- [55] ANSYS 15.0 **Release Documentation**, 2015.
- [56] Lasan, B. **Damping of materials and members in structural mechanics**, Oxford Pergamon, 1968.
- [57] Bachmann, H. **Vibration problems in structures**, practical guidelines/Basel, Boston, Berlin, 1995.